Colorado's Full-Scale Field Testing of Rockfall Attenuator Systems

DETAILS

AUTHORS

BUY THIS BOOK

FIND RELATED TITLES

TRANSPORTATION RESEARCH
CIRCULAR

Number E-C141   **October 2009**

Colorado's Full-Scale Field Testing of Rockfall Attenuator Systems

TRANSPORTATION RESEARCH BOARD
OF THE NATIONAL ACADEMIES

TRANSPORTATION RESEARCH CIRCULAR E-C141

Colorado's Full-Scale Field Testing of Rockfall Attenuator Systems

Ben Arndt
Yeh and Associates, Inc

Ty Ortiz
Colorado Department of Transportation

A. Keith Turner
Colorado School of Mines

October 2009

Transportation Research Board
500 Fifth Street, NW
Washington, DC 20001
www.TRB.org

TRANSPORTATION RESEARCH CIRCULAR E-C141

ISSN 0097-8515

The **Transportation Research Board** is one of six major divisions of the National Research Council, which serves as an independent adviser to the federal government and others on scientific and technical questions of national importance. The National Research Council is jointly administered by the National Academy of Sciences, the National Academy of Engineering, and the Institute of Medicine. The mission of the Transportation Research Board is to provide leadership in transportation innovation and progress through research and information exchange, conducted within a setting that is objective, interdisciplinary, and multimodal.

The **Transportation Research Board** is distributing this Circular to make the information contained herein available for use by individual practitioners in state and local transportation agencies, researchers in academic institutions, and other members of the transportation research community. The information in this Circular was taken directly from the submission of the authors. This document is not a report of the National Research Council or of the National Academy of Sciences.

Transportation Research Board
500 Fifth Street, NW
Washington, DC 20001
www.TRB.org

Preface

The purpose of this circular is to provide the results of a recently completed study to geotechnical engineers and engineering geologists responsible for managing and mitigating rockfalls. The study, sponsored by the Colorado Department of Transportation (CDOT), was conducted to provide a better understanding of the durability and performance of several currently available mesh and cable net products that can be used to construct rockfall attenuator systems, for which no design guidelines exist. With the technical support of consultant Yeh and Associates, Inc., of Denver, Colorado, CDOT developed a test site and completed research that resulted in CDOT's development and construction of an attenuator system at a very difficult rockfall site. The testing described in this circular provides useful data that practitioners may use as they make design decisions when considering attenuator systems.

Rockfall mitigations are generally grouped into one of three major categories: avoidance, stabilization, or protection measures. Avoidance measures rely on relocating the endangered facility. Stabilization techniques are used to support or secure potential rockfalls in place to keep them from initiating. The goal of protection measures is to control or capture rockfalls once they initiate and restrict them from endangering a structure or facility, such as a highway. Attenuator systems fall into the protection category.

Attenuators are used to intercept rockfalls and dissipate the energy of moving rock blocks as they pass through the attenuator system, slowing them down so that they are retained in a designated collection area, generally a roadside ditch. An effective attenuator is positioned on the slope where rockfalls can be intercepted. These systems generally consist of several mesh or cable net panels that are connected together laterally and supported on a wire rope raised above the ground on a series of posts. In most cases, the only attachment of the mesh panels to the support system is by the upper support rope. The panels hang down freely with a specific length of the draped mesh resting on the ground down-slope of the posts.

When a rockfall strikes the raised impact area, it is directed downward and beneath the mesh resting on the ground. The free-hanging nature of the mesh allows it to deflect when struck by a rock, which reduces impact damage to the system. The interaction between falling rock and the mesh dissipates the rockfall energy by impacting and lifting the mesh, by changing the direction of the rock downward to strike the ground surface, and by forcing the rock to work its way between the draped mesh and ground surface in order to continue down the slope. These actions slow the rockfall velocity and produce a significant reduction in kinetic energy as rock exits the system.

This circular is authored by Ty Ortiz, CDOT; Ben Arndt, Yeh and Associates, Inc.; and Keith Turner, Colorado School of Mines. Critical reviews were provided by Tom Badger, Washington State Department of Transportation; Vanessa Bateman, Tennessee Department of Transportation; John Duffy, California Department of Transportation; Peter Ingraham, Golder and Associates; and Dave Stanley, Alaska Department of Transportation and Public Facilities. Special thanks are expressed to G. P. (Jay) Jayaprakash, Transportation Research Board, for his input and support.

—Lawrence A. Pierson
Chair, Engineering Geology Committee

iii

Overview

This circular presents the results of an applied research study to test various mesh materials that could be used in constructing rockfall attenuator systems, also referred to as hybrid rockfall fences. At the time of the study, no design guidelines were available for these systems. The goal of the evaluation was to subject these systems and materials to realistic loading and impact conditions in order to better understand the durability of the mesh and net materials and their effectiveness in dissipating rockfall energy and thereby mitigating rockfall hazards.

The study was initiated by the Colorado Department of Transportation in response to a lack of success with previous rockfall mitigation efforts along Interstate-70 near Georgetown, Colorado, 100 km (45 mi) west of Denver. Recognizing that the site conditions required a new mitigation approach, the Colorado Department of Transportation contracted with Yeh and Associates, Inc., of Denver, Colorado, to assist with research that would help them put an improved rockfall protection system into service.

At the Georgetown Incline, rockfall source areas are up to 600 m (2,000 ft) above the highway; the slope averages between 35 and 45 degrees but includes steeper, near-vertical sections where many of the rockfall events initiate. Due to the slope angle and geometry, rockfalls develop considerable rotational energy and achieve significant bounce heights as the blocks progress down the slope. Several rock-rolling tests were performed at the site, but a more comprehensive suite of testing that did not affect Interstate-70 traffic was needed.

Accepted system testing protocols evaluate the total kinetic energy capacity of proprietary barrier systems but these testing procedures typically do not include rotation of the test rocks. Rotating rocks, especially ones with sharp, angular, or protruding edges, cause additional damage to components of barrier systems, adversely affecting their performance, service life, and maintenance requirements. To better model these effects, a testing facility was constructed to more closely reproduce the rotational component of observed rockfall. In these tests, rotational energy accounted for up to 32% of the total kinetic energy.

Evaluations of 11 different mesh panel materials and two different post configurations were undertaken with 125 rock-rolling tests. Six sizes of test rocks weighing up to 3,800 kg (8,360 lb) were manufactured as steel-reinforced concrete cuboctahedrons. High-speed cameras recorded each test, and analysis of the video records determined rotational and total kinetic energies. Strain gauges attached to the posts measured direct impacts on the posts. The materials were evaluated on their ability to attenuate (reduce) rockfall energy, the amount of deformation each material suffered, the maintenance required, the amount of tail (drape length) required to adequately attenuate the rockfall energies, the durability of the post-to-foundation connections, and the amount of fly-up of the drapery tail that occurred upon rock impact.

Evaluations and testing of each system continued until it was deemed to no longer function as intended. The results of the tests have been tabulated and are presented in the appendixes. On the basis of the test results, a new series of attenuator systems have been installed at various elevations on the slope above Interstate-70 at the Georgetown Incline site. Recently, a 730 kg (1,800 lb) rock was dropped from a helicopter onto the slope above the highest attenuator. The new system performed as intended, and the test rock was retained in a catchment ditch adjacent to the Interstate after passing through the series of attenuators.

Contents

LIST OF FIGURES

LIST OF TABLES

Colorado's Full-Scale Field Testing of Rockfall Attenuator Systems

BEN ARNDT
Yeh and Associates, Inc.

TY ORTIZ
Colorado Department of Transportation

A. KEITH TURNER
Colorado School of Mines

Rockfall hazards are frequently encountered along highways in mountainous areas. Rockfalls pose safety risks to the traveling public and, by disrupting the proper functioning of the transportation facility, cause economic hardship by interrupting commerce and restricting access to adjacent communities. Mitigation of these rockfall hazards has thus become an important concern of transportation authorities, especially those located along heavily traveled major highways.

1 INTRODUCTION

Rockfall mitigation procedures are grouped into one of the following three major categories: avoidance, stabilization, and protection measures. Avoidance measures rely on relocating the endangered facility. Stabilization techniques are used to support and/or secure potential rockfalls in place to keep them from initiating. The goal of protection measures is to control or mitigate rockfalls once they initiate and restrict the rockfalls from endangering a structure or facility.

Over the past decade, considerable technological advances have greatly improved the design and performance of rockfall protection measures. New materials have been developed that allow the construction of stronger and more efficient protection systems; while enhanced analysis of rockfall processes, coupled with more sophisticated design procedures, permit the selection of suitable protection systems.

Rockfall hazards are particularly severe when a highway is located in a valley bordered by extensive mountain slopes. In these locations, rockfall source zones may exist high above the road and far outside the right-of-way. As dislodged rock blocks travel down these long slopes from the source areas, they accelerate and experience multiple impacts with the uneven slope surface, causing them to spin and bounce with increasingly large energies along erratic and unpredictable trajectories. Yet, at many of these locations, mitigation by avoidance is impractical, due to the constraints imposed by the terrain and economics; stabilization measures often cannot be applied to widely-dispersed rockfall source areas located outside the right-of-way; and protection measures placed near the road have often proven ineffective.

At the base of long slopes, rockfall blocks are traveling at velocities that produce high impact energies. While the most rugged of the existing fence systems have been reported as capable of withstanding up to 5,000 kJ (1,850 ft-tons) impacts, and many experienced practitioners believe that rock diameters less than 1.5 m (5 ft) are unlikely to produce impact energies in excess of 1,000 kJ (370 ft-tons), several practical issues often restrict our ability to design adequate rockfall protection devices at the base of long slopes.

Rockfall events on these long slopes often do not consist of single rocks; usually there are multiple rocks traveling as a group, either because the initial failure included more than one block, since the rolling rock triggered other rockfalls as it traversed the slope, or because larger blocks tend to break up during the descent. As a result, it is important to have a rockfall protection system that is capable of absorbing multiple impacts in close succession. This consideration translates into the need for a fence system that has a high-impact design capacity, or alternatively the use of some type of barrier wall, and there is often insufficient space to construct either a barrier wall or provide an adequate catchment area. In addition, field observations confirm the predictions of rockfall simulation models that some rockfalls will travel along trajectories that allow them to pass over any fence or barrier of feasible height placed at the base of the slope. Together, these considerations suggest that it is often impractical to rely solely on protection measures installed at the base of long, elevated slopes to adequately mitigate the rockfall hazard.

In some cases, effective fence or barrier systems could be placed higher up on the slope to intercept rockfalls. However, once they are filled with rockfall debris, or have been exposed to several rockfall events, these installations generally require maintenance. In many locations, the steepness of the slope makes access for maintenance operations impractical, risky, and costly.

Consequently, assessments of a new type of protection measure, termed an attenuator system, began at locations in several western states. Rather than trying to arrest the rocks on the slope, attenuator systems are designed to intercept and dissipate the velocities and energies of the rockfall blocks as they pass through the system, and, as a result, the blocks can be retained in a designated collection area, such as a roadside ditch, along the base of the slope. As these systems combine the attributes of standard drapery with a flexible rockfall fence/barrier, they are in some instances also referred to as "*hybrid drapery*" or "*hybrid barrier*" (Badger et al., 2008).

Most rockfalls along Colorado highways are relatively small events involving rock blocks that are less than 0.7 m (2 ft) in diameter. In many locations, rockfall events are quite frequent, although individual events are unpredictable. Rockfalls are caused by the disintegration of weathered rock faces, erosion of block-in-matrix slopes, and wildlife activity. Freeze–thaw events in the winter and spring, and intense summertime precipitation events, often initiate rockfalls. Variable message warning signs along major roads are used to alert the traveling public to the potential for rockfall at these times. The most common methods of mitigating these smaller rockfall events are catchment ditches, draped netting, and rock scaling.

However, some sections of Colorado highways, including several heavily-traveled and important highways, are located in mountain valleys or canyons, and are thus exposed to the increased rockfall velocities and energies associated with locations at the base of long and steep natural slopes. These locations have been the focus of much more intensive rockfall mitigation efforts.

A 3.54 km (2.2 mile) section of Interstate 70 west of Denver, located between the towns of Georgetown and Silver Plume (Figure 1), is one of the highest-ranked rockfall risk locations in Colorado because of its high traffic volumes and the frequency of rockfall events. This location became the first in the state to be considered for the installation of attenuator systems constructed with net panel materials that had been used in rockfall barrier protection fences.

Georgetown Incline

Hidden Valley Test Site
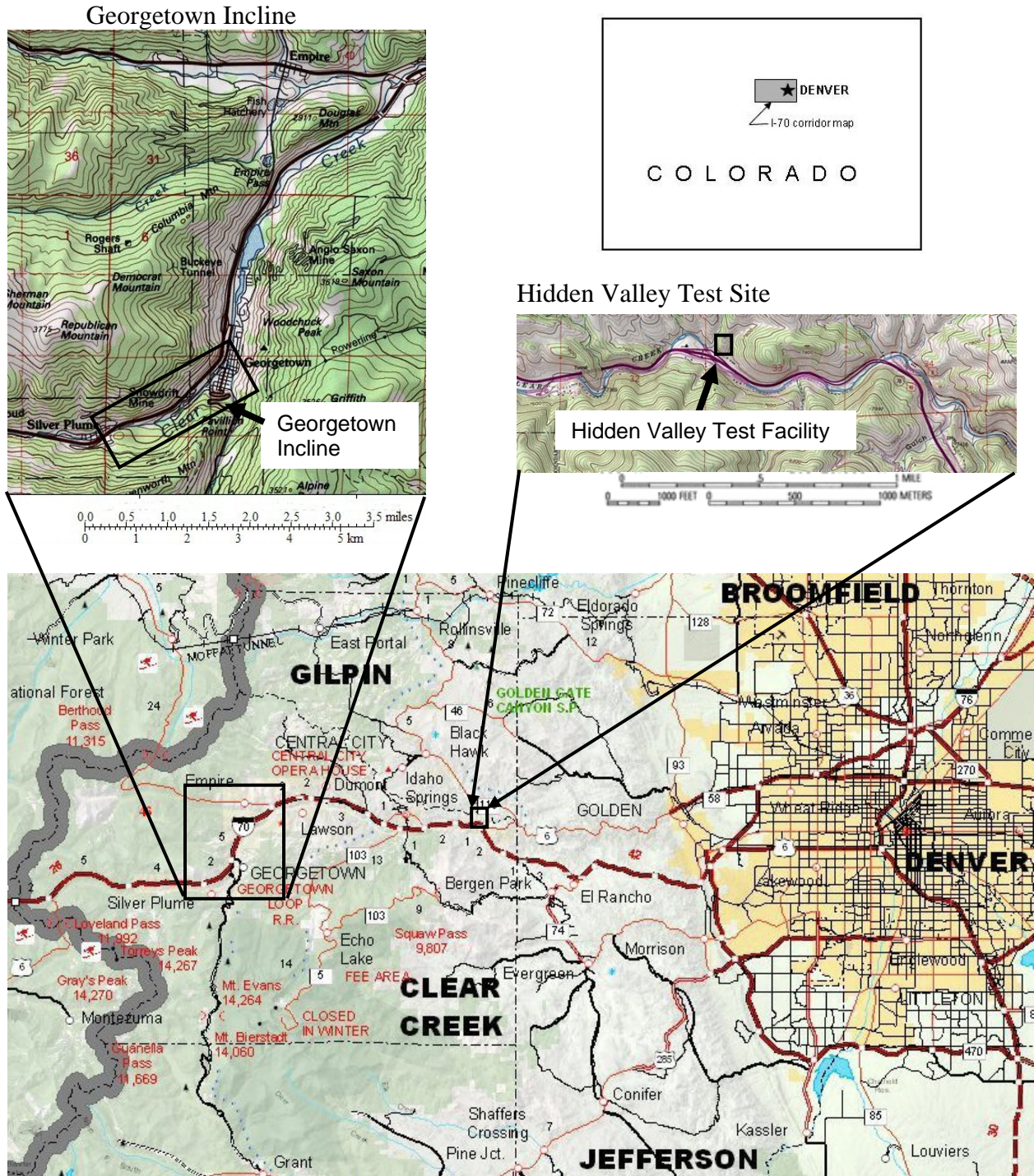
FIGURE 1   Interstate 70 corridor west of Denver, with detailed maps showing locations of Georgetown Incline section, between Georgetown and Silver Plume, and Hidden Valley test site (based on Colorado Travel Map, Colorado Department of Transportation; detailed location maps from U.S. Geological Survey topographic map sheets).

FIGURE 2 Composite photograph of Georgetown Incline.

1.1 Rockfall Protection Actions Along Interstate 70 at Georgetown, Colorado

Interstate 70 forms the principal transportation link between Denver and the ski resorts and recreation areas in the Rocky Mountains west of Denver, as well as being part of a major East-West transportation corridor for the nation (Figure 1). Traffic volumes are considerable; the average annual daily traffic volume through this section of Interstate 70 is approximately 30,000 vehicles, but national holidays and many weekends experience traffic volumes that are much higher than this average.

 The section of Interstate 70 between the towns of Georgetown and Silver Plume (see detailed map in Figure 1) is locally referred to as the "Georgetown Incline" because this 3.54-km (2.2-mile) section of roadway climbs approximately 150 m (500 ft) with a continuous steep grade ranging from five to eight percent, which is steeper than typical Interstate design standards. The highway alignment is cut into steep mountainous slopes that exceed 1H:1V in many places. Numerous exposed bedrock outcrops are located above the highway. There was little opportunity to create rockfall catchment ditches of adequate width during construction. The natural slopes rise over 600 m (2,000 ft) above the current highway alignment along most of this section. Rock cuts and disturbed areas just above the highway, created to accommodate the multilane roadway, generally range from 6 to 45 m (20 to150 ft) high, and have slope angles ranging from vertical to 60º (Figure 2).

 The bedrock geology consists of Idaho Springs Formation that includes pegmatite intrusions, and Silver Plume Granite. The surficial materials covering the steep slopes above the roadway consist of colluvium, talus, and isolated mine tailings; these deposits include materials ranging from silt to boulders. Numerous bedrock outcrops form vertical cliff faces, creating potential source areas for rockfall. In addition, the local elevations range between approximately 2,500 m and 3,500 m (8,400 ft and 11,700 ft) and thus experience climate conditions that are conducive to rockfall, including periods of intense precipitation and extended freeze-thaw events. The combination of climate, steep slopes, fractured bedrock outcrops, and relatively loose surficial materials that include many large fragments, creates an extensive rockfall hazard

area. Multiple rockfall source areas are located as much as 600 m (2,000 ft) above the roadway. Well-defined rockfall chutes channel the rockfall down to the roadway (Figure 3). Many rockfall events at the Georgetown Incline involve rock blocks that are less than 1.5 m (5 ft) in diameter.

Rockfall events have led to accidents and fatalities along the Georgetown Incline. Approximately 100 rockfall-related accidents have occurred in the past 24 years, and these have resulted in 17 injuries. Between 1999 and 2003 there were three rockfall related fatalities. Rock-filled ditches along the westbound lanes and numerous rock blocks located on the embankments along the eastbound lanes, provide physical evidence that there is a much greater incidence of rockfall activity than is indicated by the reported accidents (Yeh and Associates, Inc., 2005). Rockfall debris that impacts the eastbound lanes, or the adjacent bike path, must have experienced high energies and extreme bounce heights. Examination of Figure 3 reveals a scenic overlook parking area, accessible from the eastbound lanes, that is directly opposite several of the active rockfall chutes.
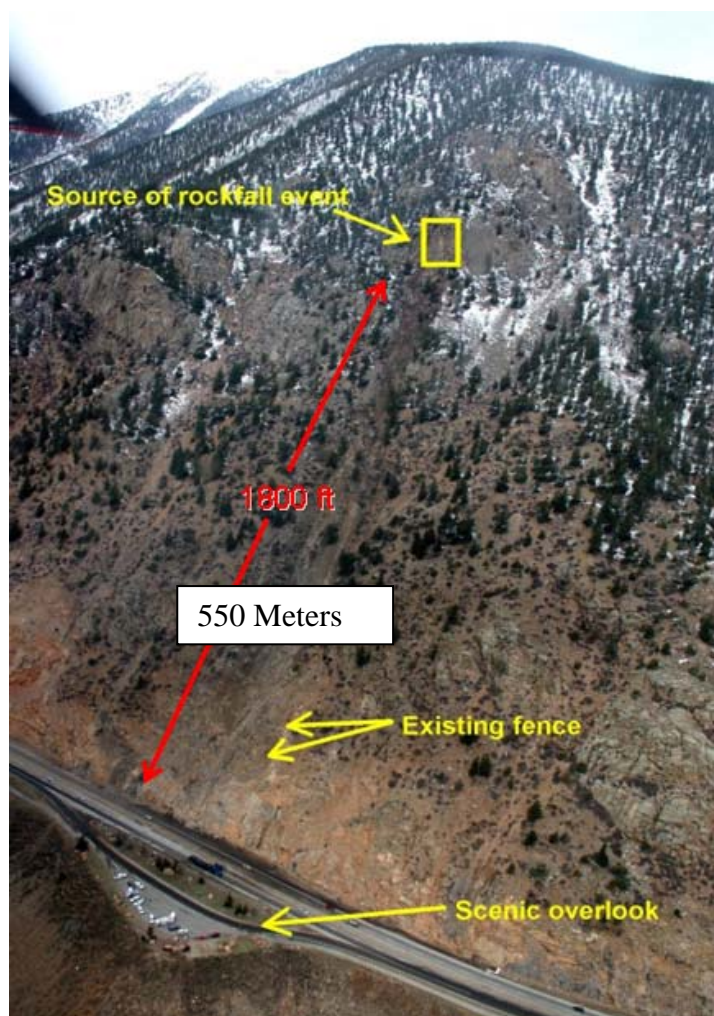
FIGURE 3 Aerial view of Georgetown Incline section of Interstate 70 showing extensive slope distance between source area and roadway for rockfall event of April 2004.

**TABLE 1 Sequence of Events Affecting Rockfall Attenuator Development by
Colorado Department of Transportation, 1999–2009**

Event Number	Date	Description
1	May 1999	Rockfall event on Georgetown Incline resulting in one fatality
2	December 1999	Rockfall event on Georgetown Incline resulting in one fatality
3	2000	First rockfall fences constructed approximately 50–100 m (150–300 ft) above the roadway on Georgetown Incline. These fences thus were installed fairly near the base of the 600 m (2,000 ft) slope.
4	May 2001	Rockfall event on Georgetown Incline causes two accidents as vehicles hit debris. Several rocks cross all Interstate lanes and land on bike path beyond/below roadway.
4a	September 2003	Rockfall event on Georgetown Incline resulting in one fatality
5	April 2004	Severe rockfall event on Georgetown Incline destroys fences and causes accidents that result in temporary closure of Interstate 70.
6	June 2004	First field rock-rolling experiments conducted at Georgetown Incline site. These require temporary traffic-stops on the Interstate during the experiments.
7	September–November 2004	Construction of prototype attenuators at Georgetown Incline
8	March 2005	Second field rock-rolling experiments conducted at Georgetown Incline site. Rocks bounce over installed prototype attenuator that was 4.5 m (15 ft) tall.
9	August–November 2007	Construction of Hidden Valley attenuator test facility.
10	December 2007–April 2008	Full-scale field tests of attenuator systems conducted at Hidden Valley test facility.
11	February 2009	Additional field rock-rolling experiments conducted at Georgetown Incline site. Prototype attenuator damaged and support post impacted by block.
12	March–April 2009	Series of three new attenuator systems installed at Georgetown Incline site above the prototype attenuator, which is also repaired.
13	May 2009	Field rock-rolling experiments conducted at Georgetown Incline site that verify the effectiveness of the newly designed and installed attenuator systems.

Over several decades, a series of rockfall mitigation installations, ranging from draped wire mesh to rockfall fences, have been designed and constructed to protect Interstate 70 at the Georgetown Incline site. Despite these mitigation efforts, multiple rockfalls have reached the traveled lanes from sources and slope areas that have been provided with rockfall mitigation. Table 1 provides a summary of the sequence of significant rockfall events and mitigation responses undertaken at the Georgetown Incline site over the past decade. Table 1 also shows how the full-scale attenuator testing, that is the subject of this circular, is related to the continuing efforts to provide adequate rockfall protection at the site.

1.2 Sequence of Events Affecting Rockfall Attenuator Development by the Colorado Department of Transportation, 1999–2009

In 2007 the Colorado Department of Transportation decided to construct a specialized field test facility where full-scale tests of potential rockfall attenuator systems could be conducted. This decision resulted from the experiences with rockfall mitigation installations at several locations in Colorado, but especially at the Georgetown Incline section of Interstate 70 since 1999, as defined in Table 1. The following paragraphs provide some additional information on several of these events.

1.2.1 Rockfall at Georgetown Incline Between 1999 and 2005

Between 1999 and 2004 five large rockfall events occurred on the Georgetown Incline (Events 1, 2, 4 and 5 in Table 1). In addition, a smaller rockfall event (Event 4a in Table 1) occurred in September 2003, which caused an additional fatality, and made it clear that even small rockfall events can have tragic consequences.

On May 16, 1999, a woman was killed after boulders, reported to be the "size of bathtubs," struck her Toyota. On December 9, 1999, a man was killed when a rock came through the window of the shuttle van in which he was riding. These two events resulted in the construction of the first rockfall protection fences to be installed at the Georgetown location. They were constructed across several prominent rockfall chutes at some considerable distance, approximately 50 to 100 m (150 to 300 ft) above the highway lanes.

A rockfall event that occurred May 6, 2001, caused two accidents when cars encountered rock debris in the road. This 2001 event occurred after 4 days of mixed rain and snow precipitation. Rockfall debris from this event was found in widely dispersed locations: in the ditch of the westbound lane, adjacent to the slope; on the shoulder of the eastbound lane, indicating the rocks had to have crossed the entire multilane roadway. Other rocks were observed on a bike path located below the highway embankment, indicating that some rocks traveled even further from the base of the slope. This observation demonstrated that at least some of the rockfall debris must experience high energies and extreme bounce heights.

In April 2004, a much larger rockfall event occurred that originated high above the Interstate (Figure 3). It destroyed the existing rockfall barrier fences (Figure 4) and spread rockfall debris across the Interstate. The 200 kJ (74 ft-tons) barrier fences, although constructed approximately 50 to 100 m (150 to 300 ft) above the highway, were located comparatively near the base of the rockfall chute and were unable to withstand the energies associated with the rockfall impacts. Numerous vehicles collided with the debris; a tractor trailer jackknifed and nearly crossed the median barrier (Figure 5). Fortunately no fatalities or serious injuries resulted from these multiple accidents. The rockfall event occurred around 1 a.m., and the Interstate was closed to traffic until about 8 a.m. while the rockfall debris was removed and the potential for further rockfall assessed.

A feasibility study was conducted by the Colorado Department of Transportation and Yeh and Associates, Inc. (Yeh and Associates, Inc., 2005) to evaluate possible rockfall mitigation systems for use at the Georgetown Incline location based on the following factors:

FIGURE 4 Damaged fence following April 2004 rockfall event.

**FIGURE 5 An eastbound tractor trailer encountered a rockfall event and
jackknifed into westbound lanes through median barrier, April 2004.**

maintenance, effectiveness, constructability, environmental constraints, and cost. The methods evaluated consisted of avoidance, stabilization, and protection methods such as tunneling around the area, stabilizing the source areas, and rockfall barriers. Installation of rockfall fence systems combined with attenuators placed higher on the slope was judged to be the best mitigation alternative.

An initial rock-rolling exercise was conducted in June 2004 (Event 6 in Table 1) for the purposes of validating the rock-rolling models used by the Colorado Rockfall Simulation Program (CRSP Version 4.0) which had already been used in the evaluation. Specifically,

validation of bounce heights was the primary concern, since CRSP modeling indicated 9 to 12 m (30 to 40 ft) bounce heights were achievable. Therefore, the rocks rolled during the exercise were launched from locations within 30 to 60 m (100 to 200 ft) of the initiation point of the April 2004 event, approximately 550 meters (1,800 feet) above Interstate 70 (Figure 3). The actual source was difficult to access and rocks that could be launched by hand had to be selected from among the rocks already lying on the slope. The rocks ranged in diameter from 1.2 to 2.1 m (4 to 7 ft). As the tests were qualitative in nature, the impact energies were not calculated. Visual examination of the video-recordings of the experiments allowed estimation of the bounce heights achieved by the blocks. Bounce heights in excess of 12 m (40 ft) were estimated based on observing the trajectories relative to nearby trees. Additionally, it was observed that rocks greater than 1 m (3 ft) in diameter generally broke in to smaller rocks as they traveled down the slope.

These rock-rolling experiments were conducted with a portable fence protection system of 80 kJ (30 ft-ton) design capacity located on the shoulder of the road, while remnants of the previously destroyed fences had not been removed from the slope. The rocks traveled down the slopes and onto, even across, the Interstate lanes and consequently the experiments had to be conducted during periods when all traffic on the Interstate, in both directions, was temporarily stopped.

Following these experiments, during the fall of 2004, a prototype attenuator system was installed at the Georgetown location (Event 7 in Table 1 and Figure 6). As no design methodology for attenuator systems existed at the time, the system was designed based solely upon performance of previous successful installations and engineering judgment.

The prototype attenuator system consisted of post-supported netting with a length of net draped on the ground. The system was supported on posts 4.5 m (15 ft.) tall that consisted of W8x48 steel columns mounted on a pinned base. The posts were battered downslope at about 15 degrees. The nets consisted of an 8 mm (0.31 in.) diagonally woven cable net with 150 x 150 mm (6 x 6 in.) openings. Tail lengths were about 4.5 m (15 ft). The intermediate posts utilized single, uphill, tieback anchors from the top of the post. The end posts utilized one uphill tieback and one lateral tieback anchors. When this installation was being designed and installed, it was believed that rolling rocks had cut the net support ropes on the fence that had been destroyed. Therefore, the support ropes for these attenuators were constructed with dual 25 mm (1 in.) diameter wire ropes. Double-twist wire mesh was attached with hog rings to the uphill side of the cable net panels.

The attenuators were not intended to stop rock blocks, but to reduce the kinetic energy associated with rockfall debris and allow the rock blocks to continue down the slope for collection at the base of the slope. Therefore, a 500 kJ (185 ft-ton) fence was built on the shoulder of Interstate 70 as part of the complete system. It was anticipated that the attenuators would not accumulate rockfall debris and thus would not require maintenance operations to clean them out. Although there were no specific design guidelines to aid in the placement of the attenuators, it was believed that if they could be placed in a sequence, then the kinetic energies of the rockfall debris would be controlled and the rockfall material could be collected within the limited area available at the base of the slope (Figure 7). If this could be achieved, then the overall installation and maintenance costs would be as low as possible, while the level of rockfall protection would be improved.

**FIGURE 6 View of prototype attenuator system installed
above Georgetown Incline.**
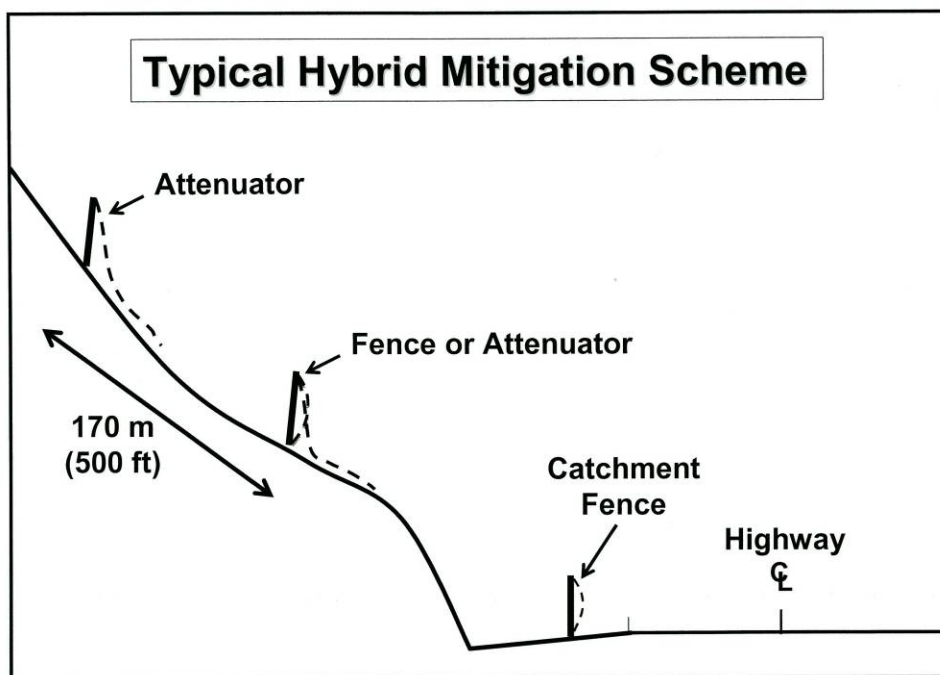
FIGURE 7 Conceptual diagram showing installation of attenuator sequence.

Following the installation of the prototype attenuator system, a second series of rock-rolling experiments was conducted at Georgetown in March 2005 (Event 8 in Table 1). As in the previous case, to ensure the safety of the traveling public, traffic on Interstate 70 was stopped for relatively short periods while these rock-rolling experiments were conducted. The rocks ranged in diameter from 0.7 to 1 m (2 to 3 ft) and were rolled from locations approximately 70 to 100 m (200 to 300 ft) upslope of the attenuator. Slope angles ranged between 35 and 40 degrees. This testing was also qualitative in nature, and no velocity or energy measurements were made. Energies were estimated from measurements made on individual frames of video recordings. Grid lines were painted on the slope at 10 m (30 ft) intervals to provide a reference for some measurements. However, x and y coordinates of a block were measured on individual sequential image-frames, and these allowed computation of velocities. The rock block densities and sizes were used to determine their masses. Energies could then be calculated from the mass and velocity values. From these procedures, these experiments produced impact energies that were no greater than 200 kJ (75 ft-tons). These tests failed to fully establish the functionality of the attenuator system. The experiments involved seven test-rolls. In two of these tests, the rock blocks bounced over the 5 m (15 ft) high attenuator. Once again the possibility of large bounce heights was demonstrated. The remaining five tests did not generate sufficient impact energies, and so the reactions of the attenuator system were not definitive.

However, after a period of use, periodic inspections of this prototype attenuator system revealed that the system had experienced multiple rockfall impacts. Damage consisted of ripped netting, post damage, and general stretching and/or ripping of the panels (Figure 8). The prototype attenuator appeared to function as intended, but the lack of guidelines to design this type of attenuator system hindered the more widespread adoption of attenuators. Based on the performance and testing of the prototype barrier and the large observed bounce heights, a more rigorous testing program was required, and this program is the subject of this Circular.

1.2.2   Hidden Valley Attenuator Test Facility

After some consideration, and based on the apparent success of the prototype attenuator, the Colorado Department of Transportation decided to initiate a full-scale testing program to provide a framework for evaluating attenuator systems. The initial objectives of the testing program included:

- Determine the reaction of various types of panel materials to rock impacts,
- Assess the effects of rock rotation on the attenuator components,
- Assess exit velocities of rock blocks associated with various "tail" lengths,
- Assess the kinetic translational and rotational energies of the experimental test blocks and determine if these values are consistent with results obtained by CRSP modeling, and
- Evaluate and test various post-to-foundation connections.

These testing objectives dictated the characteristics of an appropriate test site. The site should be accessible to construction equipment, provide a controlled environment to ensure safety to both workers and the public, and have the capability for test rocks to develop adequate levels of both rotational and translational energies. After some searching, the Colorado Department of Transportation selected a site located along Interstate 70 between Georgetown and Denver, at the Hidden Valley Interchange (Figure 1). Section 2 of this Circular describes the test facility

constructed at this site and the tests that were conducted there in late 2007 and early 2008 (Events 9 and 10 in Table 1).

1.2.3   Further Activities at Georgetown Incline Location, 2009

Following completion of the attenuator testing at the Hidden Valley facility in 2008, there was renewed activity related to rockfall hazard mitigation at the Georgetown Incline location. Three distinct efforts were undertaken (Events 11, 12 and 13 in Table 1). The efforts included:

- Rock-rolling field experiments conducted in February 2009,
- Installation of a new multiple attenuator system in March and April, 2009, and
- Additional rock-rolling field experiments undertaken in May, 2009 to evaluate this new attenuator system.

Details of these efforts are provided in Section 7 of this Circular.

2   HIDDEN VALLEY ATTENUATOR TEST FACILITY

Experience with the multiple rockfall events at the Georgetown Incline between 1999 and 2005, and the apparent success of the prototype attenuator installed to mitigate the rockfall hazard, prompted the Colorado Department of Transportation to initiate a full-scale testing program to provide a framework for evaluation of updated attenuator systems. As noted in Section 1.2.2, and further discussed in Section 3, it was determined that the testing program should address five objectives, and these objectives dictated the characteristics of an appropriate test site.

FIGURE 8 Damage to prototype attenuator at Georgetown (damage caused by either stretching or cutting of 8-mm wire rope cable net).

The Colorado Department of Transportation conducted a search for a suitable site, and ultimately selected a site located along Interstate 70 between Georgetown and Denver, at the Hidden Valley Interchange (Figure 1). This location is about 25 km (16 miles) east of the Georgetown Incline.

The selected site is located on private land. The Colorado Department of Transportation, working with a rockfall contractor, negotiated an agreement with the landowner that allowed it to construct the desired test facility, perform the test series, and then reclaim the site and return it to the owner. Consequently the test facility no longer exists, and any additional full-scale tests of attenuator systems will have to be conducted at another location.

2.1 Technical Considerations Governing Selection of Test Site

Three practical operational considerations defined the basic characteristics of a suitable site:

1. The site should be accessible to construction equipment,
2. The site should provide a controlled environment to ensure safety to both workers and the public, and
3. The site should have the capability for test rocks to develop adequate levels of both rotational and translational energies.

Full-scale field tests related to rockfall catchment barrier design have been conducted for several decades in both the U.S. and Europe. The knowledge gained from these years of testing provided the basis for the tremendous advancements in the capacities of various rockfall barrier systems, including draperies, fences, walls, and ditches, to mitigate rockfall and has led to the recent official endorsement of appropriate testing methods for rockfall fence certification by European authorities.

The Colorado Department of Transportation personnel, and the personnel at Yeh and Associates, Inc., undertook the selection of the site for the full-scale attenuator testing program with a full awareness of these experiences. However, the experience gained between 1999 and 2005 at the Georgetown Incline clearly showed that the response of attenuator systems to rockfall impacts is complex, and attenuator evaluation can be best obtained from specific testing procedures.

2.1.1 Prior Full-Scale Testing Programs

Most of the prior testing had been designed to evaluate fences and fence systems. Early full-scale tests conducted in 1989 and 1990 by the California Department of Transportation evaluated rockfall fence systems designed to absorb relatively low impact energies of up to 190 kJ (70 ft-tons) (Duffy, 1990; Duffy and Smith, 1990). Natural rocks weighing from 136 to 5,897 kg (300 to 13,000 lbs) were rolled down a 34-degree natural slope that was 40 m (130 ft) high and 76 m (250 ft) long. Over 80 tests were conducted and recorded on video using high-speed cameras. These field tests led to improved fence designs and reduced maintenance, but it was obvious that the rolling rocks often traveled along erratic paths, and individual test results had a high degree of variability. Quantitative design parameters were not readily obtained from such tests. Nevertheless additional series of tests were undertaken during the following decade in several locations in California, Colorado, and other states to test the increasingly varied materials being

developed for fence designs (Andrew, 1992; Duffy, 1992; 1996; Kane and Duffy, 1993; Duffy and Hoon, 1998). At the same time additional field tests were undertaken to assess early rockfall attenuator designs and to calibrate the Colorado RockFall Simulation Program (Barrett *et al.*, 1989; Pfeiffer, 1989; Pfeiffer and Higgins, 1990; Andrew, 1992).

Rockfall field tests have also been conducted in several European countries, principally Switzerland, Italy, and Japan. There has been a considerable exchange of information and experiences among the various individuals and groups conducting these tests. Peila *et al.* (1998) reported on field tests conducted by Italian researchers. The tests were performed using a cable aligned from top to bottom of the slope, perpendicular to, and extending over the fence being tested. The test rock was loaded onto a trolley attached to the cable. As the trolley slid down the cable, the rock was detached and allowed to fall and impact the fence directly without bouncing on the ground. This direct impact permitted a relatively accurate calculation of the impact energy. Video cameras were used to monitor and record each test. The stresses or forces on the cables and posts were measured by dynamometers on the cables.

Baumann (2002) summarized full-scale rockfall barrier testing in Switzerland. Over 350 field tests have been conducted in the country since 1988, and testing methods and barrier designs have evolved considerably. Initially the Swiss followed the Italian testing examples, and attempted to drop rocks from inclined cableways, but allowed the rocks to hit the ground and roll into the fence. Later the system was modified to launch the rocks directly into the fence system. This resulted in greater repeatability among individual tests in a series, but the test rocks no longer had any rotational components.

There remained a perceived need for objective, reproducible, standardized tests of rockfall nets to allow product comparisons and provide relevant information on the capacity and maintenance characteristics (Gerber and Haller, 1997). The Swiss Agency for Environment, Forests and Landscape (SAEFL) undertook development of a certification procedure for rockfall barrier nets (Gerber, 2001; Gerber *et al.*, 2001). A permanent testing facility was constructed in an old quarry near Walenstadt, Switzerland. A vertical drop-testing method was designed to overcome deficiencies in the earlier methods. Concrete "rocks" of a specified dimension and density are dropped from a crane into rockfall barrier nets installed to project out from a vertical rock face. This configuration allows excellent control of impact velocity, energy, location of impact, and easy adjustments of those parameters. The angle of impact is constant and the ground does not contribute to energy dissipation. The tests are recorded on high-speed videotape and several measurements of loading and deformations are made. A very similar testing procedure has been developed and used by the Japanese Railway Technical Research Institute to verify rockfall fence designs (Muraishi and Sano, 1999).

The lack of consistent testing guidelines and procedures within the United States led the American Association of State Highway and Transportation Officials (AASHTO) to request a study be conducted as part of National Cooperative Highway Research Program (NCHRP) Project 20-07 (Higgins, 2003). The study was guided by a task group composed of rockfall mitigation experts from several state transportation agencies. It produced a recommended U.S. standard testing procedure for rockfall barriers that is based on the combined American and European experience to that time. In January 2008, the European Organization for Technical Approvals (EOTA) formally endorsed European Technical Approval Guideline (ETAG) 27 entitled "Guideline for European Technical Approval of Falling Rock Protection Kits" (ETAG27, 2008), thus defining the accepted formal process for testing and assessing the fitness

for use of rockfall protection fence systems, and thereby providing the basis for a European certification of these systems.

2.1.2   Conclusions Drawn from Prior Experience

Review of the past experience with conducting full-scale field testing programs suggested that:

1.   Much more consistent results are obtained when tests are conducted using manufactured concrete blocks with a standard shape. The consistency in shape, size, and mass reduces the inherent variability of natural rocks. The manufactured rocks can be designed to have reasonably angular (sharp) corners and edges; however, even when they are rotating rapidly, they may not be capable of causing as much damage to a fence panel material as an angular natural rock block.

2.   Direct "drop-tests," where a test block is dropped from a predetermined height onto a system being tested, provides the most consistent and readily determined energy of impact. Test rocks can be hoisted to the desired height by a crane and then dropped using a suitable release mechanism. The point of impact on the tested fence system can be precisely defined. However, these tests do not provide a means of imparting rotational energies to the test rock and, in general, the angle of impact is not easily modified.

3.   High-speed digital recording systems, some capable of up to 1,000 frames per second, provide a means for very accurate analysis of the test conditions during and after the impact.

These three conclusions greatly influenced the selection of the site for the test facility and also the design of the test facility.

However, experience with the rockfall events at the Georgetown Incline, and elsewhere, also suggested that it is ideal to test attenuator systems with rocks that are rotating and are traveling down the slope at considerable velocity. Thus, a simple drop-test would not be suitable to evaluate system performance.

2.2   Description of Test Site

One of the features that led to the selection of the Hidden Valley site was the presence of a near-vertical rock face that was probably the result of a regional joint or shear zone–in any case it was very smooth, with few asperities and no undulation. This face was located and oriented so that it was possible to drop a test rock from a lattice boom crane in a manner that would cause the rock block to impact on the face and thus impart some horizontal translational energy, as well as some initial rotational energy to the block.

Below this rock face, there was a soil slope approximately 15 m (50 ft) long that was inclined at approximately 35 degrees. At the base of the soil slope, an earthen embankment carried an access road to another section of the property. This embankment would provide a safety measure as it would help contain any errant rocks within the test facility.

It was decided that the test facility should be constructed so that a test rock could be dropped from a crane, free-fall a predetermined height, impact on the inclined rock face, then bounce/roll down an inclined concrete ramp constructed on the upper portion of the lower soil slope and then impact a test attenuator system installed at the base of concrete ramp. Additional space on the lower part of the soil slope would allow placement of the "tail" portions of the

attenuator system. Rocks released by the attenuator system could then be captured in a more or less level collection area extending beyond the base of the soil slope. This collection area was already partly bordered by the existing earthen embankment for the access road, but a higher embankment berm could be readily constructed to provide additional containment.

2.3   Construction of Test Facility

Figure 9 provides an aerial overview of the constructed Hidden Valley test facility. Figure 10 shows the dimensions of the facility.

Development of the test facility included constructing a concrete ramp on the soil slope below the vertical rock face. The concrete ramp was oriented at an approximate 50-degree slope angle on the upper portion of the soil slope (Figure 11).

Foundations for the attenuator posts were located at the base of the concrete ramp (Figures 12 and 13). The post foundations were constructed by drilling four No. 8 threaded bars approximately 1.2 m (4 ft) into silty-sandy, cohesionless overburden to match the spacing of the base plate of the attenuator post. The base plate was 500 mm by 500 mm (20 in. by 20 in.). The bars were grouted into the ground and No. 4 bar stirrups were placed around the No. 8 bars on 150 mm (6 in.) vertical spacing. The No. 8 bars were sleeved so the foundations could be removed for general panel testing and replaced when the posts were tested. The rough dimensions of the individual bases for the posts were 500 mm by 500 mm by 500 mm (20 in. by 20 in. by 20 in.). Figure 10 depicts a scaled drawing of the foundation bases.
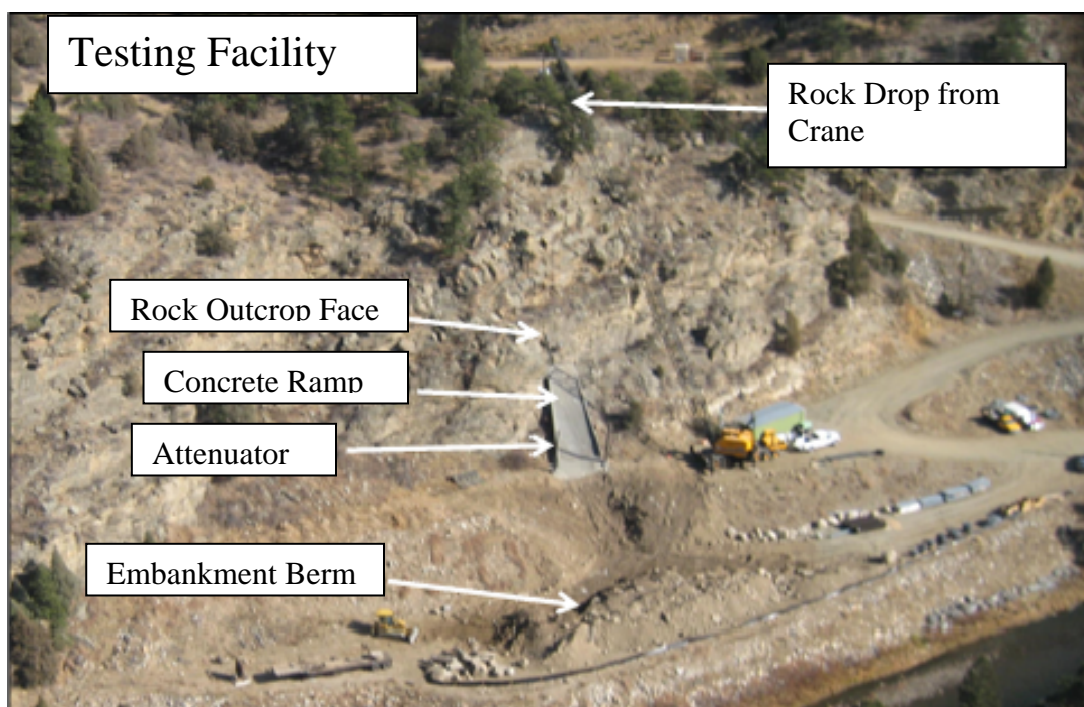
FIGURE 9. **Aerial view of Hidden Valley test facility.**
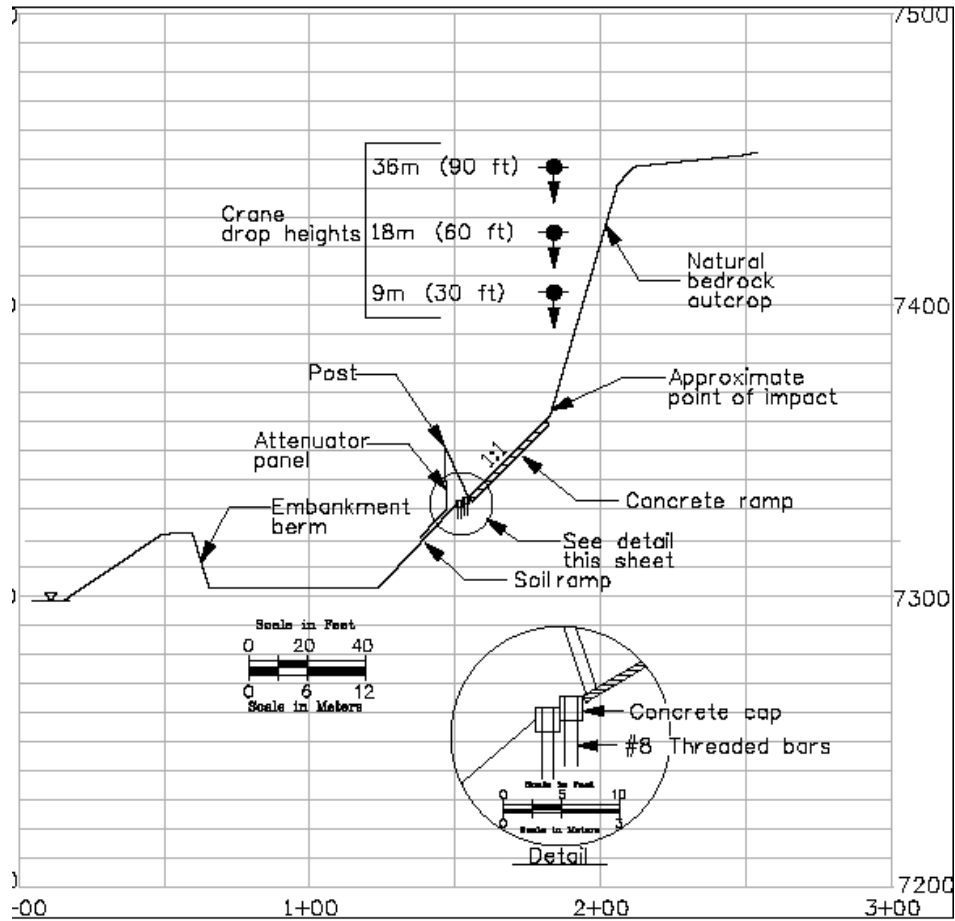
FIGURE 10 Schematic cross section of Hidden Valley test site.

FIGURE 11 Construction of concrete ramp.

FIGURE 12 Post foundation with concrete forms prior to concrete placement.

Figure 12 depicts construction of the concrete forms prior to concrete placement. Figure 13 depicts the final poured foundation. Four foundations were constructed adjacent to each other in the event one was destroyed during testing, then other foundations could be used, however only two of the foundations were used. The foundations were not embedded into the ground more than a few inches and compaction effort was minimal. The subsurface material was granular silty sand. Figure 10 depicts the general configuration of the post foundations.

The soil slope extended approximately an additional 12 m (40 ft) until it flattened. This provided adequate space to drape the tail lengths of the attenuator panels, since it was planned to assess tail lengths between 3 and 10 m (10 to 30 ft) beyond the point where the nets contacted the ground. An embankment berm was constructed to contain the runout of the rocks once they exited the attenuator system.

Because the site for the test facility was privately owned, it was deemed necessary to protect the rock face from potential damage from rock impacts. Rubber conveyor belts were draped over the rock face and onto the uppermost section of the concrete ramp; they smoothed the transition between the near-vertical rock face and the inclined concrete ramp and provided a damping effect that directed the concrete rocks into the attenuator (Figure 14). Tests without the conveyer belt resulted in greater variability in the bounce heights and trajectory paths of the boulders.

500 mm

FIGURE 13 Attenuator post attached to foundation prior to testing.

FIGURE 14 Rubber conveyor belts (trimmed to top of concrete ramp prior to testing) were used to protect rock face from impact damage (arrow depicts top of conveyor).

2.4   Test Rock Description

The test boulders that were designed for the project consisted of cuboctahedrons (Figure 15). Cuboctahedrons are polyhedrons with eight triangular faces and six square faces. They were used to provide a "rounded cube" shape with fairly sharp edges and corners. The intent of the cuboctahedrons is to provide a useful analog to the characteristics of natural rocks, but yet provide a consistent shape. Their shape contains several square or triangular faces, and thus it is relatively easy to construct the necessary concrete forms. Figure 16 shows the concrete forms with reinforcing steel, and Figure 17 shows a completed cuboctahedron "rock." The faces and edges were painted as shown to assist in the analysis of block rotations by examination of high-speed video images. Table 2 provides the mass (weight) of the six sizes of cuboctahedrons used in these tests.

FIGURE 15 Concrete form for cuboctahedrons.

FIGURE 16 Concrete form for cuboctahedrons showing rebar placement.

FIGURE 17 Finished cuboctahedrons.

TABLE 2 Cuboctahedron Rocks

Cuboctahedron Designation	Mass (kg)	Weight (lbf)	Approximate Diameter Meters	Approximate Diameter Feet
A	1,618	3,560	1	3.6
B	1,695	3,730	1	3.6
C	1,577	3,470	1.3	4.2
D	2,259	4,970	1.3	4.2
E	2,173	4,780	1.3	4.2
F	3,823	8,410	1.6	5.3

3   DATA COLLECTION PROCEDURES

As discussed in Section 1.2.2, five objectives of the testing program dictated the characteristics of an appropriate test site. They also strongly influenced the data collection procedures adopted for the testing program. In summary, the data collection procedures responded to the five objectives as follows:

Objective 1: Determine the reaction of various types of panel materials to rock impacts.

Satisfying Objective 1 resulted in the selection of 11 different net panel materials, the design and manufacture of three typical sizes of cuboctahedron concrete rock blocks, and the designation of specified drop heights. The block sizes and drop heights together defined the range of impact energies for the tests. Objective 1 also helped determine the testing sequence that repeatedly tested each net panel configuration. High-speed video recording was needed to capture the reactions of the various panel materials to the rock impacts for subsequent analysis.

Objective 2: Assess the effects of rock rotation on the attenuator components.

Objective 2 was resolved by the design of the inclined concrete ramp at the test facility, and by implementing the procedure of dropping the test rocks so that they first impacted an inclined rock face, then rolled and bounced down the ramp into the attenuators being tested. Assessment of the translational and rotational velocity of the rocks was accomplished by using high-speed video capture and subsequently by applying visual analysis techniques and motion-analysis software to the interpretation of these recordings.

Objective 3: Assess exit velocities of rock blocks associated with various "tail" lengths.

This objective was addressed by designating one camera to record the slope immediately below the attenuator installation. During testing, it became obvious that this objective could not be fully met because dust and debris frequently obscured the images obtained.

Objective 4: Assess the kinetic translational and rotational energies of the experimental test blocks and determine if these values are consistent with results obtained by CRSP modeling and observations of the rock-rolling exercises at Georgetown Incline.

The data collected is sufficient to perform the analyses required to achieve this objective. However, time has not permitted the necessary CRSP simulations to be performed; so, these comparisons have not yet been made.

Objective 5: Evaluate and test various post-to-foundation connections.

Objective 5 was addressed by constructing and testing two types of post-to-base connections. Strain-gauge data were recorded during these tests, but once again time constraints have prevented the complete analysis of this information.

3.1   High-Speed Cameras

Three high-speed cameras were used for documenting the testing. The cameras consisted of AOS Technologies X-3 high-speed cameras (Figure 18). Cameras were set at 250 frames per second.

FIGURE 18 Completed Hidden Valley test facility
(red arrows depict high-speed camera locations C1, C2, and C3).

Figures 19, 20, and 21 depict examples from each camera vantage point and are described as follows:

- Camera 1 was used to determine velocity and subsequent energy as the boulder was moving down the concrete ramp into the attenuator panel. From this vantage point, it was possible to visually compute the translational and rotational energy of the rock prior to impact with the panel using distance traveled over time.
- Camera 2 was used to evaluate the interaction of the rock with the attenuator panel as the rock traveled under the panel and exited or was entrapped by the system. Unfortunately dust and debris often obscured the photographic image, making exit velocity calculations difficult.
- Camera 3 was used to see the rock in elevation view as it traveled underneath the attenuator panel.

FIGURE 19 Example of photograph taken with Camera 1 prior to impact with net, above post support (white strips are marked on 1.5 m [5 ft] centers; white arrow depicts location of rolling boulder).

FIGURE 20 Example of photograph taken with Camera 2 during impact with net, below post support (white arrow depicts location of rolling boulder).

FIGURE 21 Example of photograph taken with Camera 3 during impact with net, below post support (white arrow depicts location of rolling boulder).

3.2   Motion Analysis

After saving the raw video data files to a hard drive, it was necessary to evaluate the motion of the rolling rocks. In cases where the rocks rolled down the concrete ramp without bouncing more than 0.3 m (1 ft) in height, it was possible to estimate average translational and rotational velocities from the images using the calibration marks on the ramp from Camera 1 (Figure 19). If the boulder bounced more than 0.3 m (1 ft) above the calibration mark, making it difficult to estimate the distance traveled between two points using visual means, it was then necessary to use the motion analysis software.

To estimate energies of moving blocks, post-processing software was used, which consisted of the two-dimensional Pro Analyst Software (Xcitex, Inc., 2007). The best results with the software occurred when the boulder rolled normal or perpendicular to the camera lens. Wobbles in the rock and/or rolling at an angle in or out of the camera field of view reduced the estimating accuracy of the software.

3.3   Strain Gauge Recording of Post-to-Base Connections

Strain gauges were not used on the panel nets or support posts. Strain gauges were used on the two posts that were tested at the end of the program. The strain gauges were welded to the posts. In order to obtain real-time readings, it was necessary to use a fiber optic system to convey the

data in a millisecond format. Each post was instrumented with four Fabry-Perot fiber optic strain gauges (model SFO-W) that were spot-welded to the posts at locations not at risk for a direct impact. The fiber optic cables used to record the data stream were placed in a trench and run to an observation station a safe distance from the runway. The fiber optic acquisition was collected at 250 samples per second. The resulting strain data versus time graphs are presented in Section 6 of this Circular. At this time the strain gauge data was used to evaluate the time interval for the rock impact with the post and no other analysis has been performed.

4   DESCRIPTION OF PANEL AND POST SYSTEMS TESTED

The panels and posts tested were purchased by the Colorado Department of Transportation. A total of 11 manufactured panel systems and two post styles were tested.

4.1   Panel Systems Tested

The 11 manufactured panel systems tested included cable nets, ring nets, cable rings, and several varieties of high-strength spiral wire nets, and regular and high-strength chain-link materials. These products exhibit a considerable range in opening sizes, deformation characteristics, strength, and weight. All these characteristics affect how the materials will react to initial impacts and to the subsequent energy dissipation as the rock blocks attempt to pass under the tail portion of the attenuator system. Table 3 summarizes some of the characteristics of each of the tested panel systems. They have been arranged according to their inherent mass per unit area, from heaviest to lightest, because this property appears to be a critical factor in how the tail portions of these attenuator systems perform.

TABLE 3 Summary of Mass–Weight per Unit Area of Panel Materials Tested

Net Type	Approximate Material Strand Diameter (mm)	Clip Type	Approximate Panel Aperture Opening (mm)	Measured Mass per Unit Area (kg/m^2)	Measured Weight per Unit Area (lbf/ft^2)
Cable Net	12	Overlap clamp	205	10.1	2.1
Cable Net	12	Wire wrap	205	10.1	2.1
Cable Net	8	Interlocking	150	6.1	1.3
Cable Net	8	Overlap clamp	150	5.4	1.1
Spiral Wire Net—High Strength	4	NA	130	4.5	0.9
Steel Wire—Chain Link	3.7	NA	50	3.7	0.8
Cable Rings (1 x 6)	8	Ferrule	350	3.6	0.7
Ring Net (1 x 6)	7/2/350	None	350	3.5	0.7
Ring Net (1 x 4)	7/3/300	Clip	300	3.5	0.7
Steel Wire—High Strength	4	NA	64	3.3	0.7
Spiral Wire Net—High Strength	4	NA	230	2.5	0.5

4.1.1   Cable Nets—12-mm Diameter, 205-mm x 205-mm Opening

Two types of 12-mm (1/2 in.) cable nets were tested with 205 mm x 205 mm (8 in. by 8 in.) openings, both were diagonal weave. ASTM 1023/A reports the tensile breaking strength of the individual wire rope to be in excess of 21,000 lbs. The connection clips did differ between the products. One product had an overlap clip and the other system had a wire wrap as shown in Figures 22 and 23.

FIGURE 22 Cable net made with 12-mm diameter wire and overlap clamp style, diagonal weave.

FIGURE 23 Cable net made with 12-mm diameter wire and wire wrap clamp style, diagonal weave.

4.1.2 Cable Nets—8-mm Diameter, 150-mm x 150-mm Opening

Two types of 8 mm (5/16 in) cable nets were tested with 150 mm x 150 mm (6 in. by 6 in.) openings; one was diagonal weave and the other was horizontal weave. Diagonal weaves were originally ordered for all the cable nets; however, one that was delivered was horizontal weave. ASTM 1023/A reports the tensile breaking strength of the wire rope to be 9,200 lbs assuming a 7 x 7 wire rope construction for both types. The connection clips did differ between the products. One product had an overlapping clip and the other system had a two-piece interlocking clip as shown in Figures 24 and 25.

**FIGURE 24 Cable net made with 8-mm diameter wire and overlap
clamp style (diagonal weave 150 mm by 150 mm).**
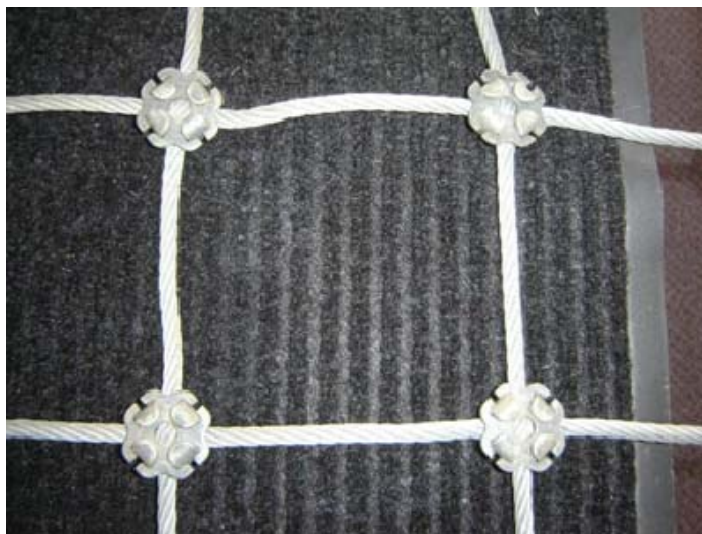
**FIGURE 25 Cable net made with 8-mm diameter wire and interlocking
clip style (horizontal weave 150 mm by 150 mm).**

4.1.3 Spiral Wire Nets

Two types of spiral wire nets were tested. The individual wires of the system are reported to have a tensile strength of 1,770 N/mm^2 (260 ksi) – three wires in a spiral; no data was provided for tensile strength of the net panel. The first spiral wire net tested had an aperture opening of 292 mm by 500 mm (11.5 in. by 19.5 in.). The aperture opening is reported to be 230 mm (9 in.). The second spiral wire net tested was reported to have an aperture opening of 173 mm by 310 mm (7 in. by 12 in.). The aperture opening is reported to be 130 mm (5 in.). Figures 26 and 27 depict the two styles of spiral wire. The first style was hung from the support rope and tested with the long axis in the vertical direction. The second style was hung from the support rope and tested with the long axis in the horizontal direction.

4.1.4 Steel Wire—3.7 mm (Chain Link)

One type of steel wire (chain link fencing) was tested in two different orientations. The individual wires of the system have a reported tensile strength of 520 N/mm^2 (75 ksi) for a 3.7 mm diameter wire (0.148 in.). The aperture opening is approximately 50 mm (2 in.). As defined in customary U.S. units the product was a 9 gauge wire – 2-inch-opening, galvanized chain link mesh. Figures 28 and 29 depict the horizontal and vertical orientation that was tested. The mesh was tested in 2 layers hog-ringed together on an approximate 300 mm by 300 mm spacing (12 in. by 12 in.).

FIGURE 26 Spiral-wire net with aperture opening of 230 mm depicted by red circle. Long axis oriented vertically showing how net was hung from support rope on attenuator system (support rope would be at top of photograph).

**FIGURE 27 Spiral-wire net with aperture opening of 130 mm
depicted by red circle. Long axis oriented horizontally showing how net
was hung from support rope on attenuator system
(support rope would be at top of photograph).**

**FIGURE 28 Close-up of steel wire (chain link), wire continuous in
a horizontal orientation showing how net was hung from support rope
on attenuator system (support rope would be at top of photograph).**

**FIGURE 29 Close-up of steel wire (chain link), wire continuous
in a vertical orientation showing how net was hung from support rope on
attenuator system (support rope would be at top of photograph).**

4.1.5   *Cable Ring Nets 1 x 6*

The cable ring net panels were made of 8 mm (5/16 inch.) wire rope that was a 300 mm diameter (12 in.). The cable ends within each ring were secured with a ferrule-type clamp. ASTM 1023/A reports the breaking strength of the individual wire ropes to be 9,200 lbs, assuming a 7 x 7 wire rope construction (Figure 30). The 1 x 6 designation indicates that each ring is interlinked with six neighboring rings.

FIGURE 30 Example of cable ring nets.

4.1.6   Ring Nets

Two types of ring net panels were tested and are designated as 7/2/350 - 1 x 6 and 7/3/300 – 1 x 4. The designation is as follows: the first number is the number of wire loops that form the ring, the second number is the wire diameter in millimeters, and the third number is the approximate diameter of the ring in millimeters. The 1 x 6 and 1 x 4 designation indicates that one ring is connected to 6 surrounding rings and 4 surrounding rings, respectively (Figures 31 and 32). The 7/3/300 individual strands are reported by the manufacturer to have a tensile breaking strength of 1,700 N/mm2 (246 ksi).

FIGURE 31   Example of 7/2/350—1 x 6 ring nets.

FIGURE 32   Example of 7/3/300—1 x 4 ring nets.

4.1.7   High-Strength Steel Wire—4 mm

One type of high-strength chain link mesh was tested in two different orientations. The individual wires of the system are reported to have an individual strand tensile strength of 1,770 N/mm^2 (260 ksi), and have a diamond shaped opening of 83 mm by 143 mm (3.25 in. by 5.63 in.). Figures 33 and 34 depict the same style of wire in the two differing orientations reflecting how the mesh was hung on the wire support rope for testing.
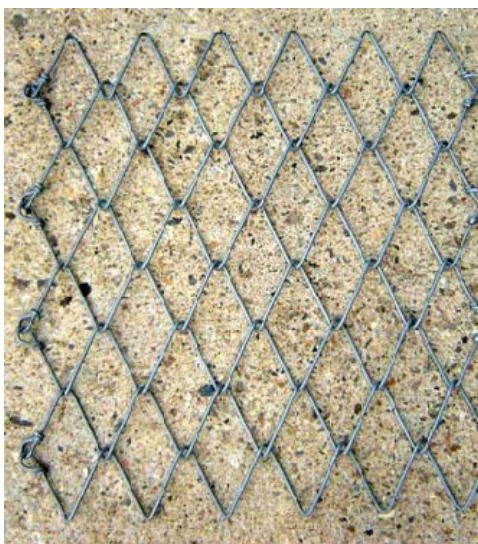
FIGURE 33 High-strength steel wire of 4-mm diameter with long axis oriented vertically showing how the net was hung from support rope on attenuator system (support rope would be at top of photograph).
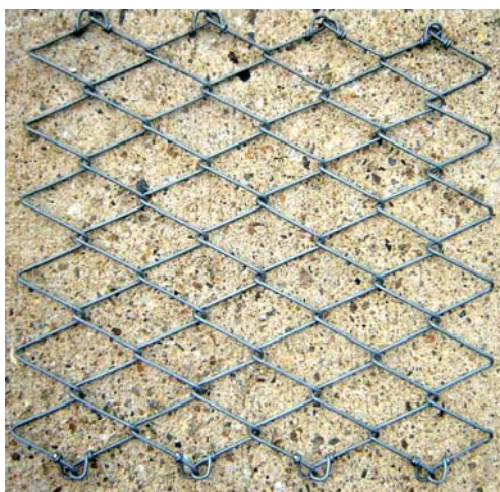
FIGURE 34 High-strength steel wire of 4-mm diameter with long axis oriented horizontally showing how net was hung from support rope on attenuator system (support rope would be at top of photograph).

4.2   Post-to-Base Connection Styles Tested

Two types of post systems were tested. The first was a post with a base plate and pin type connection. The second type of post system had a fixed base. Figure 35 depicts the base of the pinned post and Figure 36 depicts the base of the fixed post.
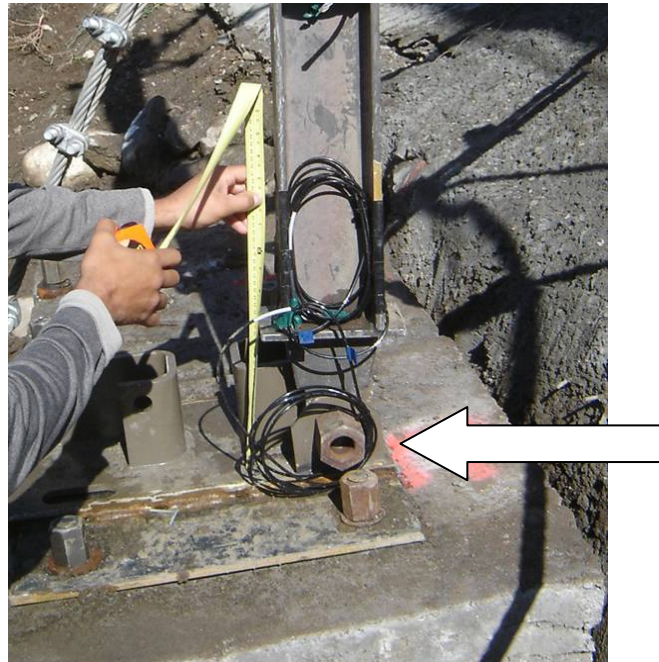
FIGURE 35 Base of pinned post (white arrow indicates pin).

FIGURE 36 Base of fixed post.

4.2.1 Post—Pinned Base

The posts were approximately 2.8 meter (9.2 ft) high and were secured with uphill anchors attached at the top, mid-span, and close to the bottom (Figure 37). Field measurement of the post indicated it would compare in the US System to a W 5 x 16, with a section modulus of approximately 4.6 cm^3/cm (8.5 in^3/ft). The base plate dimensions were 500 mm by 500 mm (20 in by 20 in). Strain gauges were also attached near the bottom and mid-span of the post (Figure 38).

**FIGURE 37 Pinned post attached to post foundation
(arrows point to uphill anchor locations).**
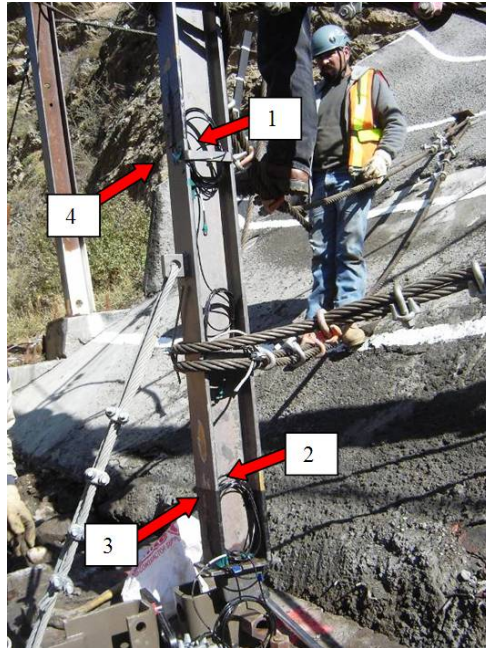
FIGURE 38 Pinned-post base attached to post foundation with strain gauges (numbers correspond to strain gauge designation and attachment location on post).
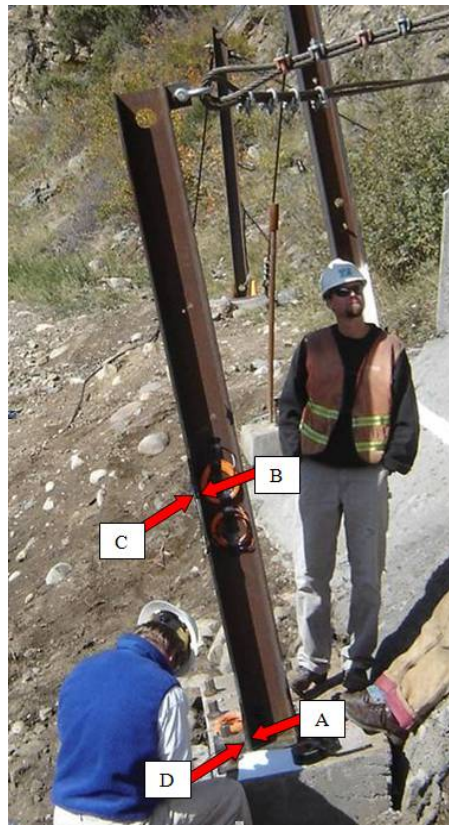
FIGURE 39 Fixed-base post attached to post foundation with strain gauges (letters correspond to strain gauge designation and attachment location on post).

4.2.2   Post—Fixed Base

The post was approximately 2.8 m (9.2 ft) high and was secured with uphill anchors attached at the top only (Figure 39). The post in the U.S. System is a W 8 x 48, with an approximate section modulus of 23.3 cm^3/cm (43.3 in.^{3}/ft). The base plate dimensions were 500 mm by 500 mm (20 in. by 20 in.). Strain gauges were also attached near the bottom and mid-span of the post (Figure 39).

5   TEST PROCEDURES

The tests were conducted by dropping the manufactured cuboctahedron concrete rocks suspended from a crane at various specified heights above the ramp onto the near-vertical rock face. Each test was recorded by three high-speed video cameras.

The initial free-fall from the selected drop-height provided a readily computed initial translational energy to the test rock. Upon impact with the conveyor belts draped over the near-vertical rock face, some of the initial vertically-oriented translational energy was converted to rotational energy, and some horizontal velocity was generated. The test rock thus began to spin and move laterally away from the rock face. The rock then would travel down the concrete ramp in a combination of rolling and bouncing movements. Results were highly variable, but in general, rocks that were released at the top of the ramp, with essentially no initial free-fall, would roll down the ramp. Those dropped from low heights would roll and bounce with very short airborne arcs. Those blocks that were dropped from greater heights traveled down the concrete ramp at the greatest velocities and might only have one or two impacts. At the base of the concrete ramp, the test rock then impacted either the attenuator system or the attenuator post that was the subject of that test. After these impacts, the rocks traveled onto the soil slope and were captured in the collection area.

The crane operator released the test rocks from predetermined locations at the top of the ramp, or from heights of 9 m (30 ft), 18 m (60 ft), or 27 m (90 ft) above the concrete ramp. These release points are defined in the database (in Appendix A) in feet (30, 60 or 90 feet), with those tests where the rock was released at the top of the ramp identified with a height of "0". A mechanical release mechanism (H44 Ram Hook), that is similar to the type used to release lifeboats from large ships, was used to release the rocks. The release mechanism was attached to the rock by a shackle and it was opened by pulling on a rope that was attached to the release mechanism (Figure 40).

The 11 different attenuator net panels were tested first. Each attenuator was subjected to multiple tests. A total of 113 individual tests were conducted, employing different-sized test blocks dropped from one of the specified heights. Appendix A summarizes the information contained in an Excel spreadsheet that contains the recorded observations for each of these tests, plus computed values of the energies exhibited by the blocks at the point of impact that have been developed for a selection of the tests. These energy computations require some fairly intensive analysis of the video records of each test, and these analyses have not been completed for all the tests.

Subsequently, an additional series of 12 tests were conducted to evaluate two types of post-to-base connections. All the tests for both the attenuator panels and the posts were recorded with the high-speed video cameras. These video recordings were retained by the authors and are available to researchers upon request.

**FIGURE 40 Release mechanism attached
to a cuboctahedron test block.**

5.1   Attenuator Geometry

The initial tests of the attenuator net-panels employed a two-post, single-panel-width system with two 6-m (20-ft) posts spaced 6 m (20 ft) apart (Figure 41) This design was initially selected because it corresponded to the 6 m (20 ft) height that was expected to be used for future attenuator projects at the Georgetown Incline. However, observations of impacts encountered in these tests showed panel net reactions that were very different from those observed during the 2005 field tests of the prototype attenuator at the Georgetown Incline. With the attenuator constructed with only a single 6-m (20-ft) panel-width of material, the net panel would wrap around the rocks, thereby trapping them (Figure 42). Field tests at the Georgetown Incline used multiple panels seamed together. These installations never entirely enveloped the impacting rock, but only partially deformed around it. Muhunthan and Radhakrishnan (2007) modeled several attenuator widths using finite-element techniques, and found that attenuator systems consisting of narrow panels tended to wrap around the rocks and trap them. Washington State Department of Transportation has observed the same behavior at one narrow-panel system they installed (Tom Badger, Washington State Department of Transportation, personal communication, 2009).

Faced with this response of the single-panel test attenuator, a second attenuator design was constructed using four posts to support multiple net panels. This design utilized four 6-m (20-ft) posts spaced 6 m (20 ft) apart (Figure 43). This configuration reduced the enveloping effect of the attenuator on the impacting test rocks.
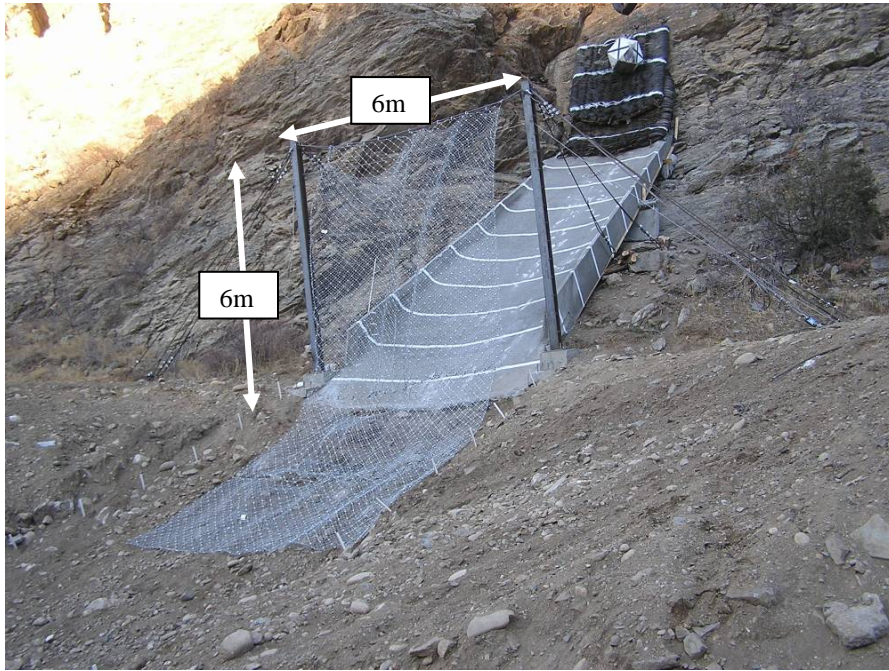
**FIGURE 41 Initial two-post system depicting two vertical posts
6 m high and 6 m apart.**

FIGURE 42 Example of single-panel system wrapping and entangling a rock.
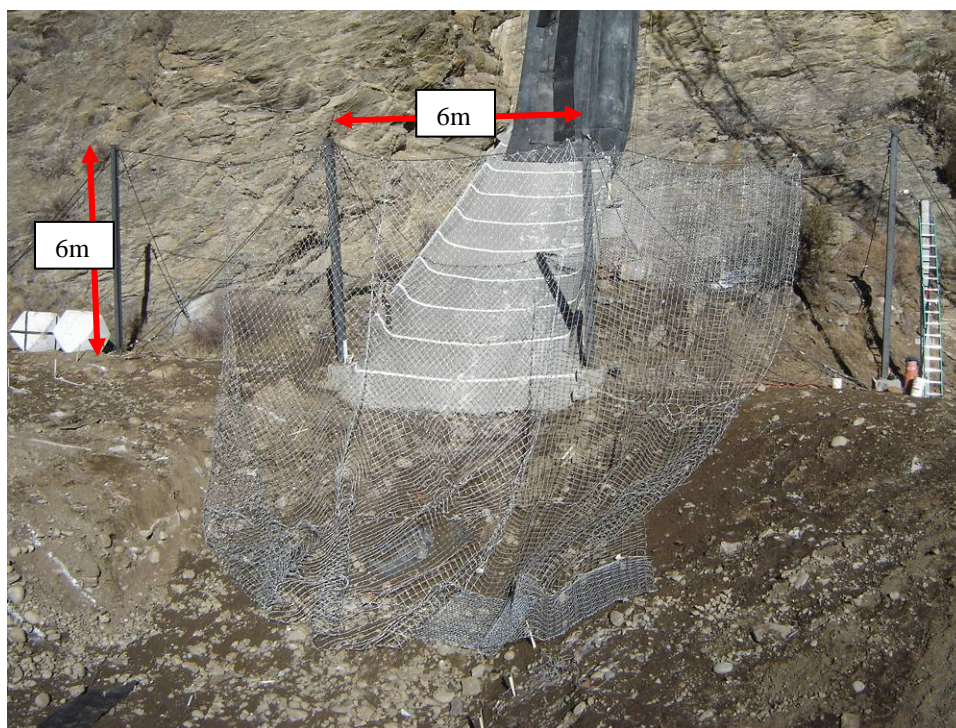
**FIGURE 43 Four-post system depicting four vertical posts
6 m high and 6 m apart.**

However, the decision to use this expanded configuration required the use of considerably more mesh and net panel materials than had been purchased for the test program when only the narrow, single-panel, design was anticipated. There was insufficient material to construct all the desired attenuators that incorporated tail lengths greater than 5 m (15 ft). Faced with material shortages, a third attenuator design was constructed at the test facility using four posts to support the net panels. This design utilized four 3-m (10-ft) posts spaced 6 m (20 ft) apart (Figure 44). The outer two posts were cut from 6 m to 3 m tall and holes were drilled in the inner two posts for the support rope. For these tests, the tails of the two outer panels were sometimes constructed with a different net material, but a net material of similar weight to that being subjected to the test was always used. Because these outer tail components were located outside the impact zone of the attenuator system, the use of substitute materials of similar weight to that being tested was believed to not greatly influence the test results.

5.2   Tail Length and Chain Link Backing

The tail lengths were varied from 5 to 30 feet. For most fabrics, a short tail was first placed on the ground and a preliminary test was conducted. More tail was added if it appeared the rock rolled too freely through the net panels and little reduction in velocity was observed. The tail length was measured where the panel was in contact with the ground (Figure 45).
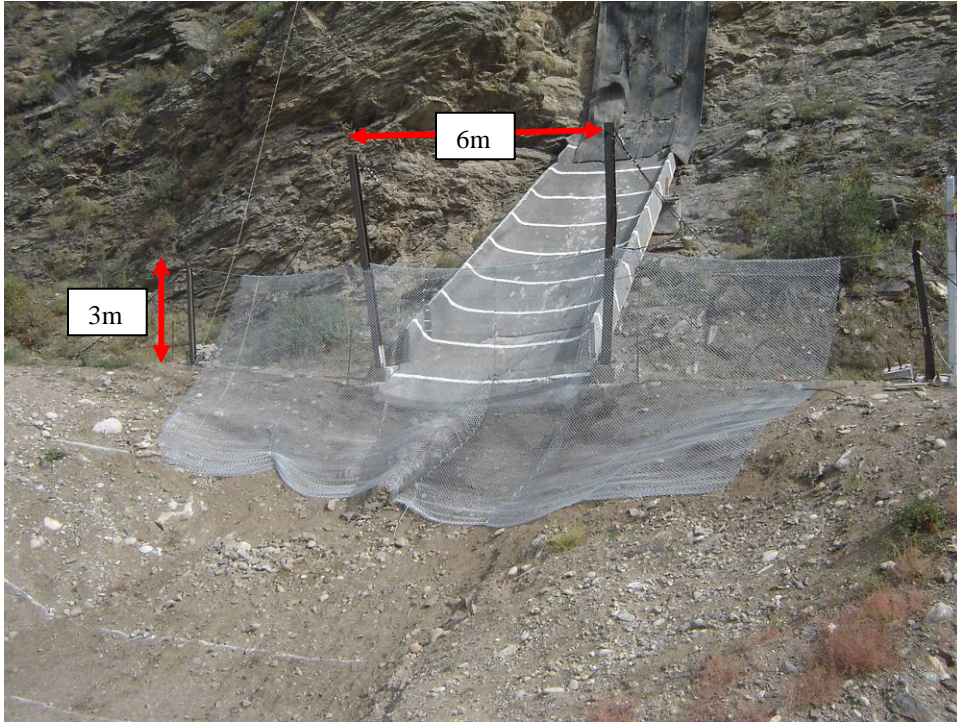
**FIGURE 44 Four-post system depicting four vertical posts with
support wire rope 3 m high and post spacing at 6 m.**

**FIGURE 45 Measurement of tail length for net panel
in contact with ground.**

Some of the panels tested were fastened with 3.7 mm steel wire (chain link) backing mesh on the impact side of the panels. The masses provided in Table 3 do not reflect the additional mass for the 3.7 mm steel wire (chain link). It was observed during the field testing that the 3.7 mm steel wire mesh backing worked well as a sacrificial layer that probably provided some damage protection to a panel, but typically after one or two hits the chain link would be torn off the net panel or damaged to an extent that it failed to offer further protection.

5.3   Attenuator Net Panel Test Sequence

In many cases, for each new net-panel material being tested, the initial tests were conducted with the test rock released at the top of the ramp. The testing sequence then progressed with the use of progressively greater drop heights. Most test sequences were limited to a maximum drop height of 18 m (60 ft) above the concrete ramp. The 27 m (90 ft)-drop height was not routinely used, because the bounce heights after the initial impact with the concrete ramp were often greater than the height of the 3 m (10 ft) posts. They also caused significant damage to the concrete ramp.

High-speed video recordings of each test were collected by three cameras placed so as to obtain distinct views of the rock trajectory before, during and after its impact with the attenuator, and the reactions of the attenuator system to the impact (section 3.1 and Figures 19, 20, and 21). Figures 46 to 52 provide seven sequential images, representing selected frames from one high-speed camera recording, of a typical test, in this case a 12 mm cable net system being impacted by an approximately 1,700 kg (3,700 lb) test rock (Type B in Table 2).

FIGURE 46 Cuboctahedron rock (in upper right corner) prior to impacting panel depicted by white arrow.

FIGURE 47 Rock traveling into panel.

FIGURE 48 Rock engaging panel and beginning to lift tail portion.

FIGURE 49 Translational velocity slowing, panel lifting vertically attenuating energy.

FIGURE 50 Rock momentum greatly reduced as panel and rock vertically rise.

FIGURE 51 Rock released from attenuator with reduced energy.

FIGURE 52 Rock fully released at much reduced velocity (at this point, would begin to reaccelerate until it impacts another attenuator or final catchment or barrier).

After each test in the sequence, the net panels were inspected for deformation and damage. If the nets were judged to be functional, the next drop in the sequence was conducted. Because of the variability in the fabrics used to construct the panels, it was difficult to set specific criteria for evaluating damage to the panels, because each category of net panels behaved quite differently from the others. Determination of the functional acceptability was based on the experience of the individual inspector. If the inspector determined that the net was damaged to a point that it would need to be replaced if it were being used in an actual field

installation, then the testing sequence was stopped. This decision was made by individuals who have experience inspecting Colorado Department of Transportation rockfall mitigation devices. For consistency, net inspection was limited to three inspectors who worked together for the entire testing program.

5.4   Post-to-Base Connection Testing

The final phase of testing evaluated the two types of post-to-base connection. The posts were placed at the base of the concrete ramp. The tests were made by aligning Rock A or B with the post and releasing the rock from the middle of the near-vertical rock face. While the two posts tested were quite different in size and bending capacity, the intent was to see how the smaller pinned base post would handle the impact energy of approximately 200 kJ (74 ft-tons) versus the heavier fixed base post subjected to a similar energy. The smaller pinned base post only withstood one impact of approximately 189 kJ (70 ft-tons) and was no longer functional. The fixed base post was subjected to a total of eight tests that hit the post, while two missed. The fixed base post withstood seven consecutive impacts of approximately 200 kJ (74 ft-tons) each and was still functional. Different uphill tieback orientations were used ranging from one to three, but after most of the testing the post was still functional. The final roll consisted of dropping Rock E (2,173 kg or 4,780 lb) into the system, and this completely destroyed the post with an impact of approximately 900 kJ (333 ft-tons) of energy.

6   RESULTS

A total of 125 tests were conducted at the Hidden Valley test facility to evaluate the alternative attenuator systems constructed with 11 different materials and two types of post-to-base connections (using an additional 12 tests, two of which missed but were still counted as tests). Appendix A provides a tabulation of the observational data collected for all tests.

Time constraints have not permitted a complete quantitative analysis or statistical evaluation of the observational data. One of the objectives in publishing this Circular is to provide access to these observations and to document the testing facilities and methods used to collect the observations. By providing these observational data along with descriptions of the "context" in which they were obtained, it is hoped that others will be able to undertake additional analyses and evaluations. These tests were not able to evaluate all of the many factors that influence the response of these attenuator systems to rockfall events. Additional test sequences will provide more information.

However, a number of analyses have been completed. The results of these analyses are discussed under four main categories:

- Evaluation of selected kinetic energies by analyzing the high-speed video recordings of the tests, using both visual analysis methods and motion-analysis software (Section 6.1)
- Assessment of the attenuator reactions to the initial impacts (Section 6.2)
- Assessment of the reactions of the attenuator tail components (Section 6.3)
- Evaluation of post-to-base connections (Section 6.4)

6.1   Evaluation of Kinetic Energies

Velocities (translational and rotational) have been estimated by visual analysis of the high-speed camera images for 41 of the 125 tests. The ProAnalyst motion-analysis software was used to estimate translational and rotational velocities for a selected 32 tests. Since the masses of the test rocks were accurately known, the velocity estimates were readily converted into estimates of kinetic energies. Both approaches were applied to 21 tests, and it is possible to compare the estimates of translational and rotational energies obtained by the two approaches.

Appendix B includes the energy estimates obtained by the visual method for the 41 tests evaluated so far. Appendix C provides the 32 resulting energy estimates obtained by using the ProAnalyst motion-analysis software. Appendix D compares the resulting energy estimates obtained by the two approaches for the 21 tests evaluated by both methods. Summaries of the detailed information contained in Appendices B, C and D are presented in Sections 6.1.1 to 6.1.3.

The process of analyzing the high-speed video images, by either the visual analysis method or by using the ProAnalyst motion-analysis software, is time consuming. Only selected tests have been evaluated by either method to date. A more complete analysis using all the tests may assist in the further evaluation of these test results.

6.1.1   Energy Estimates Obtained by Visual Analysis

For the 41 tests evaluated to date, translational kinetic energies impacting the attenuator or posts generally ranged from 75 to 460 kJ (28 to 170 ft-tons), with only two tests exceeding this range. However, one test produced a translational kinetic energy of 967.5 kJ (358 ft-tons). The mean and median values of translational kinetic energy are 322 kJ (119 ft-tons) and 309 kJ (114 ft-tons), respectively. Figure B-1 presents a summary of these results as a histogram. Appendix B provides additional details.

Rotational kinetic energies mostly ranged from nearly zero to about 64 kJ (24 ft-tons), with one test producing a maximum rotational kinetic energy of 103 kJ (38 ft-tons). The ratio of the rotational kinetic energy compared to the total kinetic energy averaged about 11%, and ranged from less than 1% to about 32%. Figures B-2 and B-3 illustrate with histograms the distribution of rotational and total kinetic energies (the total kinetic energy being the summation of the translational and kinetic energies).

The relationship between the achieved rotational kinetic energy and the total kinetic energy, as illustrated by these 41 tests, was evaluated using linear regression analysis (Figures B-4 and B-5). Figure B-4 illustrates the relationship between the percentage of rotational kinetic energy to the total kinetic energy (on the Y axis) and the total kinetic energy (on the X axis). A linear regression fitted to this relationship is significant at the 95% confidence level. There is a large scatter to the data, and the regression only "explains" 18.3% of the variability in the data, but it shows a downward trend, i.e., the ratio of the rotational energy to the total energy declines as the total energy increases.

In contrast, the relationship between rotational energy and total energy (Figure B-5) is not significant at the 95% confidence level. The trend line is essentially horizontal and "explains" only 2.1% of the data variability.

These results show that the amount of rotational energy achieved during individual tests is relatively constant, and does not increase as the total energy increases. The ratio (or

percentage) of rotational energy to total energy declines as the total energy increases (Figure B-4). The design of the test facility was intended to produce rotating rocks, and it appears to have done so, at least to a certain degree. However, the overall limited size of the test facility apparently did not permit the test rocks to achieve increased rates of rotation (or spin) as their overall velocity down the slope increased.

6.1.2   Energy Estimates Obtained Using ProAnalyst Software

Appendix C provides additional details. For the 32 tests evaluated, translational kinetic energies impacting the attenuator or posts mostly ranged from approximately 110 to 480 kJ (41 to 178 ft-tons), with only two tests exceeding this range. However one test produced a translational kinetic energy of 920.5 kJ (341 ft-tons). The mean and median values of translational kinetic energy were 322 kJ (119 ft-tons) and 285 kJ (105 ft-tons), respectively. Figure C-1 presents a summary of these results as a histogram.

Rotational kinetic energies ranged between 15 and 75 kJ (6 to 28 ft-tons). The ratio of the rotational kinetic energy compared to the total kinetic energy averaged about 12%, and ranged from 0% to about 31%. Figures C-2 and C-3 illustrate with histograms the distribution of rotational and total kinetic energies (the total kinetic energy being the summation of the translational and rotational kinetic energies).

The relationship between the achieved rotational kinetic energy and the total kinetic energy, as illustrated by these 32 tests, was also evaluated using linear regression analysis (Figures C-4 and C-5). Results were almost identical to those obtained by analyzing the estimates achieved by visual analysis. Figure C-4 shows that the ratio of the rotational energy to the total energy declines as the total energy increases. The linear regression is significant at the 95% confidence level, but there is a large scatter to the data, and the regression only "explains" 21.9% of the variability in the data. The relationship between rotational energy and total energy (Figure C-5) is not significant at the 95% confidence level, and accounts for only 0.1% of the data variability.

These results support the previous conclusions: the amount of rotational energy achieved during individual tests is relatively constant, and does not increase as the total energy increases.

6.1.3   Comparison of Energy Estimates Produced by the Two Methods

Appendix D provides an assessment of the comparison of energy estimates produced by the two methods, based on the 21 tests that were evaluated by both methods. Three linear regression analyses were conducted: one for the translational kinetic energy estimates, one for the rotational kinetic energy estimates, and one for the total kinetic energy estimates.

In each case, not only were the regression lines computed, along with their 95% confidence intervals and 95% prediction intervals, but the residuals to each regression were also evaluated. Figures D-1, D-3, and D-5 illustrate the fitted linear regression lines, along with their 95% confidence intervals and 95% prediction intervals. Figures D-2, D-4, and D-6 provide information that allows an evaluation of the residuals to each regression.

If the regression is to be a valid prediction model of the relationship between the results obtained by the two methods, then the residuals, which contain the variability in the data that is not explained by the regression, should have certain characteristics. The residuals should be distributed according to the normal distribution about the regression line. This can be evaluated

by observing them to fall along a straight line in a normal probability plot, and by a histogram of the residuals being relatively symmetrical around a central, near-zero, concentration. Furthermore, plots of residuals versus measured values, or according to the sequence of observations, should not reveal trends or correlations. Figures D-2, D-4, and D-6 each contain four graphs that provide the basic visual assessment of these desired characteristics of the residuals.

These regressions demonstrate that the translational and total kinetic energy estimates by both methods are fairly closely related. Both regressions (Figures D-1 and D-5) are significant at the 95% confidence level, and both "explain" about 50% of the variability in the data. Their residuals (Figures D-2 and D-6) meet all the desirable criteria. However these results do emphasize two points:

- There is considerable "noise" in the data. If the two methods produced closely similar results at all times then the points would mostly fall on the regression line, and the degree of variability in the data "explained" by these regressions would rise from the observed approximately 50% to a value of over 90%.
- If the two methods produced closely similar results, then the slope of the regression line should achieve a 45-degree slope, whereas the two regressions have a much lower slope, and the energy values obtained by the visual method have a smaller range than those obtained by the ProAnalyst motion-analysis software.

The comparison of the rotational energy estimates, shown by Figures D-3 and D-4, provides a very different result. The linear regression is not significant at the 95% confidence level; it "explains" only 10.8% of the data variability. The residual analysis (Figure D-4) shows a lack of a normal distribution. This is due to the presence of several very large residuals, caused by several rotational energy estimates produced by the visual method that deviate from the values anticipated by the ProAnalyst method. These show as points that plot far from the regression line in Figure D-3. The evaluation of the rotational energies thus shows that:

- The two methods do not appear to produce similar estimates of rotational energy
- The ProAnalyst method appears to estimate rotational energies between 15 and 75 kJ (6 to 28 ft-tons)
- The visual method estimates rotational energies for the same tests between 0 and 100 kJ (0 to 37 ft-tons).

The difference between the energy estimates produced by the two approaches is probably due to several factors including:

- Analysis with the motion software is much more accurate when the rock moves normal (perpendicular) to the camera viewing direction. Deviations and "wobbling" of the rock toward or away from the camera as it rolls down the concrete ramp reduce computational accuracy.
- These evaluations are based on reported results obtained by a single experienced professional user of the ProAnalyst software. They are reported as "Alt. ProAnalyst" values in Table A-3 in Appendix A. When other less-experienced individuals used the ProAnalyst

software, their calculated velocities were about 30% different. This demonstrates that the accuracy of the results depends on the way the model is set up and the assumptions used.

- The ProAnalyst motion-analysis software evaluates an instantaneous velocity at any given position along the trajectory, whereas the visual analysis method determines an average velocity between two known points. In this case the values were measured between the top of the concrete ramp and the point of impact. Motion-analysis software determinations were made at point of impact only.

Future improvements in motion-analysis software may increase the accuracy of the estimates of energies produced by this approach.

6.2   Attenuator Reactions to Initial Impacts

One of the most basic requirements affecting the design of an attenuator is that it is capable of withstanding repeated impacts by rock blocks, each impact falling within an anticipated energy range, without sustaining significant damage that would require maintenance operations on the system. This requirement often translates into attenuator systems consisting of rugged components.

The tests conducted at the Hidden Valley facility were conducted to provide additional information to assist in better defining appropriate responses to this requirement. One objective of these tests was an evaluation of the responses of the suspended "fence" portions of attenuators constructed with alternative net panel materials. The tests involved several sizes of manufactured concrete cuboctahedron rock blocks dropped from predetermined heights (Table 4). The largest number of tests (40 tests) involved B-sized rocks, with a mass of 1,695 kg (3,700 lbf), dropped from a height of 18 m (60 ft). Larger rocks and greater drop-heights were used infrequently because they tended to damage the concrete ramp. Smaller rocks and lower drop heights were used during initial "calibration" tests when each new attenuator system was first installed, but they rarely provided sufficient impact energies to fully evaluate the responses of the attenuator systems. As discussed in Section 6.1, the impact energies have been estimated for only a selected number of the tests. However, the selected tests appear representative of the entire series of tests, and the estimates show that most tests produced impacts with total kinetic energies in the range of 100 to 500 kJ (37 to 185 ft-tons). The energy estimates varied slightly between the two methods used to evaluate the high-speed video images.

Appendix E documents two additional quantitative evaluations of these energy estimates that may influence the response of the attenuators to rock impacts. Linear regression analysis was used to investigate the relationship between the rotational kinetic energies and the observed number of rotations of blocks as they traveled along the concrete ramp (Figure E-1). As expected, there is a relatively strong relationship with the estimated rotational energy increasing as the number of rotations increases. Figure E-2 shows the same relationship, subdivided according to rock size. It clearly shows that the rock size influences the relationship; the rotational kinetic energy of larger rocks increases more rapidly than smaller rocks.

Figures E-3 and E-4 summarize the relationship between bounce height and total kinetic energy. This relationship appears to depend to a considerable degree on the size of rock blocks, but these initial results are highly variable and not definitive.

TABLE 4 Summary of Rock Sizes and Drop Heights Used to Test Attenuator Net Panels

Rock Size	Mass (kg)	Number of Tests	Drop Heights				Other Heights
			0 feet	30 feet	60 feet	90 feet	
A	1,618	13	1	1	11	0	
B	1,695	51	0	6	40	5	
C	1,577	17	4	0	13	0	
D	2,259	20	2	10	9	1	
E	2,173	6	0	3	3	0	
F	3,823	5	4	0	0	0	1 from 4 feet
J	227	1	1	0	0	0	
Totals		113	10	20	76	6	1

Further evaluation of the responses of attenuators to initial impacts depends on evaluation of qualitative observations. Four aspects of the responses have been examined:

- Stretching or deformation of the net panel materials,
- Damage to the net panel materials,
- Bunching of the net panel materials along the support cable, and
- Damage to the anchor systems.

6.2.1 Stretching or Deformation of Net Panel Materials

Deformation of the system was primarily defined as how much the panel would stretch after a rock impact and how much permanent change in net configuration occurred. The stretch or deformation was assigned to three categories: negligible, defined as 0 to 0.7 m (0 to2 ft) along a single panel length; minor, defined as 0.7 to 2 m (2 to 6 ft) along a single panel length; and significant, defined as greater than 2 m (6 ft) along a single panel length.

Table 5 provides a summary of the 30 tests that produced minor or significant stretching. Only five tests produced significant stretching; two tests involved ring nets, two tests involved cable rings, and one test involved 4-mm high-tensile wire mesh. Common deformations included permanent elongation and stretch of the apertures within the net material. An additional 25 tests produced minor stretching. This type of damage was observed most frequently with 8-mm cable nets and high-tensile strength spiral wire nets (nine tests).

This type of damage was observed most frequently with cable nets (eight tests) and high-tensile spiral wire systems (nine tests) as depicted in Figures 53, 54 and 55. As evident in Figure 53, large apertures were more likely to entangle a rolling rock. However, minor stretching was observed in ring nets (five tests), when impacted with large rocks, and in high-tensile wire mesh (three tests), when impacted by small rocks.

Extreme stretching or tearing was sometimes observed at the seams between the net panels or at the connections between the net panels and the wire bearing ropes (see Section 6.2.3). This was mostly observed with 3.7-mm chain-link wire nets, and even with the 4-mm high tensile strength wire net particularly when seamed with shackles (Figure 55).

TABLE 5 Summary of Tests That Produced Minor or Significant Stretch to Attenuator Net Panels

Cells with no data indicate no stretch for that drop sequence. In cells containing data, the data describes the drop sequence that produced the described stretch.			Number of tests	Cable Net 8 mm wrapped clip	Cable Net 8 mm Interlocking clip	Cable Net 12 mm wrapped clip	Cable Net 12 mm Wire Wrap	Ring Net 350 mm	Ring Net 300 mm	Cable Ring 8mm wire rope	High Tensile 4 mm	High Tensile Spiral 130 mm	High Tensile Spiral 230 mm	Chain Link
Negligible Stretch (0-2 ft)	**Drop ht. & Rock Size**	0 ft	**83 tests showed negligible stretch**											
		30 ft												
		60 ft												
		90 ft												
	Rock Action													
	Release Velocity													
Minor Stretch (2-6 ft)	**Drop ht. & Rock Size (#of drops/rock size/tail length in ft)**	0 ft	0	-	-	-	-	-	-	-	-	-	-	-
		30 ft	4	1/D/18 1/D/25	-	-	-	1/E/10 1/E/15	-	-	-	-	-	-
		60 ft	21	1/D/18 1/D/30	1/D/15	-	3/B/10	1/C/15 1/D/15	1/C/5	-	1/A/15 2/A/20	3/B/23 1/E/23	2/C/5 1/C/10 1/C/25 1/C/30	-
		90 ft	0	-	-	-	-	-	-	-	-	-	-	-
	Rock Action (# of events/action)			1/RT 2/RR,R 1/RR,S	1/SR,R	-	2/RR,R 1/RR,S	3/RR,R 1/RR,S	1/RR,R	-	2/RT 1/SR,R	3/RR,S 1/RR,R	4/RT 1/RR,R	-
	Release Velocity (# of events/velocity)			1/SL 2/RS 1/ST	1/F	-	2/SL 1/ST	2/SL 1/RS 1/ST	1/RS	-	2/F 1/SL	3/ST 1/RS	3/F 1/NA 1/SL	-
Significant Stretch (> 6 ft)	**Drop ht. & Rock Size (#of drops/rock size/tail length in ft)**	0 ft	0	-	-	-	-	-	-	-	-	-	-	-
		30 ft	1	-	-	-	-	1/D/15	-	-	-	-	-	-
		60 ft	4	-	-	-	-	-	1/C/5	1/C/5 1/C/7	1/A/20	-	-	-
		90 ft	0	-	-	-	-	-	-	-	-	-	-	-
	Rock Action (# of events/action)			-	-	-	-	1/RR,S	1/RR,S	1/RR,S 1/RT	1/RT	-	-	-
	Release Velocity (# of events/velocity)			-	-	-	-	1/ST	1/ST	1/ST 1/F	1/F	-	-	-

Codes for Rock Action and Rock Release Velocity are provided in Table A-1 of Appendix A.

FIGURE 53 Deformation of large-aperture ring net.

FIGURE 54 Typical deformation of ring-net panel
(red outlines compare deformed and unaffected apertures).

FIGURE 55 Stretching and damage along seam of 4-mm high-tensile-strength wire net.

The majority of the tests (83 tests) resulted in negligible stretching. In the case of cable nets one reason for the absence of stretching is that the connection points are fixed, not allowing the wire ropes to readily slide. The use of fixed nodes (by clips or wire knots) adds a degree of rigidity to the net panel.

6.2.2   Damage to Net Panel Materials

Damage to the attenuator net panels was assigned to four categories: negligible, defined as no observable or apparent damage; minor, defined as rips or openings less than 0.3 m (12 in.); significant, defined as rips or openings greater than 0.3 m (12 in.); and remove/replace required, defined when the damage was so severe that further testing of the attenuator was not possible. Table 6 summarizes the 16 tests that caused significant damage (eight tests), or caused damage so severe that the attenuator was categorized as remove/replace (eight tests).

The remove/replace category was fairly evenly distributed among five net panel fabrics. Two tests involving the heavier (12-mm) cable nets, and one test involving the 8-mm cable-ring material resulted from impacts by B- and C-sized rocks. In contrast, two tests with A-sized rocks caused this level of damage to the 4-mm high-tensile-strength wire mesh. An E-sized rock severely damaged the chain-link net panel, as might be expected. Two C-sized rocks severely damaged the high tensile strength spiral-wire net.

The significant damage category resulted in a total of eight tests involving rocks A, B, C and D. Three of the tests were on the 8 mm cable nets, two on the 12 mm cable nets (clamp connection), one on the 300 mm ring net and two on the 4-mm high-strength tensile wire mesh.

Much of the damage was caused when the strands forming the panel mesh were broken, developing rips or openings in the mesh. Initially, this was attributed to "cutting" of the strands by rotating rocks but, in retrospect, it is now believed that many of these breaks are due to tensile

TABLE 6 Summary of Tests That Caused Significant Damage or Required Removal or Replacement of Attenuator Net Panels

Cells with no data indicate no damage for that drop sequence. In cells containing data, the data describes the drop sequence that produced the described damage.			Number of tests	Cable Net 8 mm wrapped clip	Cable Net 8 mm Interlocking clip	Cable Net 12 mm wrapped clip	Cable Net 12 mm Wire Wrap	Ring Net 350 mm	Ring Net 300 mm	Cable Ring 8mm wire rope	High Tensile 4 mm	High Tensile Spiral 130 mm	High Tensile Spiral 230 mm	Chain Link
Negligible Damage	Drop ht. & Rock Size (#of drops/rock size)	0 ft												
		30 ft												
		60 ft												
		90 ft												
	Rock Action													
	Release Velocity													
Minor Damage (<12 inch rips)	Drop ht. & Rock Size (#of drops/rock size)	0 ft												
		30 ft												
		60 ft												
		90 ft												
	Rock Action													
	Release Velocity													
Significant Damage (> 12 inch rips)	Drop ht. & Rock Size (#of drops/rock size/tail length in ft)	0 ft	0	-	-	-	-	-	-	-	-	-	-	-
		30 ft	1	-	-	-	-	-	-	-	1/A/20	-	-	-
		60 ft	7	1/D/18	1/B/25 1/D/15	1/C/7 1/B/15	-	-	1/C/5	-	1/A/30	-	-	-
		90 ft	0	-	-	-	-	-	-	-	-	-	-	-
	Rock Action (tail length/Rx Action)			18/RR, R	25/RR, S 15/SR, R	7/RR,R 15/RR, R	-	-	5/RR, S	-	30/RT 20/RR,R	-	-	-
	Release Velocity (tail length/rel velocity)			18/RS	25/ST 15/F	7/SL 15/SL	-	-	5/ST	-	30/F 20/F	-	-	-
Remove/Replace Required	Drop ht. & Rock Size (#of drops/rock size/tail length in ft)	0 ft	0	-	-	-	-	-	-	-	-		-	-
		30 ft	0	-	-	-	-	-	-	-	-		-	-
		60 ft	8	-	-	1/C/7 1/B/10	-	1/C/7	-	-	1/A/20 1/A/30		1/C/10 1/C/30	1/E/35
		90 ft	0	-	-	-	-	-	-	-	-		-	-
	Rock Action (tail length/Rx Action)			-	-	7/S 10/S	-	7/RT	-	-	20/RT 30/RT		10/RT 30/RR,R	35/RT
	Release Velocity (tail length/release velocity)			-	-	7/ST 10/ST	-	7/F	-	-	20/F 30/F		10/F 30/SL	35/F

Codes for Rock Action and Rock Release Velocity are provided in Table A-1 of Appendix A.

FIGURE 56 Significant damage to 8-mm cable net constructed with interlocking clips.

FIGURE 57 Attaching chain-link panel to support cable.

failures of the strands. More research is required to better explain the cause of this damage. Figure 56 depicts significant damage observed to an 8 mm cable net constructed with interlocking clips.

Additional damage was also observed when clips became detached, or "lost," after the impact event. This type of damage was mostly observed with wrap-around clips on cable-net panels.

Arndt, Ortiz, and Turner   57

6.2.3   Bunching of Net Panel Materials Along Support Cable

Several of the lighter-weight net panel materials (high tensile strength wire) were attached to the support cables using a spiral looped wire connection in specific orientations (Figure 57). The ring nets and cable nets were attached to the support cable by a series of shackles. The chain link material was laced with 8 mm (5/16 in.) cable to the support rope. Upon impact, the shackles connecting the net panels tended to slide along the support cable and the net panel "bunched" laterally, rather like a shower curtain (Figure 58). This tended to cause the net panel to "wrap" around the rock, trapping it within the attenuator.

This "bunching" effect was especially apparent during the initial tests, which used a panel that was only 6 m (20 ft) wide. Such bunching had never been observed in the field with other attenuator installations. It was realized that in these field installations the attenuators included numerous panels and, thus, were much wider and laterally more continuous. To better reflect this, the test installation was modified and attenuators were constructed with a central panel and two side panels. These panels were interconnected, and the entire installation now had a much greater lateral resistance and the "bunching" effect along the support cable was reduced.

Because insufficient panel materials had been purchased to allow for the more expansive four-post design system, for many subsequent tests the side panels were fabricated from different materials than the central panel that was being tested. However, the weight (density) of the side panels was matched to that of the central panel and the validity of the test results is believed to be unaffected.

In some tests, additional "bunching" of parts of the net panel, usually at the point of primary impact, resulted when sections of the mesh panels slid together. This was most commonly observed on some of the cable nets, when the clips slid along the wires (Figure 59).

FIGURE 58 Bunching of ring net attached with shackles to support cable.

Colorado's Full-Scale Field Testing of Rockfall Attenuator Systems
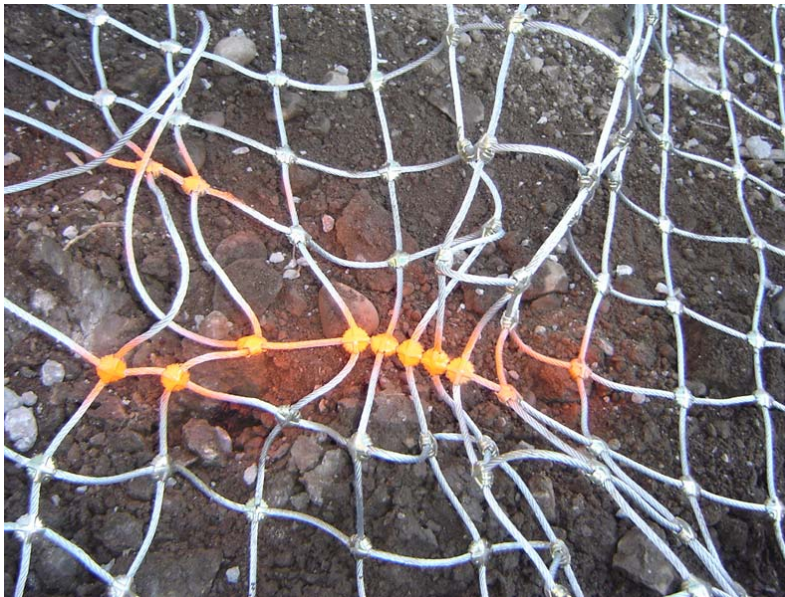
FIGURE 59 Bunching 8-mm cable net due to sliding of clips.
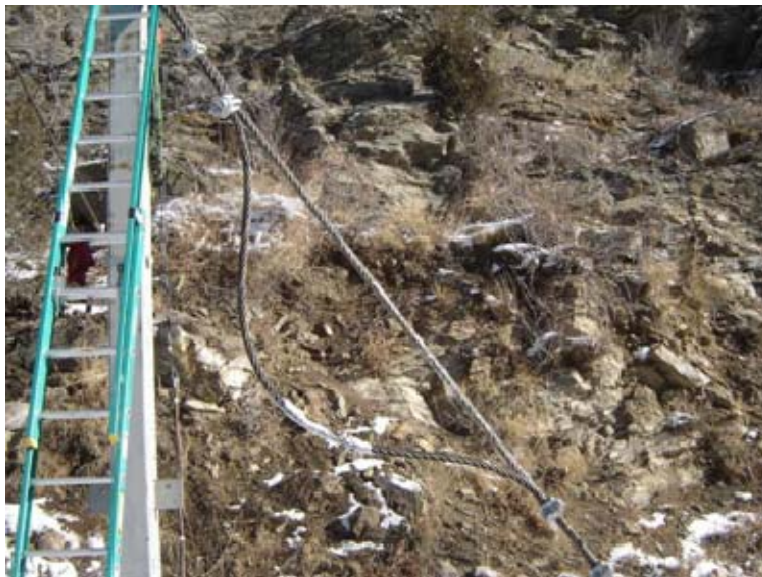
FIGURE 60 Field-designed friction-brake assembly installed on main support cable.

6.2.4   *Damage to Anchor Systems*

The Hidden Valley test facility was subjected to numerous rock-rolling tests that produced repeated impact loads on the attenuator support system that occurred at a much more rapid pace than would be expected under actual field conditions. As the testing progressed, the support system began to experience some "fatigue failures." In particular, the anchors that were attached to the support and anchoring cables began to pull out of the soil. The anchors that were grouted

in a silty sandy fill material tended to pullout after repeated tests. The depths of the anchors were 2 m (6 ft).

To reduce the instantaneous shock load from the impact that was being transmitted to the anchors, a "friction-brake" assembly was designed in the field. The assembly was constructed by attaching a short length of cable to the main support cable using cable clamps to produce and maintain slack in the main support cable (Figure 60). The clamps were tensioned below the design-load limit of the system. When the attenuator system was subjected to a large impact load, the slack in the main support cable was pulled through the clamps, which reduced the load transferred to the anchors. If the slack was reduced after a series of tests, the assembly was reset before testing resumed. This method of reducing the instantaneous shock load was not a tested component of the attenuators. It was developed to reduce the number of times the support anchors needed to be reinstalled. The ground conditions at the test facility are not similar to those at the Georgetown Incline. To date, anchor failure has not been a common occurrence with the Georgetown installations.

6.2.5 Conclusions from Test Sequence

The tests at Hidden Valley provided considerable information as to the probable maintenance requirements of the various attenuator systems that were being evaluated. This was very useful and important information, because the costs associated with maintaining earlier barrier systems at Georgetown Incline were considerable, due to their demands for excessively frequent maintenance repairs. Systems that took repeated impacts with little or no damage were deemed potentially low-maintenance systems. Conversely, systems that had greater damage were likely to result in high maintenance requirements and costs. Based on the testing, the 12 mm (0.5 in.) cable nets with wrapped connections withstood impacts with the least amount of damage after repeated impacts. The 4 mm high tensile strength wire mesh withstood multiple impacts, but experienced more permanent deformation than the 12 mm cable nets.

6.3 Reactions of Attenuator Tail Components

The successful operation of attenuator systems depends on their ability to allow rocks to pass their locations with diminished velocities. The accumulation of debris will not only stiffen the impact zone of the nets, often leading to additional damage to the attenuator components, it also makes undesirable and expensive clean-out operations necessary on a more frequent basis. In addition, if excessive damage to the attenuators is to be avoided, along with associated maintenance costs, then attenuator designs consider using significantly rugged components to ensure they can resist damage caused by anticipated rockfall impacts. In meeting these objectives, a critical aspect of attenuator design is the specification of the attenuator "tail" component; the tail consists of a length of net panel mesh material that is laid out on the ground surface downhill from the suspended attenuator fence component (Figure 45). For this test program, the length of the tail was defined as the distance over which the net panel mesh was in contact with the ground. The tail lengths evaluated at the Hidden Valley test facility ranged from 1.5 to 10 m (5 to 35 ft).

The efficient and successful attenuation of rockfall velocities, and hence their energies, by the attenuator system depends to a considerable degree on the response of the attenuator tail to the initial rock impact. Transmission of the energies generated by the initial impact often

causes the tail to rise into the air. If the attenuator tail remained elevated off the ground for a sufficiently long period, the initial rock block and any trailing blocks were more likely to pass through the attenuator system without sufficiently interacting with the net panel to effectively dissipate energy. However, if the tail length is overly long, and/or the density of the mesh materials is sufficiently large, the weight of the mesh will tend to cause the tail to remain on the ground or rapidly return to a position close to the ground following initial impact, and the rock blocks can become trapped within the attenuator.

The selection of an optimum design for an attenuator tail when draped on a relatively constant slope thus involves choices between length of the tail and density of the material used to construct the tail. Ideally, the tail should be the proper length and weight and constructed of a material type that appropriately relates to the size, shape, and energy characteristics of the anticipated rock blocks to be effective, durable and perform with less maintenance. Ideally, the choice of panel material for tail components take in to consideration the material's interaction with the rocks that are attempting to pass along and beneath the tail material. If an attenuator tail is constructed of materials with apertures that allow the corners or edges of typical rock blocks to become embedded within the net panel, then the attenuator is more likely to sustain damage requiring repairs, or will accumulate rockfall debris relatively quickly.

Thus, a major aspect of the attenuator test program at Hidden Valley was to evaluate the performance of different attenuator tail components. Tail components of several lengths were constructed using all 11 attenuator net panel materials being tested. The reactions of these tail components were recorded with high-speed video cameras as they were impacted by various sizes of test rocks. Although, the camera systems were installed to provide images of the responses of the tail components to each test impact, it was found that many test impacts produced considerable airborne dust and debris that prevented the accurate determination of quantitative measurements from the video images. As a result, the project database, provided in Appendix A, contains several qualitative observations of the responses of the attenuator tail components during these tests, rather than the more quantitative measurements that were initially anticipated.

However some quantitative measurements were obtained. These include the time the attenuator tail remained elevated in the air, and the estimated height of the attenuator tail above the ground as the rock passed beyond the end of the tail. These measurements were believed to be important because, intuitively, it seemed that the greater the time that the tail is in the air following an initial rock impact, the more likely trailing rocks could pass through the system without attenuation. Appendix F provides the results of the initial assessments of this design element and provides an evaluation of the relationships between

- The height of the tail as the rock exits the system and the time the tail remains elevated in the air,
- The time the tail remains elevated in the air and the length of the tail, and
- The height of the tail as the rock exits the system and the total kinetic energy of the test rock estimated by visual analysis of the video images.

The limited number of available energy estimates (as discussed in Section 6.1) restricted the number of tests that could be analyzed. Appendix F evaluations are based on only 36 tests, out of the total of 113 tests that were conducted.

6.3.1   Relationship Between Height of Tail as Rock Exits System and Time Tail Remains Elevated in Air

Linear regression provides evidence of a relatively strong relationship between the height of the tail as the rock exits the system and the time the tail remains elevated in the air (Figure F-1). As the time in the air increases, so does the vertical height of the tail as the rock exits the system. This regression is significant at the 95% confidence level and "explains" about 65% of the data variability.

Figure F-2 shows the same data relative to the density of the mesh. For this analysis, the various mesh materials were classified into three categories: Low Density (less than 4 kg/m^2, or 0.8 lbs/ft^2), Medium Density (4-7 kg/m^2, or 0.8-1.4 lbs/ft^2), and High Density (greater than 7 kg/m^2, or 1.4 lbs/ft^2). Figure F-2 shows that the low and medium density materials behave similarly, and similar to the combined conditions shown in Figure F-1. The high density materials appear to behave somewhat differently, but there are many fewer data points. Figure F-3 presents the same data relative to the size of the rock involved in the test. The relationship seems unaffected by rock size; rocks of size B, C, and D have almost identical trends, and although the trend for the smallest rocks (Rocks A, B and C) appears different, it is based on very few tests.

6.3.2   Relationship Between Time Tail Remains Elevated in Air and Length of Tail

Longer tails tend to spend less time elevated in the air (Figure F-4). This relationship is most apparent for medium density mesh materials (Figure F-5). Low density mesh materials show no relationship between their length and the time they are elevated; their trend line is essentially horizontal at 0.85 seconds. But this result is due to the presence of measured results ranging from 0 seconds to 1.5 seconds for any tail length. Observations during the tests noted that longer tails constructed of lower density materials tended to "whip" in the air.

When this relationship was evaluated with the data subdivided by the size of rock involved in each test (Figure F-6), it appears possible that the relationship between the time the tail remains elevated in the air and the length of the tail may be affected by the sizes of the rocks impacting the attenuator.

6.3.3   Relationship Between Height of Tail as Rock Exits System and Total Kinetic Energy of Test Rock

Linear regression shows only a weak relationship between the heights of the tail as rocks exit the system and the total kinetic energy of the test rocks, as estimated by visual analysis of the video images (Figure F-7). This relationship is not statistically significant, and the regression trend shows a diminished height as the rock impact energy increases; a counter-intuitive result. However, the data are highly erratic; the measured tail heights at the time the rocks exit the system range from low to high for all values of total kinetic energy. A subdivision of this data according to rock size (Figure F-8) fails to resolve the relationship.

6.3.4   *Additional Observations*

Some observations during the testing suggest that rocks that impact the attenuator on a rising trajectory, following a rebound from a nearby impact with the concrete ramp, are more likely to increase the tendency for the tail components to become airborne. However, this is not entirely clear from the existing data.

The amount of attenuation observed is influenced by the tail length, but is also affected by the type of net panel material used to construct the tail. Ring net and the heavier cable net materials generally only required short tail lengths of 1.5 to 3 m (5 to 10 ft) to stop or significantly slow down single rocks. The lighter cable net material required significantly longer tails to similarly slow down or stop rock blocks. In contrast, tail components of low density net panel materials, such as those constructed with 4-mm high tensile strength wire or 3.7 mm chain-link, frequently failed to significantly slow-down rock blocks, even when tails up to 10 m (30 ft) long were used.

It should be noted that the results reported in Table 6 are from tests where significant damage to the net panels occurred, and in some cases, this damage was found in the tail component. Some rock blocks tore through tails constructed of the lighter materials (Figure 61). In general, tails constructed of heavier materials remained elevated in the air for shorter periods and thus were more likely to assist in decelerating rock blocks, even when shorter tail lengths were used. Longer tails generally remained elevated in the air for shorter periods, unless they were constructed with light-weight materials; then, a whipping effect occurred.

**FIGURE 61 Severe damage to attenuator tail constructed with
relatively light-weight, double-layer chain link mesh.**

Although not evaluated by any of the tests conducted at Hidden Valley, at locations where debris-flows and/or snow avalanches are likely to occur, debris transported by these events is likely to partially bury the tail component. Since the weight of the debris will prevent the tail component from elevating to allow rock blocks to pass beneath it, rockfall debris will become trapped in the attenuator, and there is an increased likelihood of damage to the net panels, posts/post foundations, or anchors. Under these circumstances, a reduced tail length may be preferable. However, the tests at Hidden Valley have shown that tail lengths of less than 3 m (10 ft) are not very effective in providing rockfall attenuation of the rockfall sizes tested.

6.4   Evaluation of Post-to-Base Connections

A series of 12 tests were conducted to evaluate the post-to-foundation connections (Table 7). The tests were undertaken to compare two types of post to-base-connections: pin-connection and fixed-connection. These have been described in Sections 4.2.1 and 4.2.2 (Figures 35 to 41). Table 7 describes the testing with comments. It should be noted that the pin-connected post was a much lighter steel section than the fixed-connection post, but the testing was conducted to compare the effectiveness of the two different post systems to withstand similar impact energy.

The pin-connected post withstood only one impact prior to needing replacement (Figures 62 to 65), however the same foundation pad was used to test the fixed-connection post (Figure 65). The fixed-connection post was tested and withstood a direct impact with minor damage to post and foundation (Figures 66 to 69). The fixed-connection post was then moved to a lower foundation pad and withstood an additional seven impacts prior to complete failure of post and base (Table 7). The "A" rock, with a mass of 1,618 kg (3,560 lb), was used for six tests; the slightly larger "B" rock, with a mass of 1,695 kg (3,730 lb), was used for one test; and the much larger "E" and "F" rocks, with masses of 2,173 kg (4,780 lb) and 3,823 kg (8,410 lb) were used in three and two tests, respectively. Overall, the fixed-connection post withstood a total of eight impacts before requiring replacement.

Five tests have been evaluated by the ProAnalyst motion-analysis software and the estimated kinetic energies are reported in Table A-3. For two tests, the ProAnalyst software shows the rock to have no rotation, a somewhat surprising outcome that will be subsequently verified by examining the video recordings. The kinetic energies range from about 150 kJ (56 ft-tons) to about 200 kJ (74 ft-tons), except for one test where the largest "F" rock was dropped from a 20-m (60-ft) drop height, which produced an estimated impact energy of 920.5 kJ (341 ft-tons). Table A-3 provides selected energies for each of the tests.

Figures 70 and 71 provide the strain versus time intervals associated with strain gauges that were welded to the posts. Figures 38 and 39 provide the actual designation and location of the strain gauges on the posts. The strain gauge data has not been fully analyzed at this time but it is interesting to note the time interval in which the impact events occur. The x-axis data is comprised of 250 readings per second and the impact event ranged from 40 to 50 readings so it appears that the impact time interval ranges from 0.16 to 0.20 seconds. It is hoped that further evaluation of the strain gauge data will provide functional information about the post behavior.

TABLE 7 Summary of Post Testing

Test No.	Date	Post Foundation	Rock	Drop Height Above Ramp (ft)	Comments
120	10/13/2008	Pinned	B	15	Direct hit: three uphill anchors, post not functional after test. Minor spalling of concrete base (Figure 65).
121	10/13/2008	Fixed	A	15	Fixed-base post attached to same foundation base as Test 120. Rock missed on first roll.
122	10/13/2008	Fixed	A	15	Direct square hit: one uphill anchor, post functional. Significant spalling and movement of concrete base but functional (Figure 69).
123	10/14/2008	Fixed	A	15	Fixed-base post moved to lower foundation support. Glancing hit: three uphill tiebacks, post functional. Significant spalling and movement of concrete base but functional.
124	10/14/2008	Fixed	A	15	Glancing hit: two uphill tiebacks, post functional. Progressive failure of concrete base but still functional.
125	10/14/2008	Fixed	A	15	Direct hit: two uphill tiebacks, post functional. Progressive failure of concrete base but still functional.
126	10/14/2008	Fixed	A	15	Direct hit: one uphill tieback, post functional. Progressive failure of concrete base but still functional.
127	10/14/2008	Fixed	E	15	Glancing hit: one uphill tieback, post functional. Progressive failure of concrete base but still functional.
128	10/14/2008	Fixed	E	15	Rock missed
129	10/14/2008	Fixed	E	15	Direct hit: one uphill tieback, post functional. Progressive failure of concrete base but still functional.
130	10/14/2008	Fixed	F	15	Glancing hit: one uphill tieback, post functional. Progressive failure of concrete base but still functional.
131	10/14/2008	Fixed	F	60	Direct hit: one uphill tieback, post not functional after test. Concrete base destroyed.

**FIGURE 62 Test 120 prior to release of rock at mid-height on ramp
(red arrow indicates location of rock prior to drop; white arrow indicates
pin-connection post at bottom of ramp).**

FIGURE 63 Test No. 120 (pin-connection post just prior to impact).

FIGURE 64 Test No. 120 (pin-connection post during impact).

**FIGURE 65 Minor concrete spalling as result of Test No. 120
(looking up ramp).**

FIGURE 66 Fixed-connection post just prior to impact (Test No. 122).

FIGURE 67 Fixed-connection post during impact (Test No. 122).

FIGURE 68 Fixed-connection post after impact (Test No. 122).

**FIGURE 69 Fixed connection post base placed on same base for Test No. 120
(concrete spalling after Test No. 122 looking up ramp).**

7 ACTIVITIES AT GEORGETOWN INCLINE LOCATION IN 2009

Three distinct efforts were undertaken and are described in the following sections: rock-rolling field experiments were conducted in February 2009, a new multiple attenuator system project was successfully bid and constructed March through May 2009, and additional rock-rolling field experiments were undertaken in May 2009 to evaluate this new attenuator system.

7.1 Rock-Rolling Experiments Conducted in February 2009

In February 2009, following completion of the tests at the Hidden Valley test facility, additional rock-rolling experiments were conducted at the Georgetown Incline site (Event 11 in Table 1). The purpose of these experiments was to further evaluate the performance of the prototype
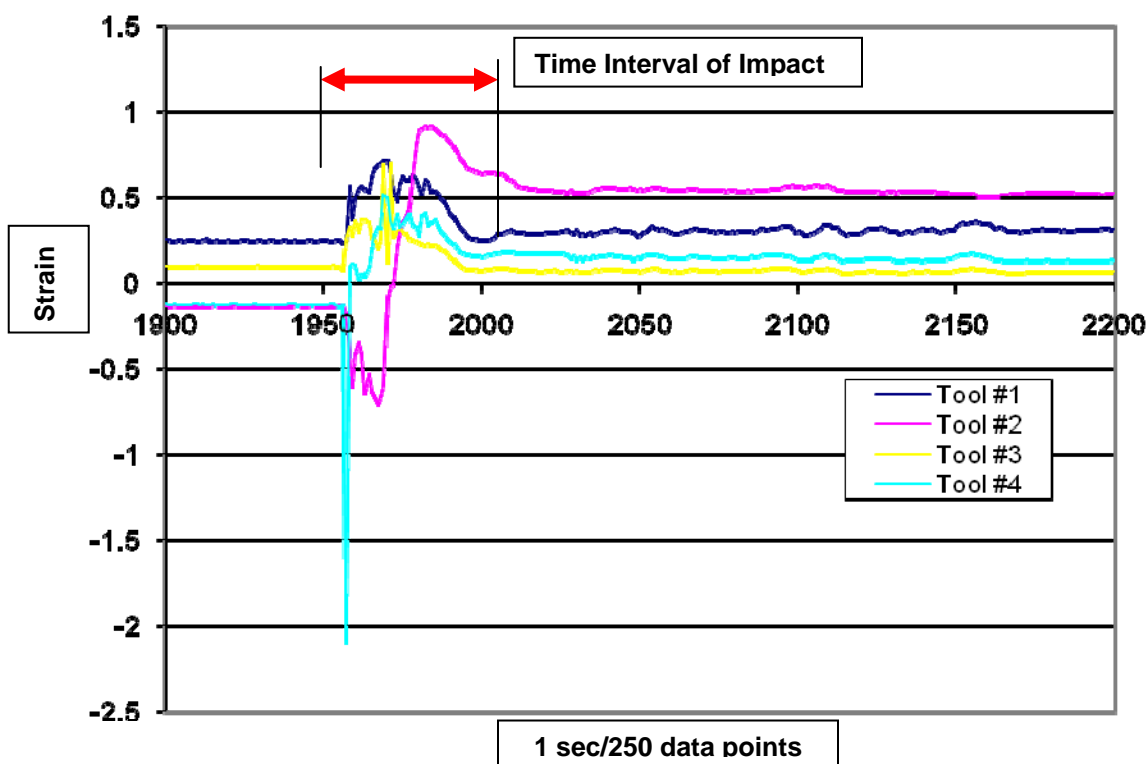
FIGURE 70 Strain gauge data collected during Test 120 for pin-connection post (time interval of impact denoted by red arrow).
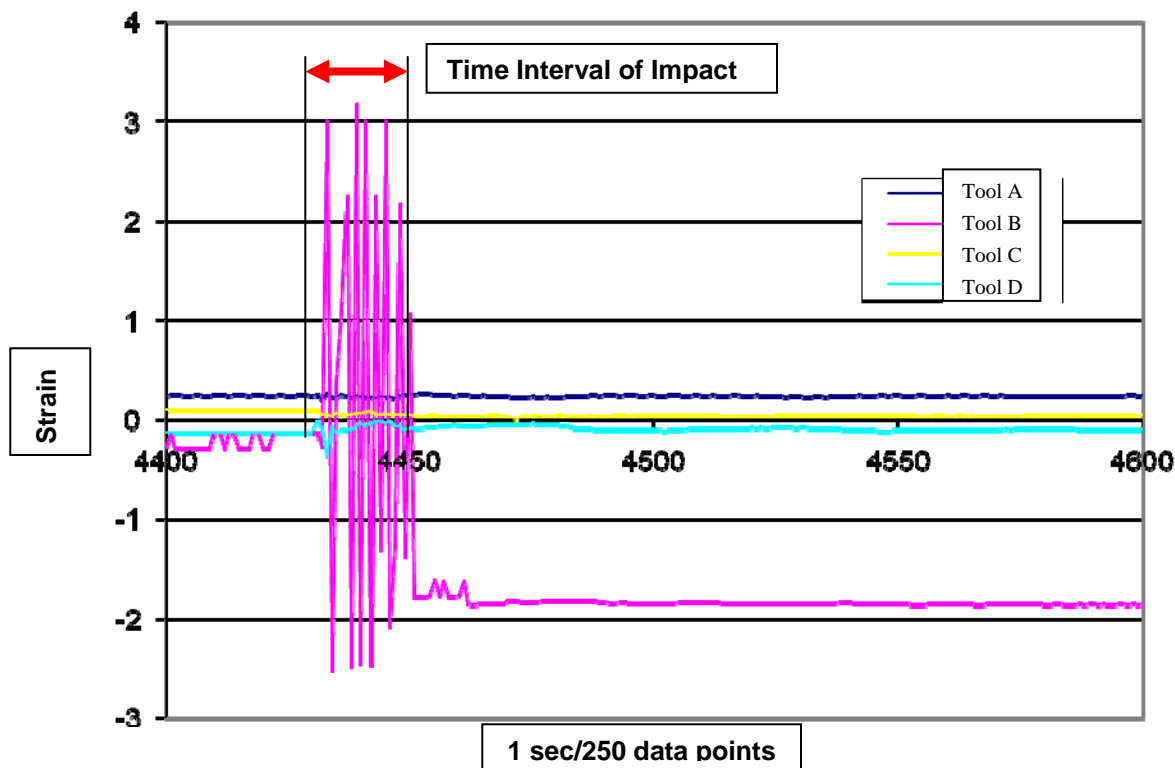
FIGURE 71 Strain gauge data collected during Test 122 for fixed-connection post (time interval of impact denoted by red arrow).

attenuator previously installed at Georgetown, in light of the experience gained with the tests at the Hidden Valley facility. The experiments were recorded with high-speed video cameras. These experiments resulted in damage to the prototype attenuator, which sustained impacts of fairly large, rapidly moving blocks with considerable rotational energy. One of the attenuator support posts was knocked off its concrete base and a second post was bent and damaged by a direct impact of a test block. Subsequently, the first post was restored and re-used; the second post was replaced. Although high speed video was obtained, it was very difficult to calibrate the video given the difficult access at the site. Further calibration at the site will be necessary to provide meaningful results from the test data and has not been undertaken at this time.

7.2   Installation of New Multiple Attenuator System

In March and April of 2009, the Colorado Department of Transportation applied the test results from the Hidden Valley test facility to design and install a multiple attenuator system above the Georgetown Incline (Event 12 in Table 1). The design consisted of a series of three separate attenuators that were located approximately 100 and 150 m (300 and 500 ft) apart. The two prototype attenuators located lower on the slope were also repaired, and the barrier fence adjacent to Interstate 70 was extended. Appendix G reproduces five selected plan sheets from the project, including a typical cross section of the recently constructed test site that consists of a total of five attenuators. The upper three attenuators were constructed as additional attenuators

under this project. The lower two attenuators have been referred to as the prototype attenuators that have been built and re-built at various stages per descriptions in Table 1.

The attenuators were specified to have a total drape length of 13.7 m (45 ft) so that at least 7.6 m (25 ft) would be in contact with the ground. Based on the results observed during a test of the system that involved dropping a block from a helicopter, as described in Section 7.3, future designs will likely have a total length of 16.7 m (55 ft) so that at least 10.6 m (35 ft) will be in contact with the ground.

For the conditions and slope geometries at Chute 4 of the Georgetown Incline the following attenuator materials were used for construction:

Cable Net: The 12 mm (1/2 in) diameter, 205 mm by 205 mm (8 in. by 8 in.) diagonal weave, cable net, with interlocking clips was chosen based on the empirical data gathered from testing that suggested this panel system incurred the least damage, had the greatest unit mass to attenuate rockfall energies and minimize tail lift, required the least maintenance, and had small enough aperture sizes so that rocks would not easily become entangled in the panel. Chain link was attached to the uphill side of the cable net as a sacrificial layer to extend the functional life of the system. Based on the bids for the project, the cable nets item costs ranged from the low bid of $21.62/square foot to a high bid of $25.69/square foot. The awarded bid cost was $21.62/square foot for the cable net system which included the chain link attached to the panels.

Posts: The fixed based W 8 x 48 posts were also chosen since they were able to withstand multiple impacts and still functioned at holding the attenuator panels off the ground with little maintenance. Based on the bids for the project, the post costs (which included the post and the reinforced foundation) ranged from a low bid of $3,265 per post to a high bid of $22,928 per post. The awarded bid cost was $3,796 per post.

It is emphasized that the selected attenuator components at the Georgetown Incline site were chosen based on almost a decade of field experience and the unique conditions specific to this area but may not be appropriate for other sites.

7.3   Rock-Rolling Experiments to Evaluate New Attenuator System

Near the end of construction of the new attenuator system, in May 2009, the Colorado Department of Transportation directed the contractor to undertake some field rock-rolling experiments to evaluate the performance of the new attenuator installations (Event 13 in Table 1). As a first step in the experiment, five concrete rocks with a mass of 730 kg (1,600 lb) were rolled into the three lowest attenuators as depicted in the cross section in Appendix G. Data was collected using standard video recorders that recorded at 25 frames per second; since, using the high speed cameras was determined to be too labor and time intensive to set up and generally did not provide outstanding results. Energy results from this roll have not been evaluated at this time.

The five rocks were released as a group. Four of the five rocks hit the first attenuator and were slowed down. However, the fifth rock rolled under the attenuator while the net was lifted into the air by the impacts of the initial four rocks, and did not slow down. This rock was the first to hit the next attenuator downslope and was attenuated then. This demonstrated the value of having redundancy provided by the series of attenuators.

The Colorado Department of Transportation also had the contractor drop a single 730 kg (1,600 lb) rock from a helicopter approximately 300 vertical meters (1,000 ft) above the roadway into the top attenuator while traffic was stopped. The rock then bounced over the second attenuator at a height estimated to be in excess of 7 m (23 ft). Upon reaching the third attenuator

system, the rock was estimated to have a velocity between 18 and 21 m/s (60 to 70 ft/s). The third attenuator nearly stopped the rock, but upon exiting this third attenuator it continued down-slope, and was eventually deposited in the rockfall catchment area adjacent to Interstate 70. All six tests were considered successful, and the attenuators performed as intended when they were designed. Figures 72 and 73 depict Attenuator A as described in the plans of the recently installed attenuator system.

FIGURE 72 View of Attenuator A (looking southwest).

FIGURE 73 View of Attenuator A (looking west).

8   CONCLUSIONS

The full-scale testing of rockfall attenuator systems, combined with the experience with rockfall events and attempts at rockfall hazard mitigation at the Georgetown Incline both before and after the full-scale testing at the Hidden Valley facility provides a series of conclusions.

8.1   Limitations of Full-Scale Tests Conducted at Hidden Valley

The experiences and observations obtained during the series of full-scale tests conducted at Hidden Valley provided valuable insights and information that have assisted in the preparation of designs for new rockfall attenuator installations at the Georgetown Incline.

Although only a short period of time has elapsed, initial field tests with manufactured rocks at the Georgetown location indicate that the new attenuators are likely to perform much better than the earlier installations. Testing at the Hidden Valley Site assisted in evaluating the system for the project site conditions. However, the observations and data collected from these tests have limitations that prevent them from being entirely representative of conditions that can be anticipated for other locations and slope geometries. The principal limitations of these tests are:

1.   The test site was too small to replicate the lengths of natural slopes between attenuators which were typically constructed at 150 m (500 ft) spacing. The concrete ramp at the test facility only allowed the test rock blocks to gain modest levels of translational and rotational kinetic energies, levels that did not cover the full range of energies to be expected at a location similar to Georgetown Incline.

2.   The performance of any attenuator tail component is likely to be affected by the slope inclination over which it is placed. The test facility only had a single slope inclination (of about 35 to 40 degrees) over which all the tail components were placed. The test results cannot fully evaluate the interaction of attenuator tail components at different slope inclinations.

3.   Prior to undertaking the tests at Hidden Valley, it was believed that the observed damage to fences and attenuators installed at the Georgetown Incline location was caused by "cutting" of the panels and support ropes by rapidly spinning rocks. However, none of the damaging rockfall events at the Georgetown Incline location were directly observed, so this belief in the "cutting" process was unsubstantiated. It was hoped that the impacts of rotating cuboctahedron manufactured test blocks would damage the test panels in a similar manner to what was observed at field locations.

4.   The damage observed to the attenuator components during the Hidden Valley testing sequence appears similar to the damage previously attributed to "cutting" after one of the "real" Georgetown rockfall events. However, the testing at Hidden Valley did not produce any direct evidence of failures due to the "cutting" actions of rotating rock blocks. The damage observed during the Hidden Valley tests can be attributed to the failure in tension of net panel fabrics or support components. However, this conclusion remains partly speculative, as insufficient quantitative data were measured during these tests.

5.   In retrospect, although considerable damage was observed on several panel systems, it appears likely that the tests did not fully duplicate the severity of the actual field conditions since: (a) the cuboctahedrons do not contain edges and corners that are as sharp as some naturally occurring, disc-shaped, sharp-edged rocks, and (b) the total kinetic energies, and their

translational and rotational components, may not be as extreme as can be expected on longer slopes. The tests at Hidden Valley demonstrated that block rotation is a critical factor in causing damage to net panels, but the tests did not define the full reaction of a net panel to block rotation.

6.   The determination of the kinetic energies achieved by each individual rock block requires a detailed analysis of the high-speed video records. These video images can be evaluated manually or by the use of specialized motion-analysis software. Time constraints prevented the complete analysis of each test by either approach, and, to date, energies have been determined by manual visual analysis for only about 33% (41/125) of the tests, and by use of the motion-analysis software for 25% (32/125) of the tests. A more complete evaluation of the energies developed by individual rocks is highly desirable.

7.   The experience with the motion-analysis software demonstrated that this technology holds some promise, but that its use requires some experience and skill. The motion-analysis methods work best if the block rotation is relatively simple and in the plane of the image; that is: the block is not "wobbling" or rotating toward or away from the camera.

8.   The visual and automated preliminary analyses suggest that rotational energy of the rocks in these tests was as much as 32% of the total kinetic energy. Yet, the relationship between the amount of "spin" (or rotational energy) achieved by the rock blocks and their overall velocity (and hence total kinetic energy) is relatively complex. It is unclear if the test procedures were especially good at inducing the test rocks to rotate, as was hoped for, or if the relatively short length of the concrete ramp prior to the attenuator restricted the translational energy and thus affected the ratio between rotational and translational energy components.

9.   Individual attenuator designs were installed and subjected to a series of rockfall impacts. Each test potentially caused some damage to the attenuator. It was observed that an individual attenuator might respond to a series of relatively high-energy impacts without apparent severe damage, it might then fail when subjected to an impact with a much smaller energy. Obviously the attenuator was undergoing progressive deterioration as the series of tests progressed.

8.2   Lessons Learned Concerning Success of Attenuator Installations

The following comments are based on experiences gained at the Georgetown Incline in the period 1999–2005, observations obtained from the full-scale tests conducted at the Hidden Valley test facility in 2007–2008, and the subsequent rock-rolling exercises conducted in May 2009 with the most recently installed attenuator systems at the Georgetown Incline. In the absence of definitive design guidelines, which cannot yet be developed without further testing and analysis, the collected information is presented for consideration by practitioners interested in the installation of attenuators to mitigate rockfall hazards.

1.   The attenuator systems described in this Circular have a suspended height of 6 m (20 ft). This height was used during the tests conducted at Hidden Valley, and for the 2009 multiple attenuator installation at the Georgetown Incline. These attenuators were able to control the velocities, energies and trajectories of rockfall blocks traveling down the long and steep natural slopes with the first attenuator located no further than 150 m (500 ft) below the rockfall source area, and subsequent attenuators spaced no further apart than 150 m (500 ft) down the slope specific for the 6 m (20 foot) post heights. If an attenuator has a height less than 6 m (20 ft), then the distance between attenuators may need to be decreased. Such an arrangement, using a series

of attenuators, has the potential to prevent rockfall blocks from gaining too large a velocity, and thus translational and rotational kinetic energies that are too great for attenuator components to handle without sustaining significant damage.

2.   The design of an attenuator is related to the impact energies of the rockfall blocks arriving at the attenuator location. Frequently attenuators are impacted by multiple rockfall blocks that arrive essentially simultaneously as a group. The suspended attenuator panels and support components to be effective are constructed of materials that are sufficiently rugged to accept these multiple, near-simultaneous, impacts without excessive loss of suspended height or compromised capacity.

3.   The successful operation of these attenuator systems also depends to a considerable degree on the appropriate response of the attenuator tail components. If the tail component is too short or too light, it tends to be lifted into the air for too long a period when initially impacted, allowing subsequent blocks involved in the rockfall event to pass unaffected by the system. If the tail component is too long, then it could trap rock blocks which would reduce the flexibility of the system and compromise the intended self-cleaning characteristic of the attenuator. Selecting the appropriate length and weight-per-unit-area of attenuator tail components is a complex task because these values are related to the slope inclination; the slope characteristics; and the velocities, energies, and shapes of the rock blocks impacting the attenuator.

4.   The trajectories, velocities and kinetic energies of natural rockfall blocks are unpredictable, and are likely to vary much more than observed during full-scale tests using manufactured cuboctahedral blocks. Although highly dependent on site conditions, it should be expected that some individual rockfalls in an event will not impact a specific attenuator. For example, some blocks may bounce over a given attenuator. Constructing a series of attenuators spaced down the slope can provide system redundancy and greater confidence in achieving rockfall hazard mitigation.

5.   The combinations of panel weight, tail length, and aperture size are critical elements to the function of the attenuator system. These elements can be designed on a case-by-case basis, after considering: the local slope inclination, the available space for the tail component, the length, steepness, and characteristics of uphill distance over which the incoming rock blocks will have traveled, and the potential for debris flows and avalanches to bury the tail.

6.   A successfully operating attenuator system directs a stream of rockfall debris toward the base of the slope. A catchment area and/or rockfall barrier is needed to retain the rockfall debris prior to reaching the roadway/facility.

8.3   Future Work

The tests performed at the Hidden Valley facility were unable to answer all questions concerning the design of attenuator systems. The purpose of this Circular is to provide a description of the rationale that led to the tests being performed, to document the test facility and the tests performed, and to present the data collected during the testing.

The data are recorded in Appendix A. In addition, the video records of the tests, obtained with high-speed digital video-recording equipment, have been retained and can be made available to other researchers upon request to the authors.

As is the case with most, if not all, research endeavors, further work is desirable. There is potential for the following additional work:

1.   A complete quantitative and statistical analysis of all the data collected during the full-scale tests at Hidden Valley, including: (a) the data reported in Appendix A, (b) analysis by both manual and automated means of the video records of these tests to assess the energies achieved by each block.

2.   Further analysis of these tests using rockfall simulation software such as the Colorado Rockfall Simulation Program (CRSP) would allow a comparison of the observed energy levels developed by analysis of the video records with the predicted energy levels computed by the software. This may provide insight into the performance of the attenuators during the tests, but it would also provide further understanding of the accuracy and limitations of computer simulations.

3.   Further testing is needed before definitive attenuator design guidelines can be developed. Additional tests may address some of the limitations attributed to the Hidden Valley tests described above.

4.   Undertake additional tests to better evaluate the two major aspects of attenuator performance: (a) how the attenuator absorbs the initial impact in the "fence" portion of the system, and (b) how the "tail" portion of the system contributes to the further attenuation of the kinetic energy of the rockfall blocks as they pass through the system.

5.   It appears important that future tests evaluate the interaction between the characteristics of the attenuator "tail" and the inclination and other characteristics of the slope over which the tail is draped.

6.   Consideration could be given to additional testing to better quantify the loads placed on the bearing ropes and anchors. Simple load scales were installed at the test site but after a few tests the 44 kN (10,000 lbf) scale capacity was exceeded and the scale no longer functioned. The field designed "friction-release" devices were not studied at this time.

7.   Post spacing is a significant attribute of the system, however, due to the construction constraints of the test site there were no variations in the 6 m (20 ft) post spacing. The recently constructed attenuators at Georgetown used post spacings in excess of 15 meters (50 feet). Future testing may define a functional limit.

ACKNOWLEDGMENTS

REFERENCES

1. Andrew, R. D. Selection of Rockfall Mitigation Techniques Based on Colorado Rockfall Simulation Program. In *Transportation Research Record 1343*, TRB, National Research Council, Washington, D.C., 1992, pp. 20–22.
2. Badger, T. C., J. D. Duffy, F. Sassudelli, P.C. Ingraham, P. Perreault, B. Muhunthan, H. Radhakrishnan, O. S. Bursi, M. Molinari, and E. Castelli. Hybrid Barrier Systems for Rockfall Protection. *Proc., Interdisciplinary Workshop on Rockfall Protection* (A. Volkwein, et al., eds.*)*, Morschach, Switzerland, 2008, pp. 10–12.
3. Barrett, R. K., T. Bowen, T. Pfeiffer, and J. D. Higgins. *Rockfall Modeling and Attenuator Testing*. Colorado Department of Transportation Report CDOH-DTD-ED3/CSM-89-2. Denver, Colo., 1989.
4. Baumann, R. The Worldwide First Official Approval of Rock-Fall Protection Nets. *Proc., 53rd Annual Highway Geology Symposium*, California Department of Transportation, San Luis Obispo, Calif., 2002, pp. 40–51.
5. Duffy, J. D. *Field Testing and Evaluation of Rockfall Restraining Nets*, Report No. CA/TL-90-05 (Videos). California Dept. of Transportation, Transportation Materials and Research, Sacramento, Calif., (Video) 1990.
6. Duffy, J. D. *Field Tests and Evaluation of Flexible Rockfall Barriers*. Brugg Cable Products, Oberbuchsiten, Switzerland, 1992.
7. Duffy, J. D. *Field Tests and Evaluation of Hi-Tech Low Energy Chain Link Rockfall Fence.* Report No. CA/05-96-01. California Dept. of Transportation, San Luis Obispo, Calif., 1996.
8. Duffy, J. D., and W. Hoon. *Field Tests and Evaluation of Chain Link Fence, Gawk Screen, Fence and Jersey Barrier*. Report No. CA/05-98-01. California Dept. of Transportation, San Luis Obispo, Calif., 1998.
9. Duffy, J. D., and D. D. Smith. Field Tests and Evaluation of Rockfall Restraining Nets. *Proc., 41st Annual Highway Geology Symposium,* 1990, pp.125–142.
10. ETAG27. *Guideline for European Technical Approval of Falling Rock Kits*, (February, 2008), European Organisation for Technical Approvals, Brussels, Belgium, 2008.
11. Gerber, W. *Guideline for the Approval of Rockfall Protection Kits*. Swiss Agency for the Environment, Forests and Landscapes (SAEFL), and the Swiss Federal Institute (WSL), Berne, Switzerland, 2001. www.environment-switzerland.ch/publications.
12. Gerber, W., and B. Haller. Safe and Economical Rockfall Protection Barriers. *Proc., Congress Environmental and Safety in Underground Construction,* Balkema, Rotterdam, 1997, pp. 915–920.
13. Gerber W., H. Grassl, A. Böll, and W. Ammann. Flexible Rockfall Barriers–Development, Standardisation and Type-Testing in Switzerland. In *International Conference on Landslides–Causes, Impacts and Countermeasure*. (M. Kuehne, H. H. Einstein, E. Krauter, H. Klapperich, and R. Poettler, eds.)*, 17-21 June 2001, Davos, Switzerland,* Verlag Glueckauf Gmbh, Essen, 2001, pp. 515–524.
14. Higgins, J. D. *Recommended Procedures for the Testing of Rockfall Barriers*. Report prepared as part of NCHRP Project 20-07, Task 138, National Cooperative Highway Research Program, Transportation Research Board, Washington, D.C., 2003.
15. Kane, W. F., and J. D. Duffy. *Brugg Low Energy Wire Rope Rockfall Net Field Tests*. Technical Research Report 93-01. Dept. of Civil Engineering, University of the Pacific, 1993.
16. Muhunthan, B., and H. Radhakrishnan. *Finite Element Analysis of Hybrid Barrier for Rock Fall Slope Protectio*n. Final Report, Department of Civil and Environmental Engineering, Washington State University, 2007.
17. Muraishi, H., and S. Sano. Full-Scale Rockfall Test of Ring Net Barrier and Components. In *Seminar of Rockfall Tests and Standardization*, Davos, Switzerland, 1999.
18. Peila, D., S. Pelizza, and F. Sassudelli. Evaluation of Behavior of Rockfall Restraining Nets by Full Scale Tests. In *Rock Mechanics and Rock Engineering*, Springer-Verlag, Vol. 31, No.1, 1998, pp. 1–24.

19. Pfeiffer, T. J. *Rockfall Hazard Analysis Using Computer Simulation of Rockfalls.* Master of Engineering Report, Colorado School of Mines, Golden, Colo., 1989.
20. Pfeiffer, T. J., and J. D. Higgins. Rockfall Hazard Analysis Using the Colorado Rockfall Simulation Program. In *Transportation Research Record 1288*, TRB, National Research Council, Washington, D.C., 1990, pp. 117–126.
21. *ProAnalyst User Guide*, Xcitex, Inc., Cambridge, Massachusetts, 2007.
22. Yeh and Associates, Inc. *I-70 Georgetown Incline Rockfall Mitigation Feasibility Study*. Consulting Report to Colorado Department of Transportation, Region 1, 2005.

APPENDIX A

Tabulations of Hidden Valley Test Data

A total of 125 tests were conducted at the Hidden Valley test facility to evaluate the alternative attenuator systems constructed with 11 different materials (using a total of 113 tests) and two types of post-to-base connections (using an additional 12 tests). Time constraints have not permitted a complete quantitative analysis or statistical evaluation of the observational data.

However, a number of analyses have been completed. The results of these analyses are discussed under four main categories:

- Appendices B, C, and D contain evaluations of kinetic energies produced by analyzing the high-speed video recordings of the tests, using both visual analysis methods and motion-analysis software. These are discussed further in Section 6.1 of the Circular.
- Appendix E provides an assessment of the attenuator reactions to the initial impacts by rockfall blocks. These are discussed further in Section 6.2 of the Circular.
- Appendix F provides assessments of the reactions of the attenuator tail components to the passage of rockfall blocks. These are discussed further in Section 6.3 of the Circular.
- Evaluations of post-to-base connections are discussed in Section 6.4 of the Circular.

One of the objectives in publishing this Circular is to provide access to these observations and to document the testing facilities and methods used to collect the observations. By providing these observational data along with descriptions of the "context" in which they were obtained, it is hoped that others will be able to undertake additional analyses and evaluations. These tests were not able to evaluate all of the many factors that influence the response of these attenuator systems to rockfall events. Additional test sequences will provide more information.

This appendix contains tabulations of the results obtained from the tests. Table A-1 documents the codes used within the Tables A-2, A-3, and A-4. Tables A-2 and A-3 summarize the observations for the 113 tests used to evaluate the alternative attenuator systems constructed with 11 different materials. Table A-2 provides information describing the attenuator configurations and their reactions to rock impacts; Table A-3 provides quantitative kinetic energy estimates developed by initial evaluations of high-speed video recordings and observations of rock bounce height and reactions of panel tail components to each test impact.

Table A-4 contains the recorded observations for the 12 tests used to evaluate the two types of post-to-base connections, and repeats and expands upon the data contained within Table 7 of the Circular.

Tables A-2 and A-3 have been produced from the original project database contained as an Excel file that can be obtained by contacting the authors using the following e-mail addresses:

Ben Arndt: barndt@yeh1.net
Ty Ortiz: ty.ortiz@dot.state.co.us
A. Keith Turner: kturner@mines.edu

TABLE A-1 Explanation of Codes
Used in Tables A-2, A-3, and A-4

Test Rock Mass Key:	
Rock Mass Code:	*kg*
A	1618
B	1695
C	1577
D	2259
E	2173
F	3823
J	227

Rock Action Key:	
Observation:	*Key*
Rotation Reversed	RR
Released	R
Missed Net	MN
Rolled Through	RT
Stopped	S
Skimmed Net	SN
Stopped Rotation	SR
Bounced Over Net	BON

Slope Protection Key:	
Observation:	*Key*
Blast Mat	BM
Conveyor Belt	CB
Magic Carpet	MC

Rock Release Velocity Key:	
Observation:	*Key*
Stuck in Net	ST
Released and Stopped	RS
Slowly Rolled Away	SL
Rolled Away with Speed	F

Panel Tail Vertical Height at End of Test:	
Observation:	*Key*
0-1 m (0-3 ft)	Very Low
1-2 m (3-6 ft)	Low
2-3 m (6-9 ft)	Medium
3-4 m (9-12 ft)	High
> 4 m(> 12 ft)	Very High

Net Damage Key:	
Observation:	*Key*
Negligable	Neg
Minor (<0.3 m (1 ft) rips/opening)	Min
Significant (>0.3 m (1 ft) rip/opening	Sig
Remove/Replace Needed	Rep

Net Stretch Key:	
Observation:	*Key*
Negligable (0-0.7 m (0-2 ft))	Neg
Minor (0.7-2 m (2-6 ft))	Min
Significant (> 2 m(> 6 ft))	Sig

TABLE A-2 Tabulation of 113 Tests Conducted to Evaluate Alternative Attenuator Systems Constructed with 11 Different Materials: Attenuator Configurations and Reactions to Rock Impacts

Test No.	Date	Net Type	Approx Material Strand Diameter (mm)	Approx Panel Aperture Opening (mm)	Orientation or Long Axis Direction	Clip Type	Rock Size	Drop Height (ft)	Post Connect Height (ft)	Tail Length (ft)	Panel Width (ft)	Rock Action	Rock Release Velocity	Panel Tail Time in Air (sec)	Net Damage	Net Stretch
1	11/26/2007	Cable Net	8	150	Diagonal	Overlap	B	30	20	15	20	RR, R	SL	1.40	Neg	Neg
2	11/26/2007	Cable Net	8	150	Diagonal	Overlap	B	30	20	15	20	SN	F	N/A	N/A	N/A
3	11/27/2007	Cable Net	8	150	Diagonal	Overlap	B	30	20	15	20	RR, S	ST	1.30	Neg	Neg
4	11/27/2007	Cable Net	8	150	Diagonal	Overlap	B	60	20	15	20	RT	F	1.84	Neg	Neg
5	11/27/2007	Cable Net	8	150	Diagonal	Overlap	B	60	20	25	20	RR, S	ST	0.27	Neg	Neg
6a	11/27/2007	Cable Net	8	150	Diagonal	Overlap	B	90	20	25	20	MN	N/A	N/A	N/A	N/A
6b	11/27/2007	Cable Net	8	150	Diagonal	Overlap	B	90	20	25	20	SN	F	N/A	NA	NA
1	12/5/2007	Cable Net	8	150	Square	Interlocking	B	30	20	15	20	RR, R	SL	1.17	Neg	Neg
2	12/5/2007	Cable Net	8	150	Square	Interlocking	B	60	20	15	20	RR, R	SL	1.56	Neg	Neg
3	12/5/2007	Cable Net	8	150	Square	Interlocking	B	90	20	15	20	RT	F	1.98	Neg	Neg
4	12/6/2007	Cable Net	8	150	Square	Interlocking	B	30	20	15	20	RR, R	RS	1.56	Min	Neg
5	12/6/2007	Cable Net	8	150	Square	Interlocking	B	60	20	15	20	RR, R	SL	1.78	Min	Neg
6	12/6/2007	Cable Net	8	150	Square	Interlocking	B	30	20	25	20	RR, S, R	RS	1.63	Min	Neg
7	12/6/2007	Cable Net	8	150	Square	Interlocking	B	30	20	25	20	RR, S	ST	0.95	Min	Neg
8	12/6/2007	Cable Net	8	150	Square	Interlocking	B	60	20	25	20	MN	N/A	N/A	N/A	N/A
9	12/6/2007	Cable Net	8	150	Square	Interlocking	B	60	20	25	20	SN.RT	F	N/A	Neg	Neg
10	12/10/2007	Cable Net	8	150	Square	Interlocking	B	60	20	25	20	RR, S	ST	0.31	Neg	Neg
11	12/12/2007	Cable Net	8	150	Square	Interlocking	B	60	20	25	20	RR, S	ST	0.22	Sig	Neg
12	12/13/2007	Cable Net	8	150	Square	Interlocking	D	30	20	15	20	SN, RT	F	N/A	Neg	Neg
13	12/13/2007	Cable Net	8	150	Square	Interlocking	D	30	20	15	20	SN, RT	F	N/A	NA	NA
14	12/13/2007	Cable Net	8	150	Square	Interlocking	D	30	20	15	20	RR, R	SL	1.29	Min	Neg
15	12/14/2007	Cable Net	8	150	Square	Interlocking	D	60	20	15	20	SN, RT	F	N/A	NA	NA
16	12/14/2007	Cable Net	8	150	Square	Interlocking	D	60	20	12	20	SR, R	F	2.22	Neg	Neg
17	12/14/2007	Cable Net	8	150	Square	Interlocking	D	60	20	15	20	SR, R	F	0.93	Sig	Min
18	12/14/2007	Cable Net	8	150	Square	Interlocking	D	30	20	18	20	RR, R	ST	1.43	Neg	Neg
19	12/17/2007	Cable Net	8	150	Square	Interlocking	D	60	20	18	20	RR, R	SL	1.90	Neg	Neg
20	12/18/2007	Cable Net	8	150	Diagonal	Overlap	D	30	20	18	60	RT	SL	1.62	Min	Min
21	12/18/2007	Cable Net	8	150	Diagonal	Overlap	D	30	20	18	60	SR, R	SL	1.73	Min	Neg
22	12/18/2007	Cable Net	8	150	Diagonal	Overlap	D	60	20	18	60	RR, R	RS	1.44	Sig	Min
23	12/19/2007	Cable Net	8	150	Diagonal	Overlap	D	30	20	25	60	RR, R	RS	1.09	Neg	Min
24	12/19/2007	Cable Net	8	150	Diagonal	Overlap	D	60	20	30	60	RR, S	ST	0.00	Min	Min
25	12/20/2007	Cable Net	8	150	Diagonal	Overlap	D	60	20	25	60	RR, S	ST	0.00	Neg	Neg
26	12/20/2007	Cable Net	8	150	Diagonal	Overlap	B	60	20	25	60	RR, S	ST	0.00	N/A	N/A
27	12/20/2007	Cable Net	8	150	Diagonal	Overlap	D	90	20	25	60	RR, S	ST	0.00	Neg	Neg
28	12/21/2007	Ring Net	7/2/350	350	N/A	None	D	30	20	15	20	SN, RT	F	N/A	N/A	N/A
29	12/21/2007	Ring Net	7/2/350	350	N/A	None	D	30	20	15	20	RR, S	ST	1.68	Min	Sig
30	12/21/2007	Ring Net	7/2/350	350	N/A	None	D	30	20	15	20	RR, R	SL	1.74	NA	NA
31	12/21/2007	Ring Net	7/2/350	350	N/A	None	D	60	20	15	20	SN.RT	F	N/A	Neg	Neg
32	12/21/2007	Ring Net	7/2/350	350	N/A	None	D	60	20	15	20	RR, R	SL	1.51	Min	Min
33	1/2/2008	Ring Net	7/2/350	350	N/A	None	E	30	10	10	60	RR, R	SL	1.52	Min	Min
34	1/3/2008	Ring Net	7/2/350	350	N/A	None	E	30	10	15	60	RR, R	RS	2.03	Neg	Min
35	1/3/2008	Ring Net	7/2/350	350	N/A	None	C	60	10	15	60	RR, S	ST	0.00	Neg	Min
36	1/8/2008	Cable Rings	8	350	N/A	Ferrule	C	60	10	5	60	RR, S	ST	0.00	Min	Sig
37	1/8/2008	Cable Rings	8	350	N/A	Ferrule	C	60	10	7	60	RT	F	N/A	Rep	Sig
38	1/9/2008	Ring Net	7/3/300	300	N/A	**Pressed**	C	60	10	5	60	RR, R	RS	1.72	Min	Min
39	1/9/2008	Ring Net	7/3/300	300	N/A	**Pressed**	C	60	10	5	60	RR, S	ST	1.06	Sig	Sig
40	1/10/2008	**Spiral Wire Net**	4	230	Vertical	N/A	C	60	10	5	55	RT	F	1.79	Neg	Min
41	1/10/2008	**Spiral Wire Net**	4	230	Vertical	N/A	C	60	10	10	55	SON	N/A	N/A	N/A	N/A
42	1/10/2008	**Spiral Wire Net**	4	230	Vertical	N/A	C	60	10	10	55	RT	F	1.46	Rep	Min
43	1/11/2008	**Spiral Wire Net**	4	230	Vertical	N/A	C	60	10	5	55	RT	F	1.45	Neg	Min

(continued)

TABLE A-2 *(continued)* **Tabulation of 113 Tests Conducted to Evaluate Alternative Attenuator Systems Constructed with 11 Different Materials: Attenuator Configurations and Reactions to Rock Impacts**

Test No.	Date	Net Type	Approx Material Strand Diameter (mm)	Approx Panel Aperture Opening (mm)	Orientation or Long Axis Direction	Clip Type	Rock Size	Drop Height (ft)	Post Connect Height (ft)	Tail Length (ft)	Panel Width (ft)	Rock Action	Rock Release Velocity	Panel Tail Time in Air	Net Damage	Net Stretch
44	1/11/2008	**Spiral Wire Net**	4	230	Vertical	N/A	C	60	10	25	55	RT	N/A	N/A	Neg	Min
45	1/11/2008	**Spiral Wire Net**	4	230	Vertical	N/A	C	60	10	30	55	RR, R	SL	0.34	Rep	Min
46	1/14/2008	Cable Net	12	205	Diagonal	Overlap	C	60	10	7	60	RR, R	SL	1.26	Sig	Neg
47	1/14/2008	Cable Net	12	205	Diagonal	Overlap	C	60	10	7	60	S	ST	1.38	Rep	Neg
48	1/15/2008	Cable Net	12	205	Diagonal	Overlap	B	60	10	10	60	RR, R	SL	1.49	Min	Neg
49	1/15/2008	Cable Net	12	205	Diagonal	Overlap	B	60	10	10	60	BON	N/A	N/A	N/A	N/A
50	1/15/2008	Cable Net	12	205	Diagonal	Overlap	B	60	10	10	60	S	ST	1.06	Rep	Neg
51	1/15/2008	Cable Net	12	205	Diagonal	Overlap	B	60	10	10	60	RT	F	1.56	Neg	Neg
52	1/15/2008	Cable Net	12	205	Diagonal	Overlap	B	60	10	15	60	RT	F	1.55	Min	Neg
53	1/15/2008	Cable Net	12	205	Diagonal	Overlap	B	60	10	15	60	RR, R	SL	1.02	Sig	Neg
54	1/15/2008	Cable Net	12	205	Diagonal	Overlap	B	60	10	15	60	RR, R	SL	1.22	Min	Neg
55	1/16/2008	Cable Net	12	205	Diagonal	Wire Wrap	B	60	10	10	60	RR, R	SL	1.34	Neg	Min
56	1/16/2008	Cable Net	12	205	Diagonal	Wire Wrap	B	60	10	10	60	RR, S	ST	0.00	Neg^	Min
57	1/16/2008	Cable Net	12	205	Diagonal	Wire Wrap	B	60	10	10	60	RR, R	SL	1.48	Min	Min
59	1/16/2008	Cable Net	12	205	Diagonal	Wire Wrap	B	60	10	15	60	RR, R	SL	1.04	Min	Neg
58	1/17/2008	Cable Net	12	205	Diagonal	Wire Wrap	B	60	10	15	60	SR, R	F	1.44	Neg	Neg
60	1/17/2008	Cable Net	12	205	Diagonal	Wire Wrap	B	60	10	15	60	RR, R	SL	0.85	Neg	Neg
61	1/17/2008	Cable Net	12	205	Diagonal	Wire Wrap	B	60	10	20	60	BON	N/A	N/A	N/A	N/A
62	1/17/2008	Cable Net	12	205	Diagonal	Wire Wrap	B	60	10	20	60	RR, S	ST	0.00	Min	Neg
63	1/17/2008	Cable Net	12	205	Diagonal	Wire Wrap	B	60	10	20	60	RR, R	SL	0.95	Neg	Neg
64	1/17/2008	Cable Net	12	205	Diagonal	Wire Wrap	B	60	10	20	60	RR, R	SL	1.07	Neg	Neg
65	1/21/2008	4 mm wire	4	64	Vertical	N/A	A	60	10	15	56	RT	F	1.36	Min	Min
66	1/21/2008	4 mm wire	4	64	Vertical	N/A	A	60	10	20	56	RT	F	1.45	Neg	Min
67	1/21/2008	4 mm wire	4	64	Vertical	N/A	A	60	10	20	56	BON	N/A	N/A	N/A	N/A
68	1/21/2008	4 mm wire	4	64	Vertical	N/A	A	60	10	20	56	RT	F	N/A	Rep	Sig
69	1/21/2008	4 mm wire	4	64	Vertical	N/A	A	0	10	20	56	RT	F	1.13	Neg	Neg
70	1/22/2008	4 mm wire	4	64	Vertical	N/A	A	60	10	30	56	BON	N/A	N/A	N/A	N/A
71	1/22/2008	4 mm wire	4	64	Vertical	N/A	A	60	10	30	56	BON	N/A	N/A	N/A	N/A
72	1/22/2008	4 mm wire	4	64	Vertical	N/A	A	60	10	30	56	RT	F	N/A	Sig	Neg
73	1/22/2008	4 mm wire	4	64	Vertical	N/A	A	60	10	30	56	RT	F	N/A	Rep	Neg
84	1/25/2008	4 mm wire	4	64	Horizontal	N/A	A	30	10	20	50	RR, R	F	N/A	Sig	Neg
85	1/25/2008	4 mm wire	4	64	Horizontal	N/A	A	60	10	20	50	SR, R	SL	0.91	Neg	Min
86	1/25/2008	4 mm wire	4	64	Horizontal	N/A	A	60	10	20	50	RR, R	SL	1.60	Min	Neg
87	1/25/2008	4 mm wire	4	64	Horizontal	N/A	A	60	10	20	50	RR, R	SL	1.86	Min	Neg
101	10/3/2008	Chain Link	3	50	Horizontal	N/A	B	30	10	15	60	RU	F	1.61	Neg	Neg
102	10/3/2008	Chain Link	3	50	Horizontal	N/A	B	60	10	15	60	RU	F	1.62	Neg	Neg
103	10/3/2008	Chain Link	3	50	Horizontal	N/A	B	30	10	25	60	RR/R	SL	1.14	Neg	Neg
104	10/3/2008	Chain Link	3	50	Horizontal	N/A	B	60	10	25	60	RR/R	SL	1.38	Neg	Neg
105	10/6/2008	Chain Link	3	50	Horizontal	N/A	B	60	10	25	60	RT	F	1.27	Neg	Neg
106	10/6/2008	Chain Link	3	50	Horizontal	N/A	B	60	10	25	60	RR/R	SL	1.17	Neg	Neg
107	10/6/2008	Chain Link	3	50	Horizontal	N/A	B	60	10	35	60	RR/R	SL	0.74	Neg	Neg
108	10/6/2008	Chain Link	3	50	Horizontal	N/A	B	60	10	35	60	RR/R	RS	0.97	Neg	Neg
109	10/6/2008	Chain Link	3	50	Horizontal	N/A	E	30	10	35	60	SR/R	SL	0.79	Neg	Neg
110	10/6/2008	Chain Link	3	50	Horizontal	N/A	E	60	10	35	60	RT	F	N/A	Rep	Neg
111	10/8/2008	Chain Link	3	50	Vertical	N/A	B	60	10	25	60	RU	F	1.31	Neg	Neg
112	10/8/2008	Chain Link	3	50	Vertical	N/A	B	60	10	25	60	RU	F	1.50	Neg	Neg
113	10/8/2008	Chain Link	3	50	Vertical	N/A	B	60	10	30	60	RR/R	RS	N/A	Neg	Neg
114	10/8/2008	Chain Link	3	50	Vertical	N/A	B	60	10	30	60	RR/R	RS	1.33	Neg	Neg
115	10/8/2008	Chain Link	3	50	Vertical	N/A	E	60	10	30	60	SR/S	ST	0.00	Neg	Neg
116	10/9/2008	Spiral Wire Net	4	130	Horizontal	N/A	B	60	10	23	60	RR/S	ST	0.00	Neg	Min
117	10/9/2008	Spiral Wire Net	4	130	Horizontal	N/A	*B*	60	10	23	60	RR/R	RS	1.31	Neg	Min
118	10/9/2008	Spiral Wire Net	4	130	Horizontal	N/A	B	60	10	23	60	RR/S	ST	0.00	Neg	Min
119	10/9/2008	Spiral Wire Net	4	130	Horizontal	N/A	E	60	10	23	60	RR/S	ST	0.00	Neg	Min

TABLE A-3 Tabulation of 113 Tests Conducted to Evaluate Alternative Attenuator Systems Constructed with 11 Different Materials: Energy Estimates, Reactions of Panel Tail Components to Rock Impacts, and Observed Rock Bounce Heights

Test No.	Rotation From Top Ramp to Panel Impact	Visual Trans KE (kJ)	Visual Rot KE (kJ)	% Rot KE	Visual Total KE (kJ)	Pro Analyst Trans KE (kJ)	Pro Analyst Rot KE (kJ)	% Rot KE	Pro Analyst Total KE (kJ)	Alt. Pro Analyst Trans KE (kJ)	Alt. Pro Analyst Rot KE (kJ)	%Rot KE	Alt. Pro Analyst Total KE (kJ)	Compare Total KE	Compare Trans KE	Panel Tail Vertical Height at End Test	Panel Tail Time In Air	Bounce Height
1	2.50	136.3	7.5	5.2%	143.8	58.6	44.0	42.9%	102.6	124.0	44.0	26.2%	168.0	-14.1%	-9.9%	High	1.40	1
2	2.50	253.5	99	3.8%	263.4											N/A	N/A	0
3	4.00	358.5	3S.7	9.7%	397.2											Medium	1.30	2
4	4.25	278.3	46.3	1+3%	324.6	128.5	82.3	32.7%	190.7	361.4	62.3	14.7%	423.7	-23.4%	23.0%	Very High	1.84	1
5	3.25	479.3	25.4	5.0%	504.7											Very Low	0.27	4
6a	N/A				N/A											N/A	N/A	N/A
6b	3.00				N/A											N/A	N/A	N/A
1	4.00	145.9	32.8	1S1%	178.7	67 .4	28.6	29.8%8	96.1	209.4	28.6	12.0%	238.0	-21.9%	30.3%	Medium	1.17	4
2	2.25	479.3	16.9	3.4%	496.2											High	1.56	10
3	300	424.6	28.1	6.2%	152.7											Very High	1.98	0
4	1.25	378.7	3.4	0.9%	382.2											Low	1.56	3
5	4.25	232.0	45.1	16.3%	277.1											Very High	1.78	0.5
6	4.00	181.5	37.7	17.2%	219.3											Very Low	1.63	2
7	4.25	213.0	32.0	13.1%	245.1											Very Low	0.95	1
8	N/A	378.7	3.5	0.9%	382.2											N/A	N/A	N/A
9	3.00	339.9	28.7	7.B%	368.6											N/A	N/A	0
1C	2.00	339.9	14.6	4.1%	354.5											Very Low	0.31	1
11	2.75	232.0	43.9	15.9%	275.9											Very Low	0.22	2
12	1.75	309.1	33.9	9.9%	343.0											N/A	N/A	2
13	0.25	337.8	2.5	0.7%	340.3											N/A	N/A	1
14	2.00	309.1	23.3	7.0%	332.4											Low	1.29	2
15	2.25	967.5	39.3	3.9%	1005.8											N/A	N/A	7
16	3.75	309.1	103.3	250%	412.4	363.2	34.5	8.7%	397.6	374.6	34.5	8.4%	409.1	0.8%	17.5%	Very High	2.22	2
17	3.25	6367	65.7	9.3%	704.4											Very Low	0.93	5
16	1.50	75.6	35.4	31.9%	111.0											Medium	.43	0
19	1.00															Very High	.90	1
20	3.25															Very High	.62	1
21	3.50	241.9	48.3	16.6%	290.2	238.8	41.4	12.5%	330.2	472.4	41.4	8.1%	513.8	-43.5%	48.8%	Very High	.73	0
22	1.25	408.8	12.3	39%	421.1	279.2	13.7	4.7%	292.9	505.1	13.7	2.6%	518.8	-18.8%	19.1%	High	.44	2
23	3.50	370.8	57.2	134%	428.0	178.5	74.7	29.5%	253.2	367.9	747	16.9%	442.6	-3.3%	-0.8%	Medium	1.09	1
24	2.50															Very Low	0.00	0
25	2.50															Very Low	0.00	8
26	4.00															Very Low	0.00	1
27	2.25	152.9	49.3	9.8%	502.2											Very Low	0.00	12
2B	1.50															N/A	N/A	0
29	2.50															Low	i.ea	1
30	2.00															Medium	1.74	1
31	3.35															N/A	N/A	6
32	1.25															Low	1.51	0
33	2.25															Medium	1.52	1
3d	2.25															Very Low	2.03	2
35	3.00															Very Low	0.00	1
36	2.75	445.9	37.8	7.8%	483.7	239.6	33.3	12.2%	3729	440.3	33.3	7.0%	473.6	2.1%	-1.3%	Very Low	0.00	6
37	3.25															N/A	N/A	9
38	2.75	285.4	21.8	7 1%	307.2	227.7	14.5	6.0%	242.3	174.1	14.5	7.7%	188.6	62.9%	-63.9%	Very High	1.72	2
33	4.00															Very Low	1.06	5
40	3.25															Very High	1.79	4
41	2.75															N/A	N/A	10
43	4.00	182.7	67.8	27.1%	250.4	99.8	67.6	40.4%	1673	224.3	67.6	23.2%	291.9	-14.2%	18.5%	Medium	1.46	0
43	2.50															Very High	1.45	4

(continued)

TABLE A-3 *(continued)* **Tabulation of 113 Tests Conducted to Evaluate Alternative Attenuator Systems Constructed with 11 Different Materials: Energy Estimates, Reactions of Panel Tail Components, and Observed Rock Bounce Heights**

Test No.	Rotation From Top Ramp to Panel Impact	Visual Trans KE (kJ)	Visual Rot KE (kJ)	% Rot KE	Visual Total KE (kJ)	Pro Analyst Trans KE (kJ)	Pro Analyst Rot KE (kJ)	% Rot KE	Pro Analyst Total KE (kJ)	Alt. Pro Analyst Trans KE (kJ)	Alt. Pro Analyst Rot KE (kJ)	% Rot KE	Alt. Pro Analyst Total KE (kJ)	Compare Total KE	Compare Trans KE	Panel Tail Vertical Height at End Test	Panel Tail Time in Air	Bounce Height
44	N/A															N/A	N/A	N/A
45	4.00	285.4	42.0	12.8%	327.3	190.2	41.1	17.8%	231.3	348.5	41.1	10.5%	389.6	-16.0%	18.1%	Very Low	0.34	1
46	2.75	316.2	38.8	10.9%	355.0	114.5	42.8	27.2%	157.4	267.7	42.8	13.8%	310.6	14.3%	-18.1%	Low	1.26	7
47	3.25	258.9	35.1	11.9%	294.0	164.9	32.6	16.5%	197.5	268.8	32.6	10.8%	301.4	-2.5%	3.7%	High	1.38	1
48	1.25															Low	1.49	1
49	2.75															N/A	N/A	12
50	2.00															Low	1.06	6
51	1.00															Very High	1.56	2
52	2.00															High	1.55	1
53	1.75															Medium	1.02	3
54	1.00															Medium	1.22	2
55	2.25															Medium	1.34	2
56	1.25															Very Low	0.00	8
57	2.25															Medium	1.48	1
59	1.75															High	1.44	0
58	2.75	378.7	37.7	9.1%	416.5	304.1	30.9	9.2%	335.0	439.9	30.9	6.6%	470.9	-11.6%	13.9%	Low	1.04	3
60	3.50	196.3	47.6	19.5%	243.9	137.6	67.9	33.0%	205.6	178.8	67.9	27.5%	246.8	-1.2%	-9.8%	Very Low	0.85	6
61	2.25															N/A	N/A	10
62	3.25															Very Low	0.00	7
63	2.50															Very Low	0.95	4
64	3.00	232.0	34.3	12.9%	266.3	100.5	29.5	22.7%	130.0	207.1	29.5	12.5%	236.6	12.6%	-12.0%	Low	1.07	4
65	2.75															High	1.36	8
66	2.75															High	1.45	7
67	3.00															N/A	N/A	10
68	2.75	293.6	43.2	12.8%	336.8	191.7	42.2	18.0%	233.9	110.3	42.2	27.7%	152.5	120.9%	-166.2%	N/A	N/A	4
69	2.00															Low	1.13	0
70	3.00															N/A	N/A	10
71	3.25															N/A	N/A	10
72	3.50	325.3	38.9	10.7%	364.2	186,0	45.5	19.7%	231.5	378.4	45.5	10.7%	423.9	-14.1%	14.0%	N/A	N/A	0
73	3.25	266.3	38.9	12.7%	305.2	152.8	51.1	25.1%	203.9	300.3	51.1	14.5%	351.4	-13.1%	11.3%	N/A	N/A	2
84	3.25															-	-	2
85	5.00															-		0
86	4.00															-		3
87	2.50															-	-	0
101	2.50															-	-	0
102	2.50															-		2
103	3.75															-		2
104	3.50															-	-	0
105	3.50															-		1
106	2.50															-	-	1
107	2.75															N/A	N/A	7
108	3.25	203.9	34.4	12.1%	283.3	194.7	23.9	10.9%	218.6	198.6	23.9	10.7%	222.6	27.3%		Low	0.91	7
109	2.75	266.3	21.6	7.5%	287.9	201.3	64.9	24.4%	266.1	194.3	64.9	25.0%	259.2	11.1%		Very High	1.60	4
110	3.50															Low	1.86	0
111	2.25															Very High	1.61	0
112	2.50															Very High	1.62	0
113	1.00															Medium	1.14	0
114	2.25															High	1.38	1
115	1.25															High	1.27	5
116	2.25						202.8	15.6	7.1%	218.4	306.6	15.6	4.8%	322.2			High	1.17	2
117	1.75						238.5	6.9	2.8%	245.4	426.7	6.9	1.6%	433.6			Low	0.74	3
118	2.00															Low	0.97	0
119	2.00															Low	0.79	0

TABLE A-4 Summary of 12 Tests Conducted to Evaluate Post-to-Base Connections

Test No.	Date	Post Foundation	Rock	Drop Ht. (ft)	Pro Analyst Trans KE (kJ)	Pro Analyst Rot KE (kJ)	% Rot KE	Pro Analyst Total KE (kJ)	Alt. Pro Analyst Trans KE (kJ)	Alt. Pro Analyst Rot KE (kJ)	% Rot KE	Alt. Pro Analyst Total KE (kJ)	Bounce Height	Comments
120	10/13/2008	Pinned	B	15	94.7	15.3	16.2%	94.7	189.3	0.0	0.0%	189.3	2	Direct Hit - 3 uphill anchors - Post Not Functional
121	10/13/2008	Fixed	A	15									2	Missed
122	10/13/2008	Fixed	A	15	57.1	13.5	19.1%	70.5	163.4	13.5	7.6%	176.9	3	Direct Square Hit - 1 uphill anchor - Post Functional
123	10/14/2008	Fixed	A	15									2.5	Glancing Hit - 3 Uphill Tiebacks - Post Functional
124	10/14/2008	Fixed	A	15									5	Glancing Hit - 2 Uphill Tiebacks - Post Functional
125	10/14/2008	Fixed	A	15	48.8	15.3	23.9%	64.1	147.2	15.3	9.4%	162.5	5	Direct Hit - 2 Uphill Tiebacks - Post Functional
126	10/14/2008	Fixed	A	15									3	Direct Hit - 1 Uphill Tieback - Post Functional
127	10/14/2008	Fixed	E	15									3.5	Glancing Hit - 1 Uphill Tieback - Post Functional
128	10/14/2008	Fixed	E	15									N/A	Missed
129	10/14/2008	Fixed	E	15	121.7	14.1	10.4%	135.9	211.5	14.1	6.3%	225.6	3.5	Direct Hit - 1 Uphill Tieback - Post Functional
130	10/14/2008	Fixed	F	15									4.5	Direct Hit - 1 Uphill Tieback - Post Functional
131	10/14/2008	Fixed	F	60	368.0				920.5	0.0	0.0%	920.5	8	Direct Hit - 1 Uphill Tieback - Post Not Functional

NOTE: This table repeats and expands information reported in the main text of this circular as Table 7.

APPENDIX B

Energy Analysis Based on Visual Methods

K inetic energy estimates have been evaluated for a selection of 41 tests by analysis of the high-speed video records using visual evaluation methods of individual frames. These results were extracted from the Xcel database (Appendix A) and analyzed using Version 15 of the Minitab statistical software.

For the 41 tests evaluated so far, translational kinetic energies impacting the attenuator or posts mostly range from approximately 75-460 kJ (28-170 ft-tons), with only two tests exceeding this range. Figure B-1 summarizes these results. Rotational kinetic energies mostly range from nearly zero to about 64 kJ (24 ft-tons), with one test producing a maximum rotational kinetic energy of 103 kJ (38 ft-tons). The ratio of the rotational kinetic energy compared to the total kinetic energy averages about 11%, and ranges from less than 1% to about 32%. Figures B-2 and B-3 illustrate the distribution of rotational and total kinetic energies.

Linear regression analysis (Figures B-4 and B-5) evaluates the relationship between the achieved rotational kinetic energy and the total kinetic energy. Figure B-4 illustrates the relationship between the percentage of rotational kinetic energy to the total kinetic energy (on the Y axis) and the total kinetic energy (on the X axis). A linear regression fitted to this relationship is significant at the 95% confidence level. Although there is a large scatter to the data, and the regression only "explains" 18.3% of the variability in the data, it shows a downward trend – that is the ratio of the rotational energy to the total energy declines as the total energy increases. In contrast, the relationship between rotational energy and total energy (Figure B-5) is not significant at the 95% confidence level. The trend line is essentially horizontal and "explains" only 2.1% of the data variability.

These results show that the amount of rotational energy achieved during individual tests is relatively constant, and does not increase as the total energy increases. The design of the test facility was intended to produce rotating rocks. It appears to have done so, at least to a certain degree. However, the overall limited size of the test facility apparently does not permit the test rocks to achieve increased rates of rotation (or spin) as their overall velocity down the slope increased.

1. Descriptive Statistics (based on 41 tests):

Translational KE (kJ)
```
     N  Mean SE Mean StDev Median Minimum Maximum
    41 322.2    23.3 149.1  309.1    75.6   967.5
```
Rotational KE (kJ)
```
     N  Mean SE Mean StDev Median Minimum Maximum
    41 34.75    2.99 19.12  35.40    2.50  103.30
```
Total KE (kJ)
```
     N  Mean SE Mean StDev Median Minimum Maximum
    41 358.0    23.4 149.9  336.8   111.0  1005.8
```
%Rotational energy/total energy
```
     N  Mean SE Mean StDev Median Minimum Maximum
    41 10.92    1.08  6.94   9.88    0.73   31.89
```

Translational Kinetic Energy Determined by Visual Methods (41 tests)
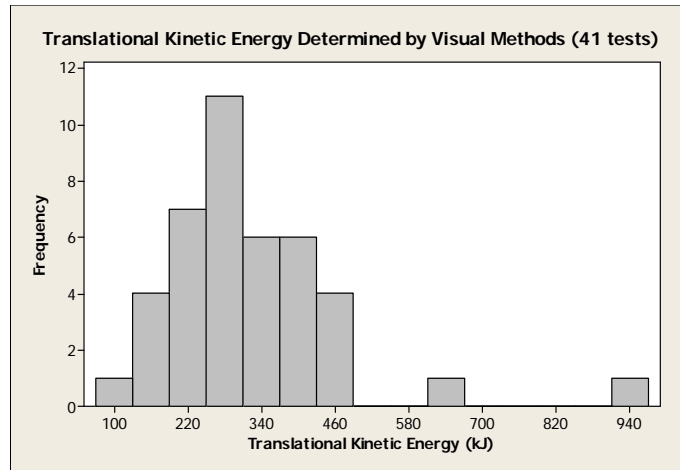
FIGURE B-1 Histogram of translational kinetic energy determined for 41 tests by visual analysis of video records.

Rotational Kinetic Energy Determined by Visual Methods (41 tests)
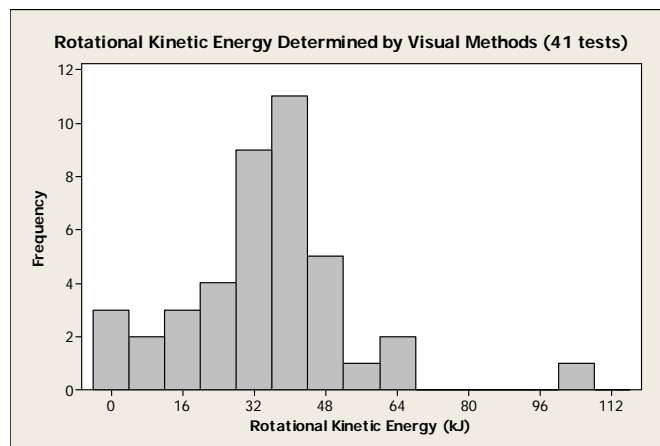
FIGURE B-2 Histogram of rotational kinetic energy determined for 41 tests by visual analysis of the video records.

Total Kinetic Energy Determined by Visual Methods (41 tests)
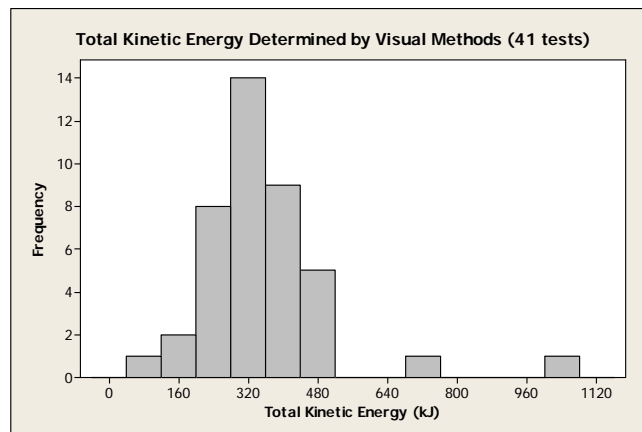
FIGURE B-3 Histogram of total kinetic energy determined for 41 tests by visual analysis of the video records.

2. Evaluation of Relationships Between % Rotational KE/Total KE and Total KE

The regression equation is
```
% Rotational KE/Total KE = 18.01 - 0.01981 Total KE
S = 6.35154  R-Squared = 18.3%
```

Analysis of variance:
```
Source     DF    SS     MS     F    P
Regression  1   352.54 352.541 8.74 0.005
Error      39 1573.34  40.342
Total      40 1925.88
```
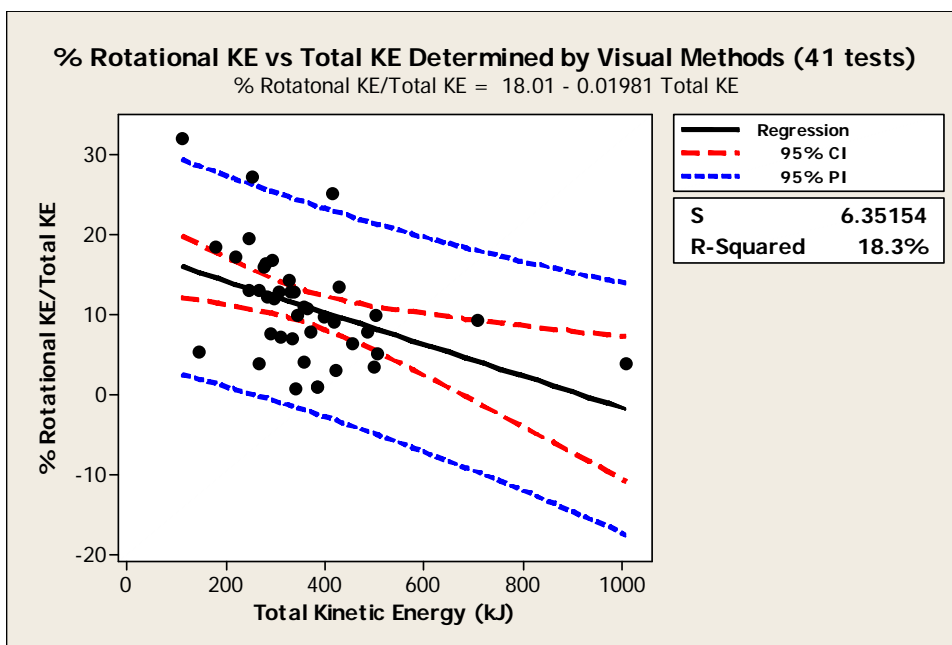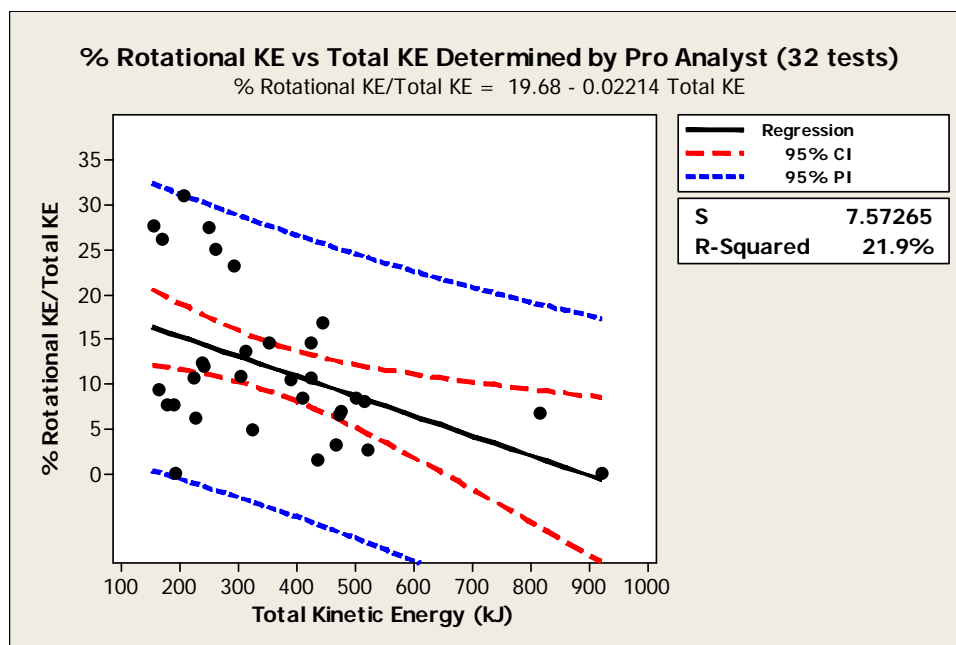

FIGURE B-4 Linear regression of percentage of rotational kinetic energy to total kinetic energy determined for 41 tests by visual analysis of the video records.

3. Evaluation of Relationships Between % Rotational KE/Total KE and Total KE

The regression equation is
```
Rotational KE = 28.12 + 0.01852 Total KE
S = 19.1544  R-Squared = 2.1%
```

Analysis of variance:
```
Source     DF    SS     MS     F    P
Regression  1   308.2 308.235 0.84 0.365
Error      39 14308.7 366.889
Total      40 14616.9
```
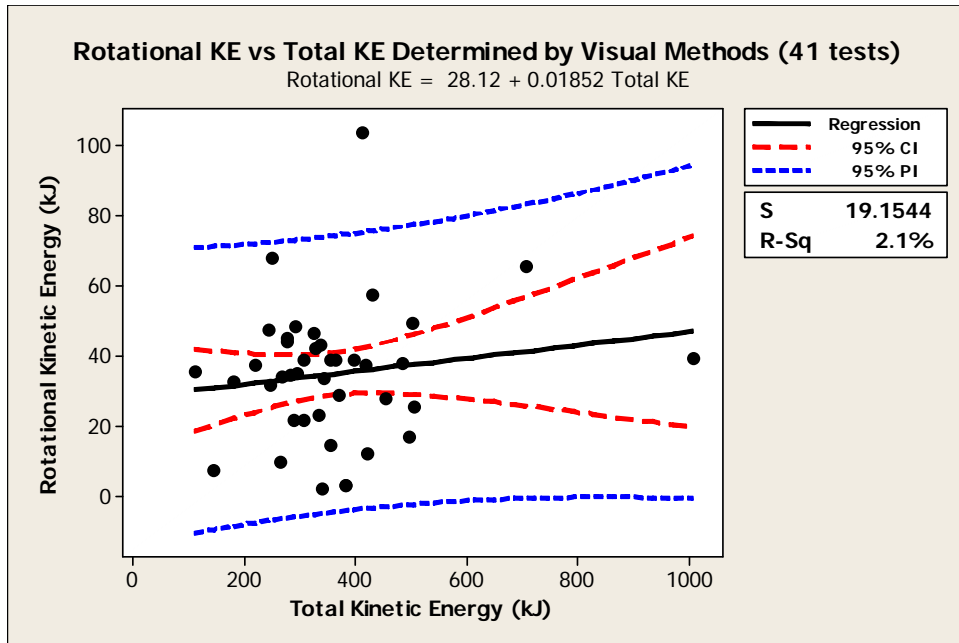
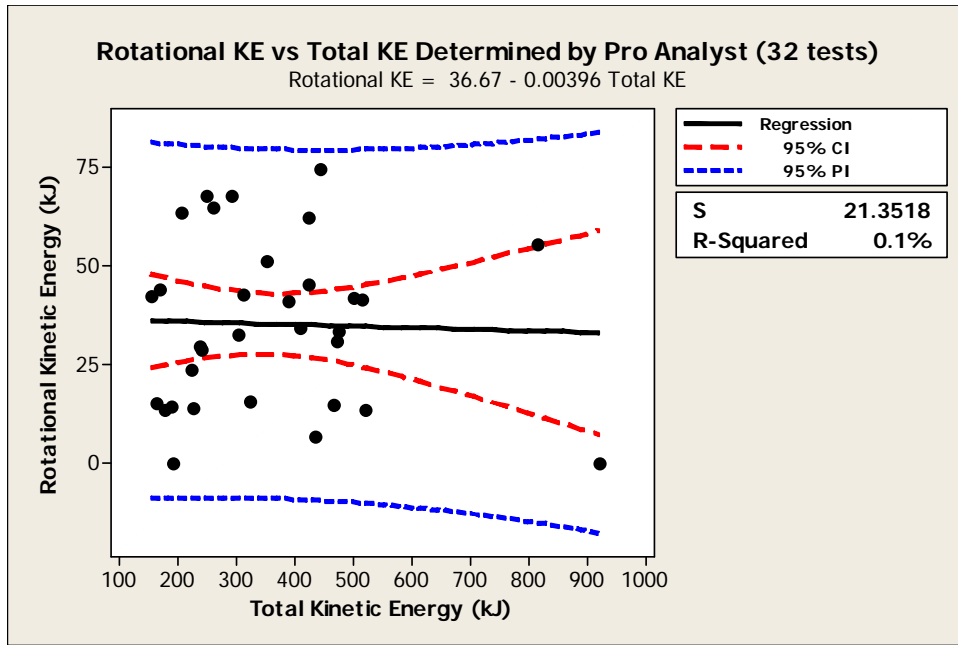**FIGURE B-5 Linear regression of rotational kinetic energy to total kinetic energy determined for 41 tests by visual analysis of the video records.**

APPENDIX C

ProAnalyst Energy Analysis

K inetic energy estimates have been evaluated for a selection of 32 tests by analysis of the high-speed video records using the ProAnalyst motion-analysis software produced by Xcitex Incorporated (Xcitex, Inc., 2007). These results were extracted from the Xcel database (Appendix A) and analyzed using Version 15 of the Minitab statistical software.

For the 32 tests evaluated so far, translational kinetic energies impacting the attenuator or posts mostly range from approximately 110-480 kJ (41-178 ft-tons), with only two tests exceeding this range. Figure C-1 summarizes these results. Rotational kinetic energies range between 15-75 kJ (6-28 ft-tons). The ratio of the rotational kinetic energy compared to the total kinetic energy averages about 12%, and ranges from 0% to about 31%. Figures C-2 and C-3 illustrate the distribution of rotational and total kinetic energies.

Linear regression analysis (Figures C-4 and C-5) evaluates the relationship between the achieved rotational kinetic energy and the total kinetic energy. Results were almost identical to those obtained by analyzing the estimates achieved by visual analysis. Figure C-4 shows that the ratio of the rotational energy to the total energy declines as the total energy increases. The linear regression is significant at the 95% confidence level, but there is a large scatter to the data, and the regression only "explains" 21.9% of the variability in the data. The relationship between rotational energy and total energy (Figure C-5) is not significant at the 95% confidence level; it "explains" only 0.1% of the data variability.

These results support the previous conclusions: the amount of rotational energy achieved during individual tests is relatively constant, and does not increase as the total energy increases.

1. Descriptive Statistics (based on 32 tests):

Translational KE (kJ)

```
 N  Mean SE Mean StDev Median Minimum Maximum
32 322.5   31.9 180.3  284.6  110.3   920.5
```

Rotational KE (kJ)

```
 N  Mean SE Mean StDev Median Minimum Maximum
32 35.26   3.72 21.02  33.90  14.93   74.70
```

Total KE (kJ)

```
 N  Mean SE Mean StDev Median Minimum Maximum
32 357.8   31.5 178.4  316.4  152.5   920.5
```

%Rotational energy/total energy

```
 N  Mean SE Mean StDev Median Minimum Maximum
32 11.76   1.49  8.43  14.66   0.00   31.04
```
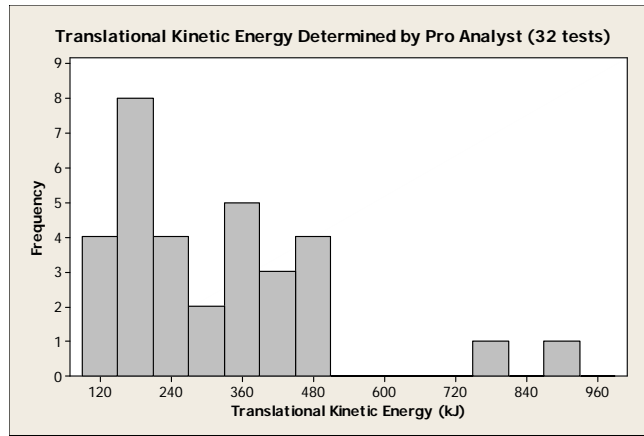
FIGURE C-1 Histogram of translational kinetic energy determined for 32 tests by applying ProAnalyst motion-analysis software to video records.
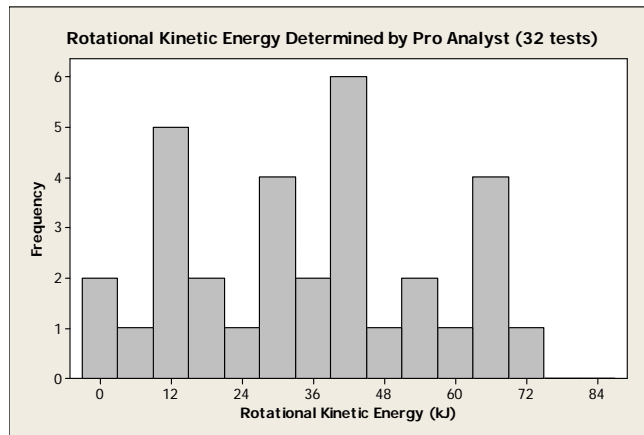
FIGURE C-2 Histogram of rotational kinetic energy determined for 32 tests by applying ProAnalyst motion-analysis software to video records.
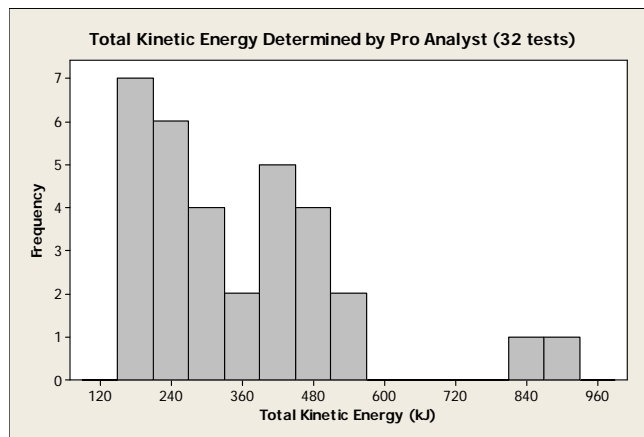
FIGURE C-3 Histogram of total kinetic energy determined for 32 tests by applying ProAnalyst motion-analysis software to video records.

2. Evaluation of Relationships Between % Rotational KE/Total KE and Total KE

The regression equation is
```
% Rotational KE/Total KE = 19.68 - 0.02214 Total KE
S = 7.57265  R-Squared = 21.9%
```

Analysis of variance:
```
Source     DF     SS     MS     F    P
Regression  1   483.27 483.272 8.43 0.007
Error      30 1720.35  57.345
Total      31 2203.62
```


FIGURE C-4 Linear regression of percentage of rotational kinetic energy to total kinetic energy determined for 32 tests by applying ProAnalyst motion-analysis software to video records.

3. Evaluation of Relationships between Rotational KE and Total KE

The regression equation is
```
Rotational KE = 36.67 - 0.00396 Total KE
S = 21.3518  R-Sq = 0.1%  R-Sq(adj) = 0.0%
```

Analysis of variance:
```
Source     DF     SS     MS     F    P
Regression  1    15.5  15.471 0.03 0.855
Error      30 13677.0 455.900
Total      31 13692.5
```

FIGURE C-5 Linear regression of rotational kinetic energy to total kinetic energy determined for 32 tests by applying ProAnalyst motion-analysis software to the video records.

APPENDIX D

Comparison of Energy Analysis Estimates Developed by Visual and ProAnalyst Methods

Kinetic energy estimates have been replicated for a selection of 21 tests by analysis of the high-speed video records following visual evaluation methods of individual frames and by use of the ProAnalyst motion-analysis software produced by Xcitex Incorporated (Xcitex, Inc., 2007). These results were extracted from the Xcel database (Appendix A) and analyzed using Version 15 of the Minitab statistical software.

Three linear regression analyses were conducted: one for the translational kinetic energy estimates, one for the rotational kinetic energy estimates, and one for the total kinetic energy estimates. In each case, not only were the regression lines computed, along with their 95% confidence intervals and 95% prediction intervals, but the residuals to each regression were also evaluated. Figures D-1, D-3, and D-5 illustrate the fitted linear regression lines, along with their 95% confidence intervals and 95% prediction intervals. Figures D-2, D-4, and D-6 provide information that allows an evaluation of the residuals to each regression.

If the regression is to be a valid prediction model of the relationship between the results obtained by the two methods, then the residuals, which contain the variability in the data that is not explained by the regression, should have certain characteristics. The residuals should be distributed according to the normal distribution about the regression line. This can be evaluated by observing them to fall along a straight line in a normal probability plot, and by a histogram of the residuals being relatively symmetrical around a central, near-zero, concentration. Furthermore, plots of residuals versus measured values, or according to the sequence of observations, should not reveal trends or correlations. Figures D-2, D-4, and D-6 each contain four graphs that provide the basic visual assessment of these desired characteristics of the residuals.

These regressions demonstrate that the translational and total kinetic energy estimates by both methods are fairly closely related. Both regressions (Figures D-1 and D-5) are significant at the 95% confidence level, and both "explain" about 50% of the variability in the data. Their residuals (Figures D-2 and D-6) meet all the desirable criteria. However, there is considerable "noise" in the data. If the two methods produced closely similar results at all times then the points would mostly fall on the regression line, and the degree of variability in the data "explained" by these regressions would rise from the observed approximately 50% to a value of over 90%. Furthermore, if the two methods produced closely similar results, then the slope of the regression line should achieve a 45-degree slope, whereas the two regressions have a much lower slope. The energy values obtained by the visual method have a smaller range than those obtained by the ProAnalyst motion-analysis software.

The comparison of the rotational energy estimates, shown by Figures D-3 and D-4, provides a very different result. The linear regression is not significant at the 95% confidence level; it "explains" only 10.8% of the data variability. The residual analysis (Figure D-4) shows a lack of a normal distribution. This is due to the presence of several very large residuals, caused by several rotational energy estimates produced by the visual method that deviate from the values anticipated by the ProAnalyst method. These show as points that plot far from the regression line in Figure D-3.

1. Translational Kinetic Energy determined by Visual and Pro Analyst Methods

The regression equation is
```
Visual Trans KE (kJ) = 136 + 0.483 Pro Analyst Trans KE (kJ)
S = 59.5610  R-Squared = 48.9%
```

Analysis of variance:
```
Source      DF   SS    MS    F    P
Regression   1  64495 64495 18.18 0.000
Residual Error 19  67403  3548
Total       20 131898
```
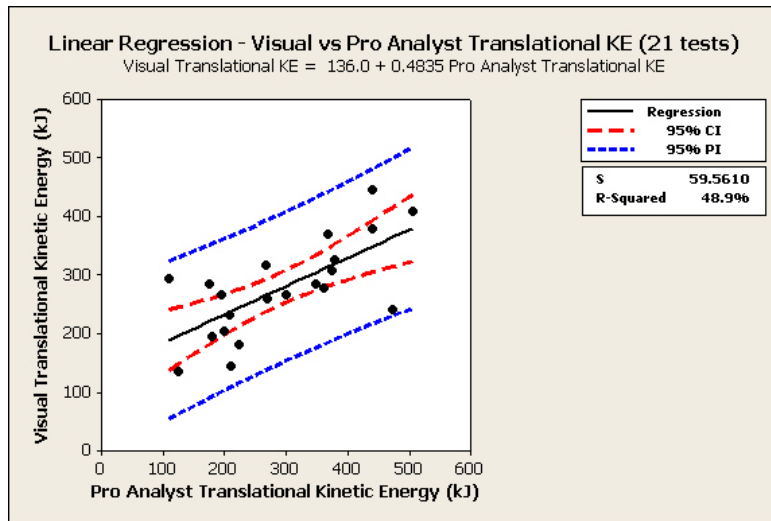

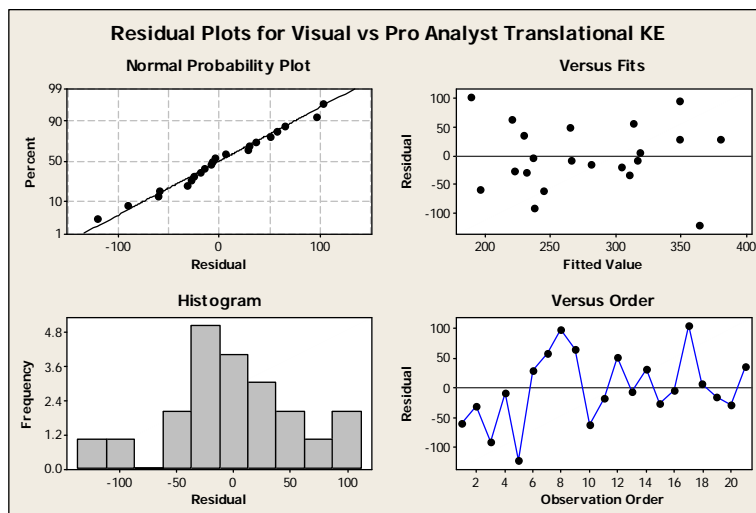**FIGURE D-1 Linear regression of translational kinetic energy estimates obtained by two methods.**

FIGURE D-2 Residual analysis for the translational kinetic energy linear regression in Figure D-1.

2. Rotational Kinetic Energy determined by Visual and Pro Analyst Methods

The regression equation is
```
Visual Rot KE (kJ) = 24.4 + 0.377 Pro Analyst Rot KE (kJ)
S = 19.2616   R-Squared = 10.8%
```

Analysis of variance:
```
Source       DF   SS    MS    F    P
Regression    1  851.3 851.3 2.29 0.146
Residual Error 19 7049.2 371.0
Total        20 7900.4
```
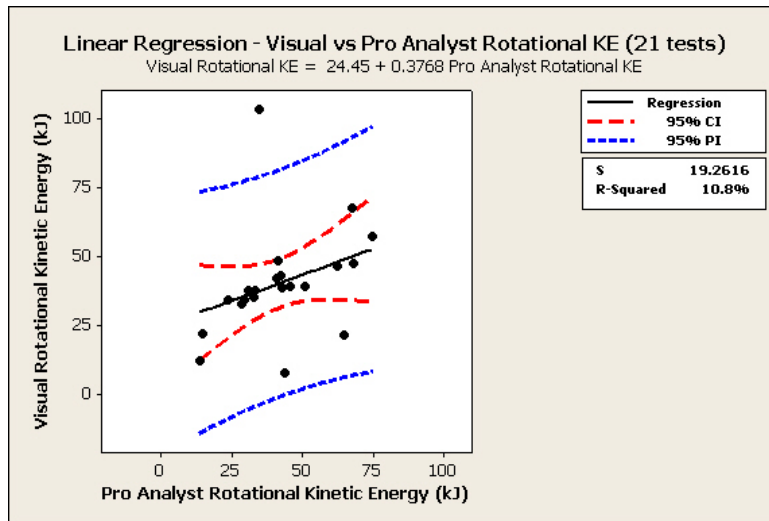

FIGURE D-3 Linear regression of rotational kinetic energy estimates obtained by two methods.
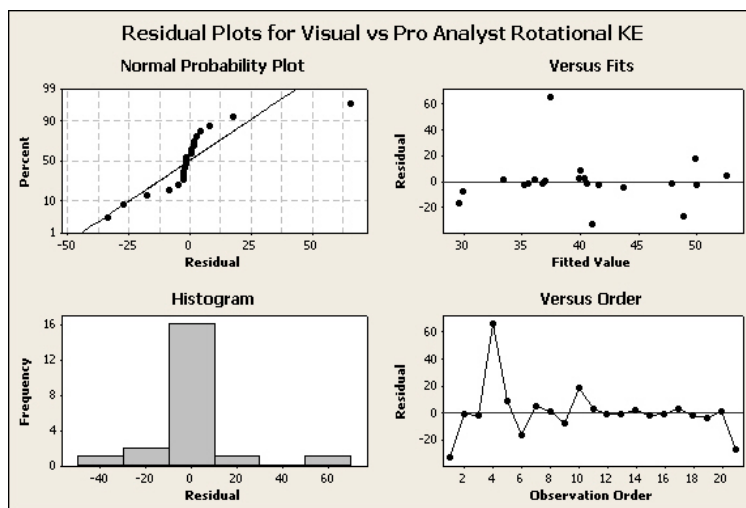
FIGURE D-4 Residual analysis for the rotational kinetic energy linear regression in Figure D-3.

3. Total Kinetic Energy determined by Visual and Pro Analyst Methods

The regression equation is
```
Visual Total KE (kJ) = 152.5 + 0.5002 Pro Analyst Total KE (kJ)
S = 61.1889  R-Squared = 48.8%
```

Analysis of variance:
```
Source      DF   SS     MS      F     P
Regression  1   67786 67786.1 18.10 0.000
Error       19   71138  3744.1
Total       20 138924
```
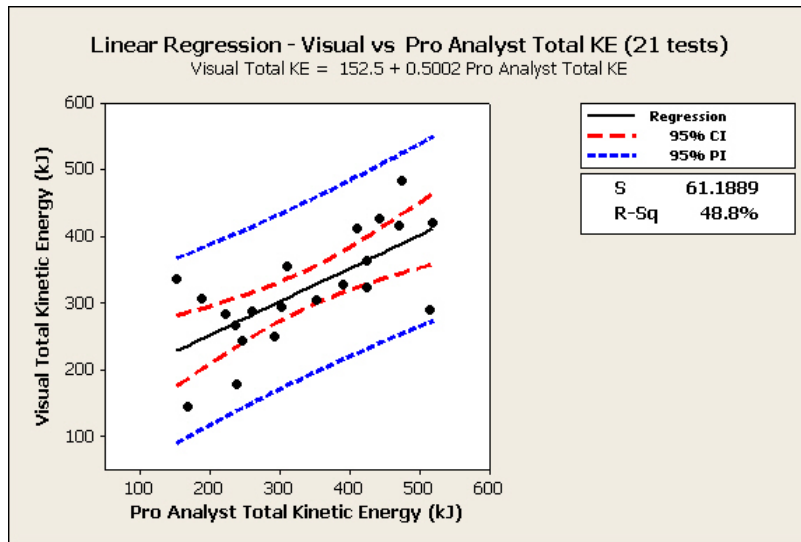

FIGURE D-5 Linear regression of total kinetic energy estimates obtained by two methods.
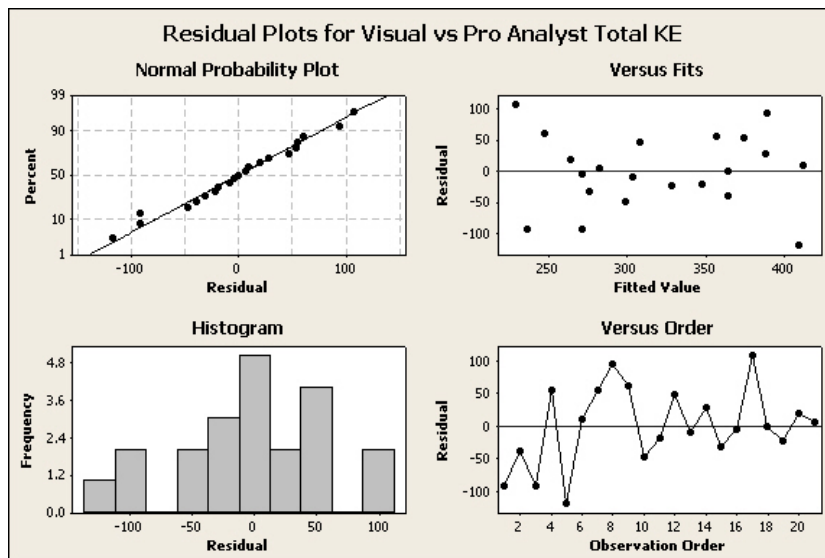
FIGURE D-6 Residual analysis for the total kinetic energy linear regression in Figure D-5.

APPENDIX E

Impact Analyses

Kinetic energy estimates that may influence the response of attenuators to rock impacts have been evaluated for a selection of 36 tests. These results were extracted from the Xcel database (Appendix A) and analyzed using Version 15 of the Minitab statistical software.

Linear regression analysis investigated the relationship between the rotational kinetic energies and the observed number of rotations of blocks as they traveled along the concrete ramp (Figure E-1). As expected, there is a relatively strong relationship; the estimated rotational energy increases as the number of rotations observed increases. Figure E-2 shows the same relationship, subdivided according to rock size. It clearly shows that the rock size influences the relationship; the rotational kinetic energy of larger rocks increases more rapidly than smaller rocks.

Figures E-3 and E-4 summarize the relationship between bounce height and total kinetic energy. This relationship appears to depend to a considerable degree on the size of rock blocks, but these initial results are highly variable and not definitive.

1. Estimated Rotational Kinetic Energy Versus Observed Number of Rotations along Ramp

The regression equation is
```
Rotational KE = - 3.410 + 13.15 (# Rotations Along Ramp)
S = 16.1764  R-Sq = 33.7%  R-Sq(adj) = 31.8%
```

Analysis of variance:
```
Source     DF    SS     MS     F    P
Regression  1  4645.1 4645.08 17.75 0.000
Error      35  9158.7  261.68
Total      36 13803.8
```

2. Bounce Height Versus Total Kinetic Energy Estimated by Visual Methods

The regression equation is
```
Bounce_Height = 0.542 + 0.006253 Visual Total KE (kJ)
S = 2.73239  R-Squared = 9.6%
```

Analysis of variance
```
Source     DF    SS     MS    F    P
Regression  1  27.800 27.8000 3.72 0.062
Error      35 261.308  7.4659
Total      36 289.108
```
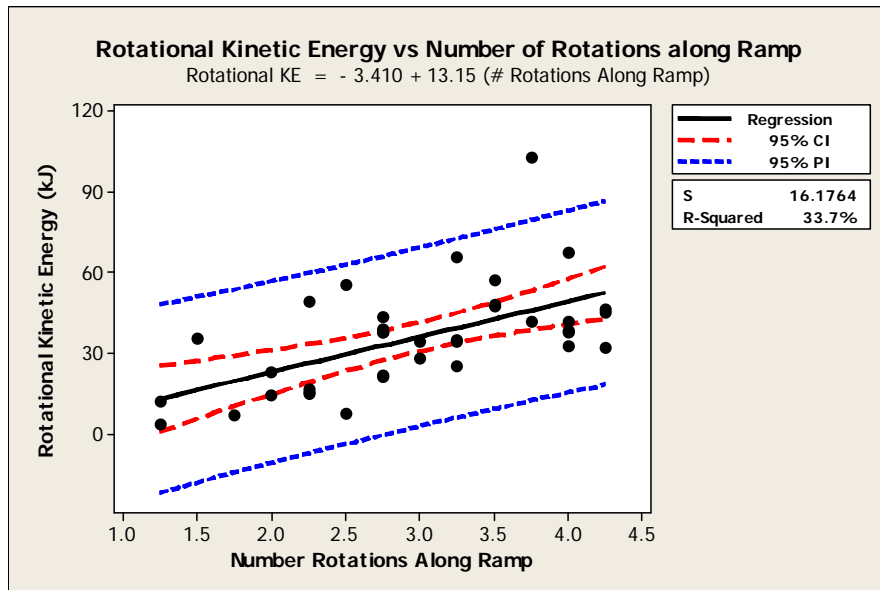
FIGURE E-1 Rotational kinetic energy estimated by visual methods versus observed number of rotations along the ramp.
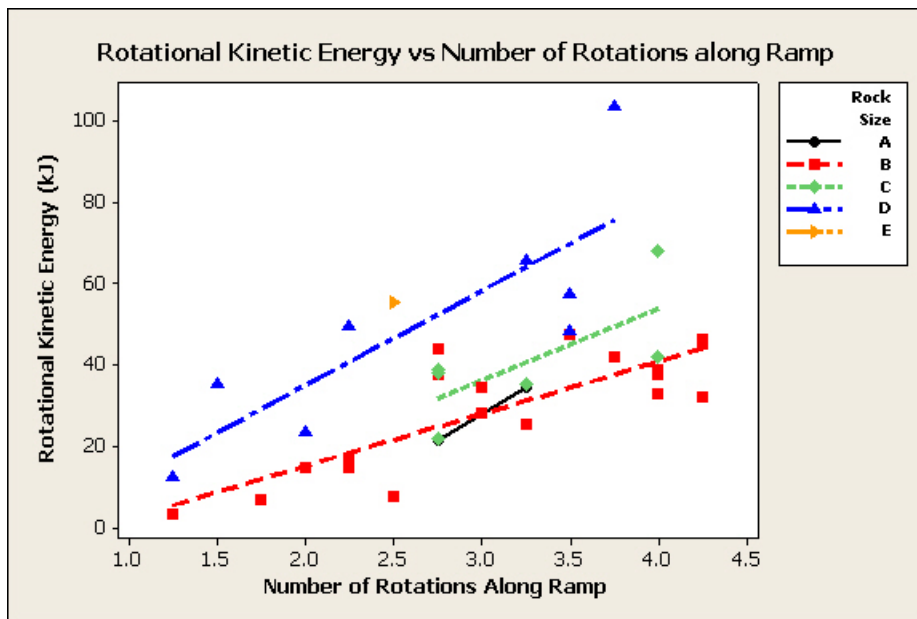
FIGURE E-2 Rotational kinetic energy estimated by visual methods versus observed number of rotations along the ramp, with subsets showing size of rock in test.
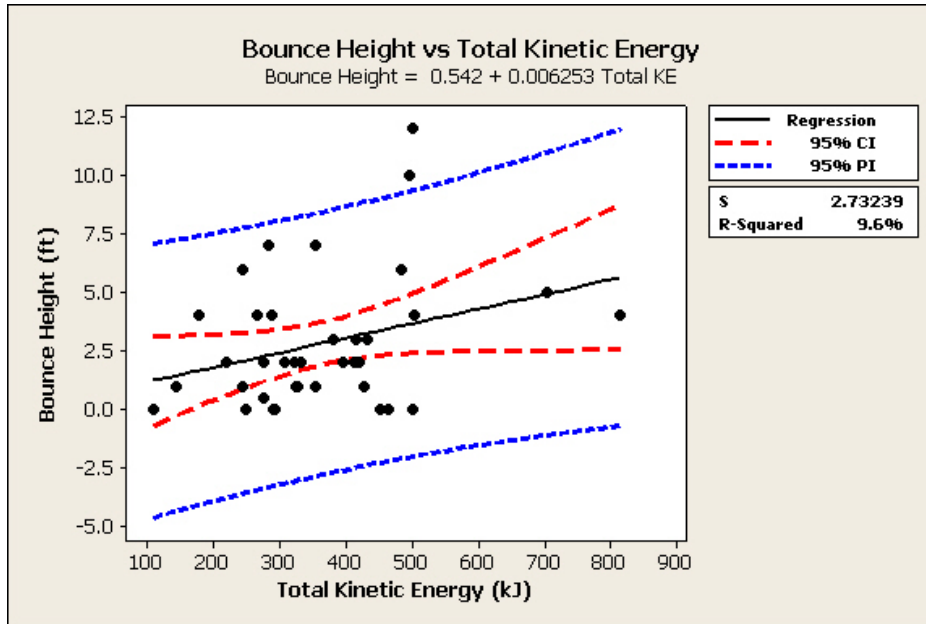
FIGURE E-3 Bounce height versus total kinetic energy estimated by visual methods.
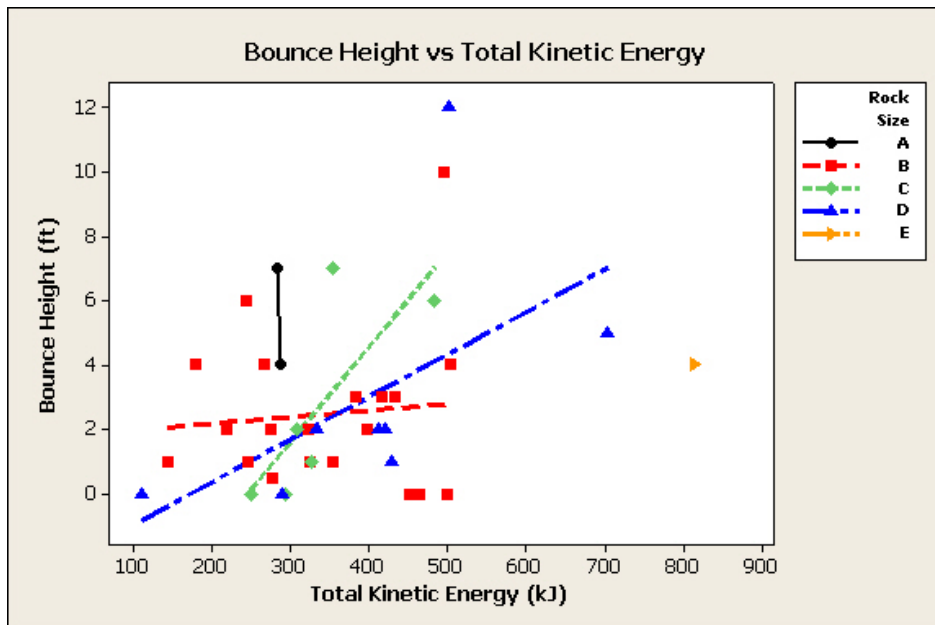
FIGURE E-4 Bounce height versus total kinetic energy estimated by visual methods, with subsets showing size of rock in test.

APPENDIX F

Responses by Attenuator Tail Components

Kinetic energy estimates that may influence the responses of attenuator tail components to rock impacts have been evaluated for a selection of 36 tests. These results were extracted from the Xcel database (Appendix A) and analyzed using Version 15 of the Minitab statistical software. Three relationships were evaluated; these evaluations are in Sections 1-3 below.

Linear regression provides evidence of a relatively strong relationship between the height of the tail as the rock exits the system and the time the tail remains elevated in the air (Figure F-1). As the time in the air increases, so does the vertical height of the tail as the rock exits the system. This regression is significant at the 95% confidence level and "explains" about 65% of the data variability. Figure F-2 shows the same data, but now subdivided according to the density of the mesh. Low density (less than 4 kg/m^2, or 0.8 lbs/ft^2) and medium density (4-7 kg/m^2, or 0.8-1.4 lbs/ft^2) materials behave similarly, and are similar to the combined conditions shown in Figure F-1. High density (greater than 7 kg/m^2, or 1.4 lbs/ft^2) materials appear to behave somewhat differently, but there are many fewer data points. Thus, at present, the relationship does not appear to be affected by material density. Figure F-3 presents the same data, now subdivided by the size of the rock involved in the test. The relationship seems unaffected by rock size; rocks of size B, C, and D have almost identical trends, and although the trend for the smallest rocks (rock A) appears different, it is based on very few tests.

Longer tails tend to spend less time elevated in the air (Figure F-4). This relationship is most apparent for medium density mesh materials (Figure F-5). Low density mesh materials show no relationship between their length and the time they are elevated; their trend line is essentially horizontal at 0.85 seconds. But this result is due to the presence of measured results ranging from 0 seconds to 1.5 seconds for any tail length. When this relationship was evaluated with the data subdivided by the size of rock involved in each test (Figure F-6), it appears possible that the relationship between the time the tail remains elevated in the air and the length of the tail may be affected by the sizes of the rocks impacting the attenuator. However, because the C-sized rocks were mostly tested with shorter tails, and the B-sized rocks with longer tails, these data may be biased and more tests need to be undertaken and evaluated before definitive conclusions can be reached.

Linear regression shows only a weak relationship between the height of the tail as the rock exits the system and the total kinetic energy of the test rock, as estimated by visual analysis of the video images (Figure F-7). This relationship is not statistically significant, and the regression trend shows a diminished height as the rock impact energy increases; a counter-intuitive result. However the data are highly erratic, the measured tail heights at the time the rocks exit the system range from low to high for all values of total kinetic energy. A subdivision of this data according to rock size (Figure F-8) fails to resolve the relationship.

1. Evaluation of Tail Vertical Height when Rock Exits Versus Tail Time in Air

The regression equation is
```
Tail Vertical Height = - 0.927 + 6.911 Tail Time in Air
S = 2.98818  R-Squared = 64.8%
```

Analysis of variance:
```
Source     DF    SS     MS     F     P
Regression  1 574.950 574.950 64.39 0.000
Error      35 312.523  8.929
Total      36 887.473
```
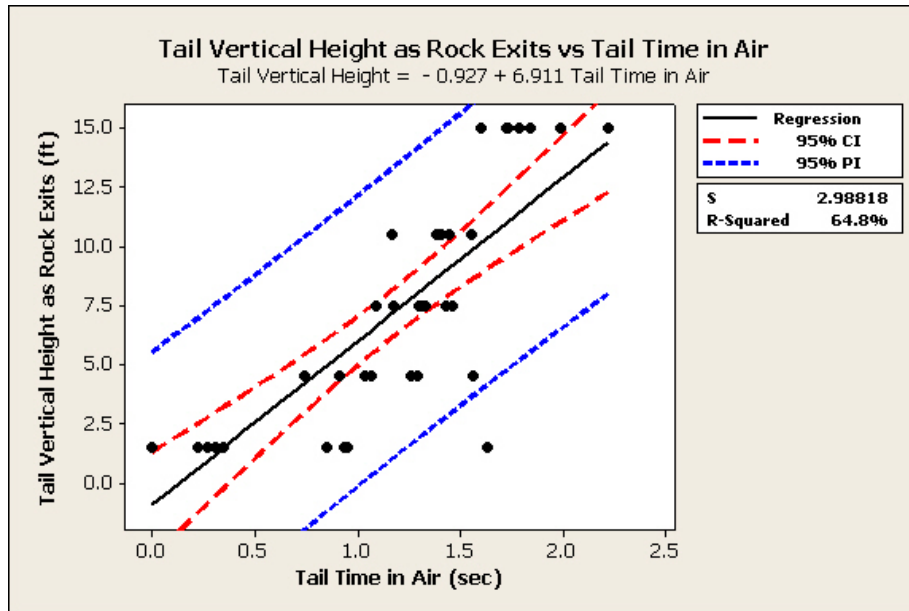

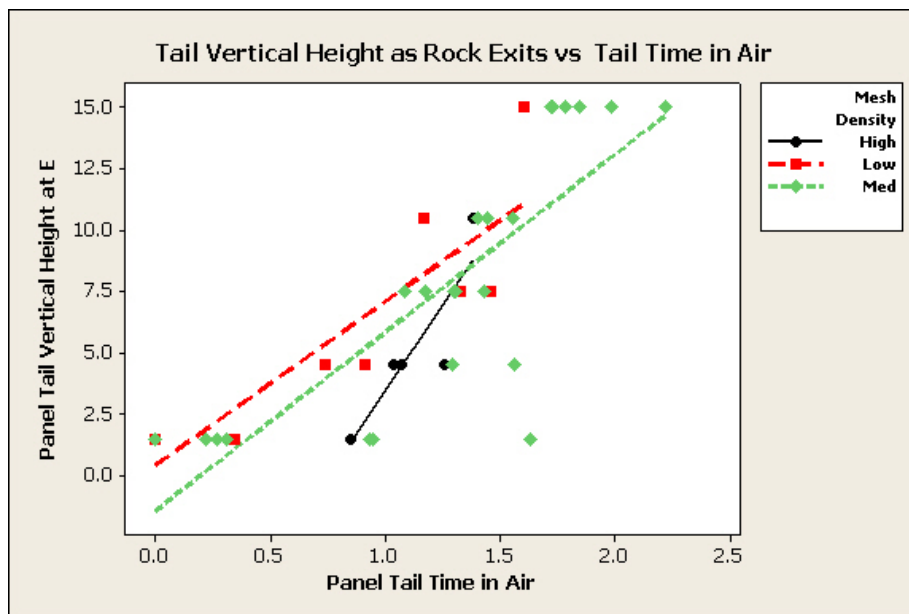**FIGURE F-1 Linear regression of panel tail vertical height as rock exits versus time in the air.**

FIGURE F-2 Panel tail vertical height as rock exits versus time in the air, with subsets showing mesh densities (Low ≤ 4 kg/m^2; Medium = 4-7 kg/m^2; High ≥ 7 kg/m^2).
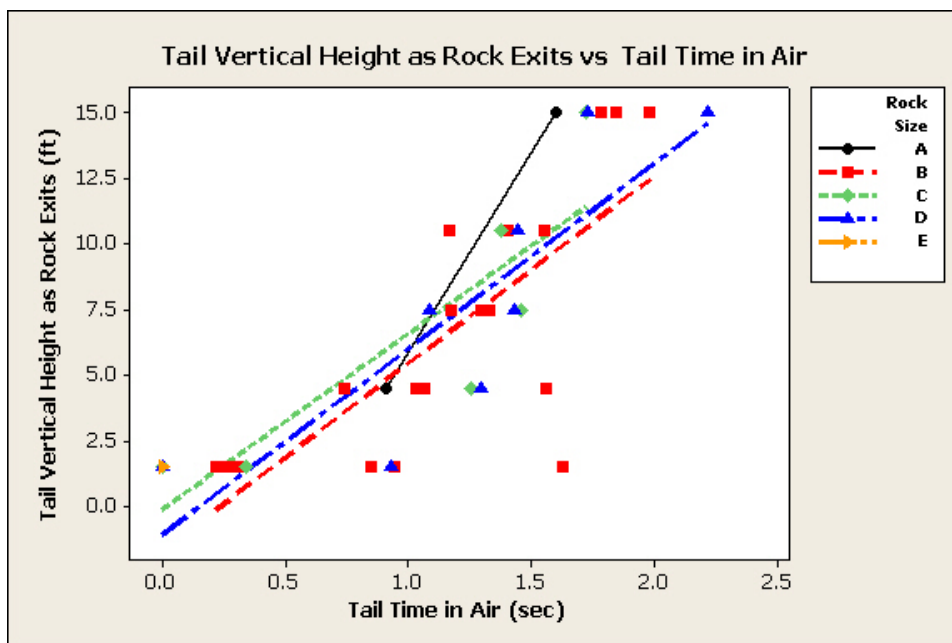
FIGURE F-3 Panel tail vertical height as rock exits versus time in the air, with subsets showing size of rock in test.

2. Tail Time in Air Versus Tail Length

The regression equation is
```
Tail Time in Air = 1.780 - 0.03425 Tail Length
S = 0.528548  R-Squared = 18.8%
```

Analysis of variance:
```
Source     DF     SS     MS     F    P
Regression  1   2.2585 2.25853 8.08 0.007
Error      35   9.7777 0.27936
Total      36  12.0362
```

3. Tail Vertical Height When Rock Exits Versus Total Kinetic Energy by Visual Methods

The regression equation is
```
Tail Vertical Height = 9.886 - 0.007980 Total KE
S = 4.90540  R-Squared = 5.1%
```

Analysis of variance:
```
Source     DF     SS     MS     F    P
Regression  1   45.269 45.2693 1.88 0.179
Error      35  842.204 24.0630
Total      36  887.473
```
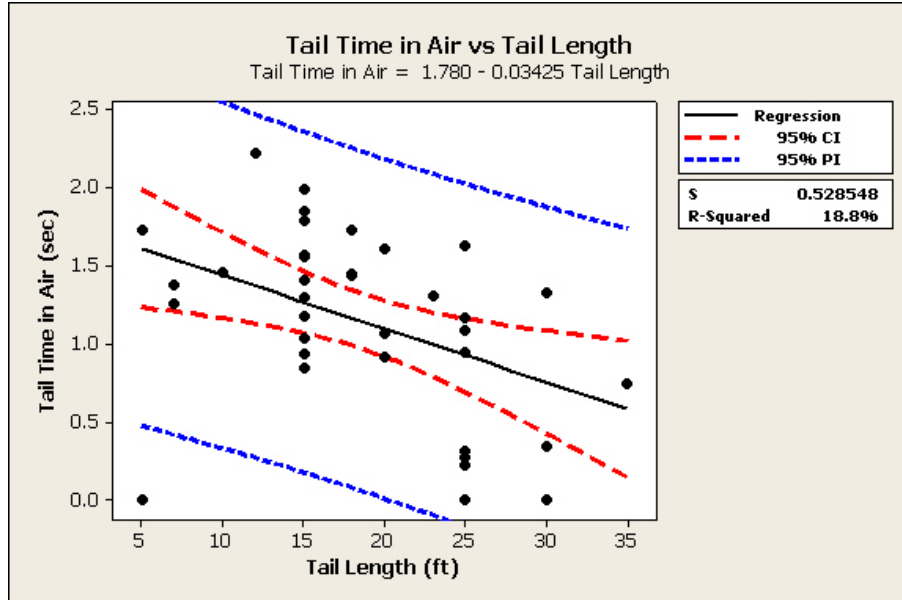
**FIGURE F-4 Tail time in the air versus tail length,
with subsets showing size of rock in test.**
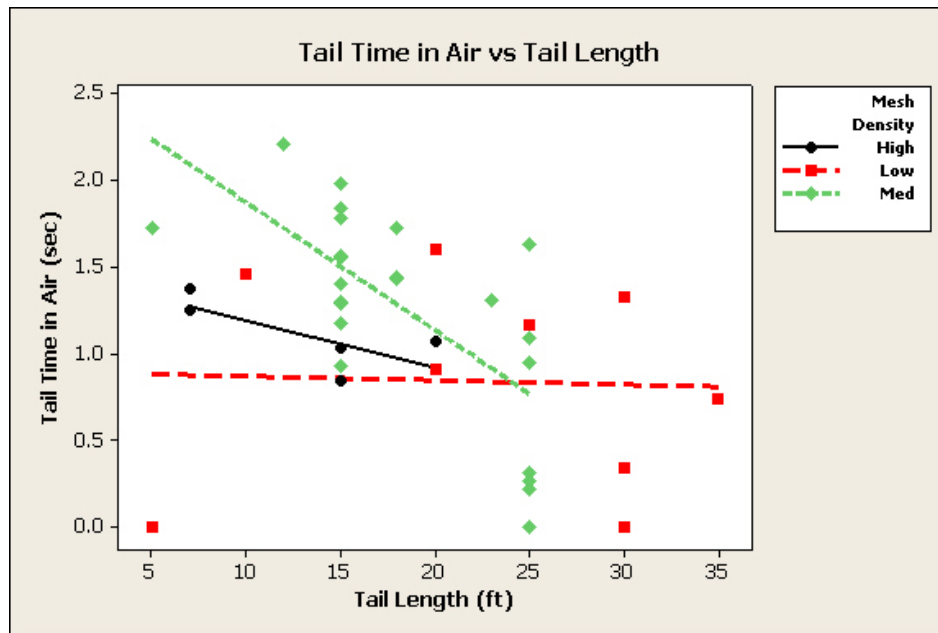
**FIGURE F-5 Tail time in the air versus tail length, with subsets showing mesh densities
(Low ≤ 4 kg/m^2; Medium = 4-7 kg/m^2; High ≥ 7 kg/m^2).**
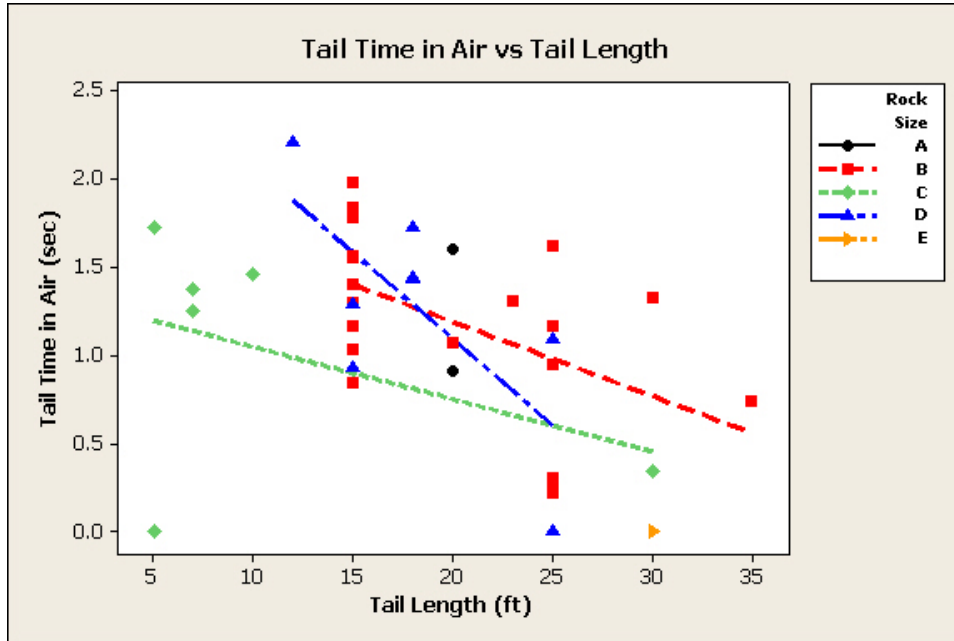
FIGURE F-6 Tail time in the air versus tail length, with subsets showing size of rock in test.
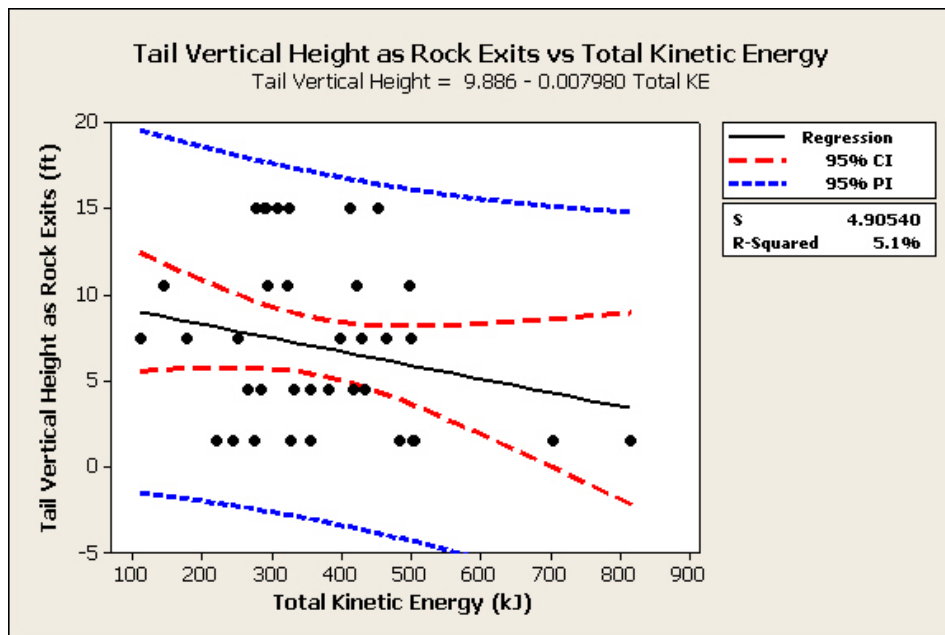
FIGURE F-7 Tail vertical height as rock exits versus total kinetic energy(est. by visual methods).
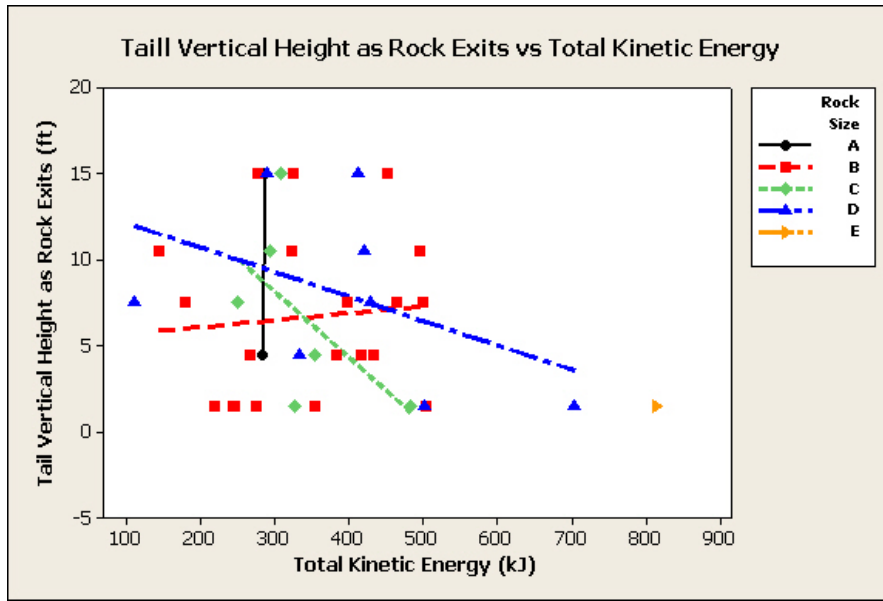
FIGURE F-8 Tail vertical height as rock exits versus total kinetic energy (est. by visual methods), with subsets showing size of rock in test.

APPENDIX G

Plans and Details of 2009 Georgetown Attenuator Installation

In March and April of 2009, the Colorado Department of Transportation applied the test results from the Hidden Valley test facility to design and install a multiple attenuator system above the Georgetown Incline. The design consisted of a series of three separate attenuators that were located approximately 100 and 150 m (300 and 500 ft) apart. The two prototype attenuators located lower on the slope were also repaired, and the barrier fence adjacent to Interstate 70 was extended.

This Appendix reproduces five selected plan sheets that define the details of this attenuator installation. They are included in Figures G-1 through G-5. Figure G-1 is a photograph of the project site, providing an overview of the three new attenuator locations, the two lower older prototype attenuators, and the catchment fences along the roadway. Figure G-2 provides a plan view of the project. Figure G-3 shows a typical section through Chute 4, the principal rockfall location being mitigated. Figures G-4 and G-5 provide details of the components used in this attenuator installation.
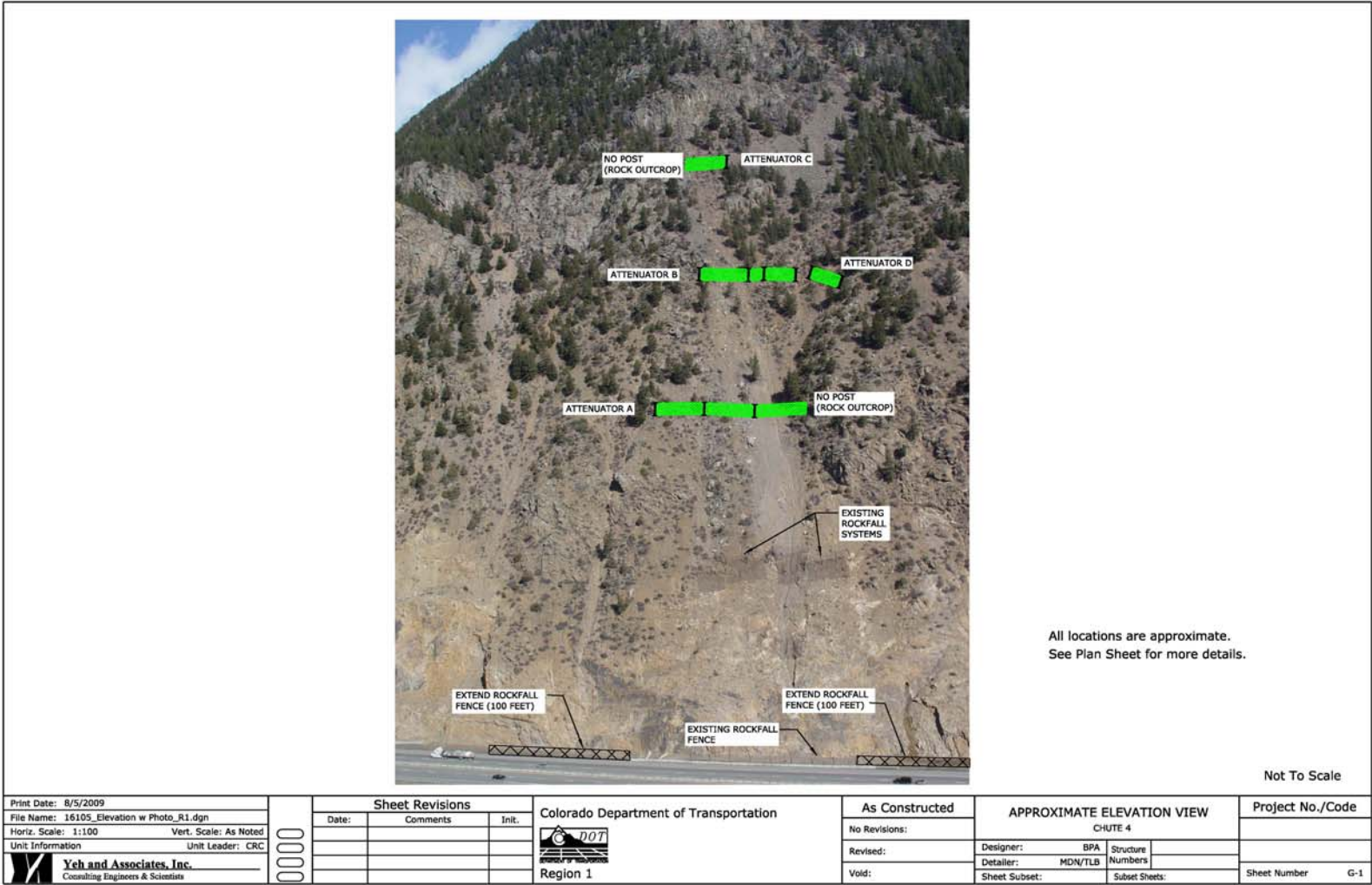
FIGURE G-1 Project site, providing overview of three new attenuator locations, two lower older prototype attenuators, and catchment fences along roadway.
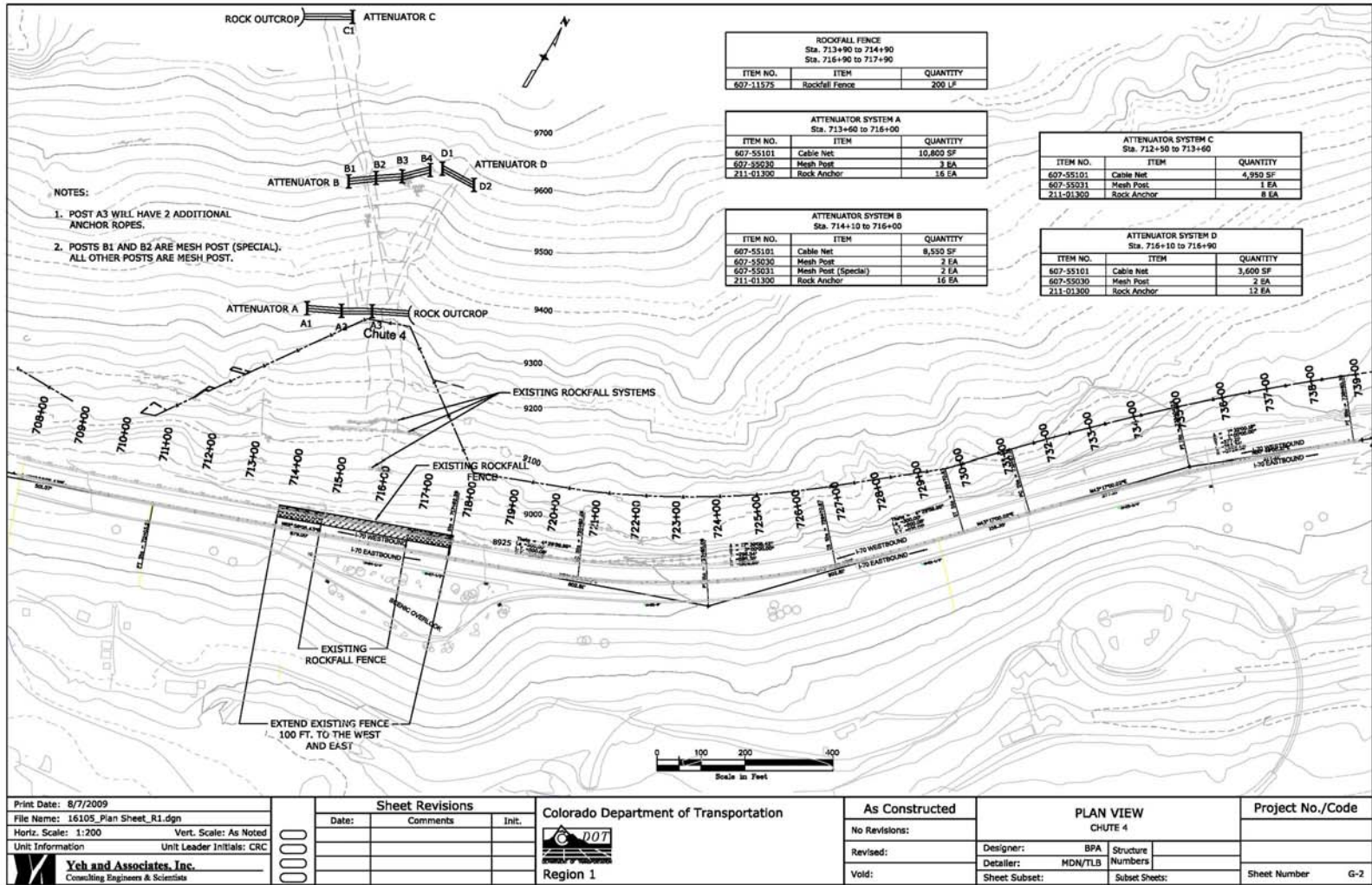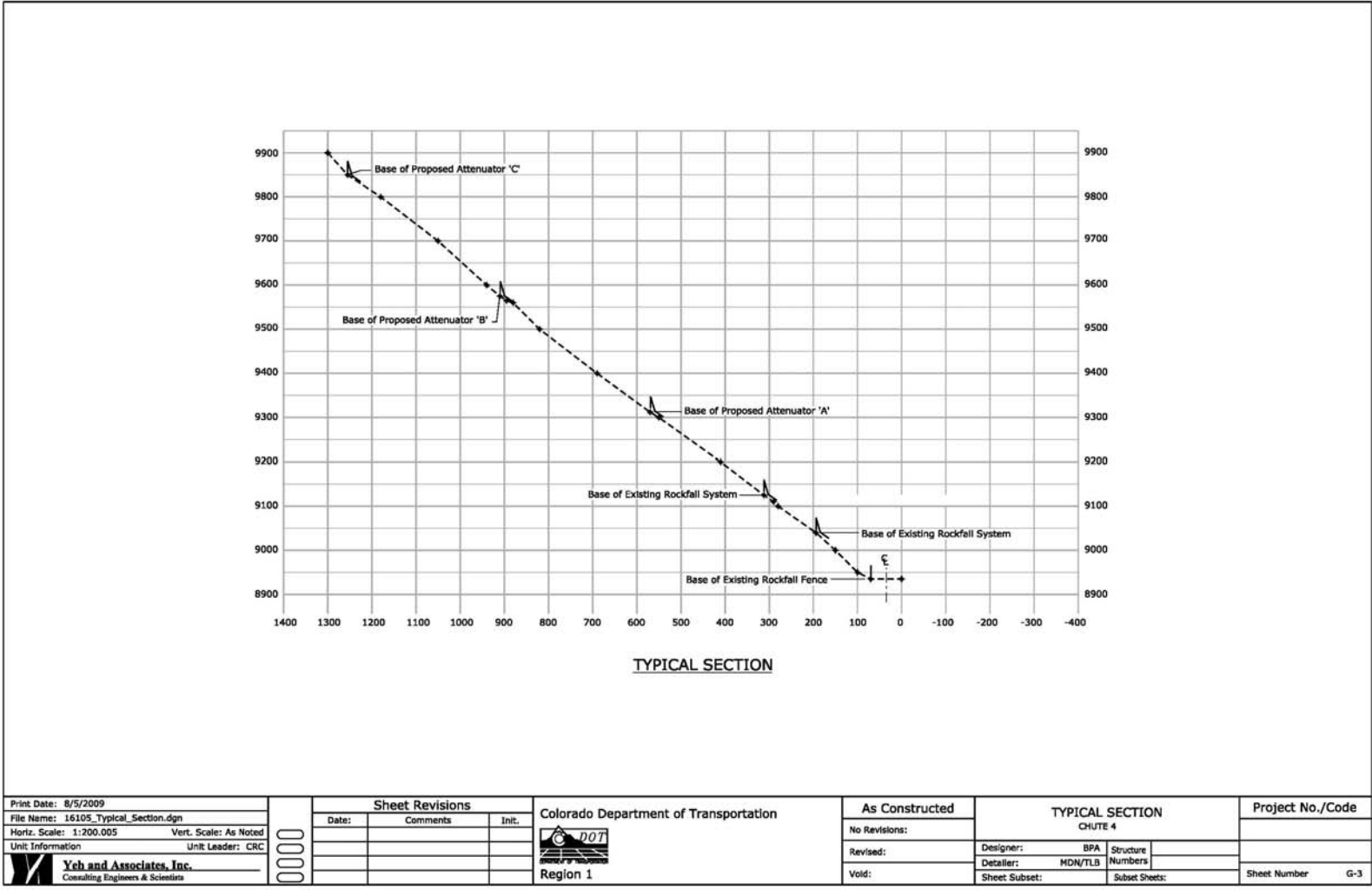
FIGURE G-2 Plan view of project.

FIGURE G-3 Typical section through Chute 4 (principal rockfall location being mitigated).
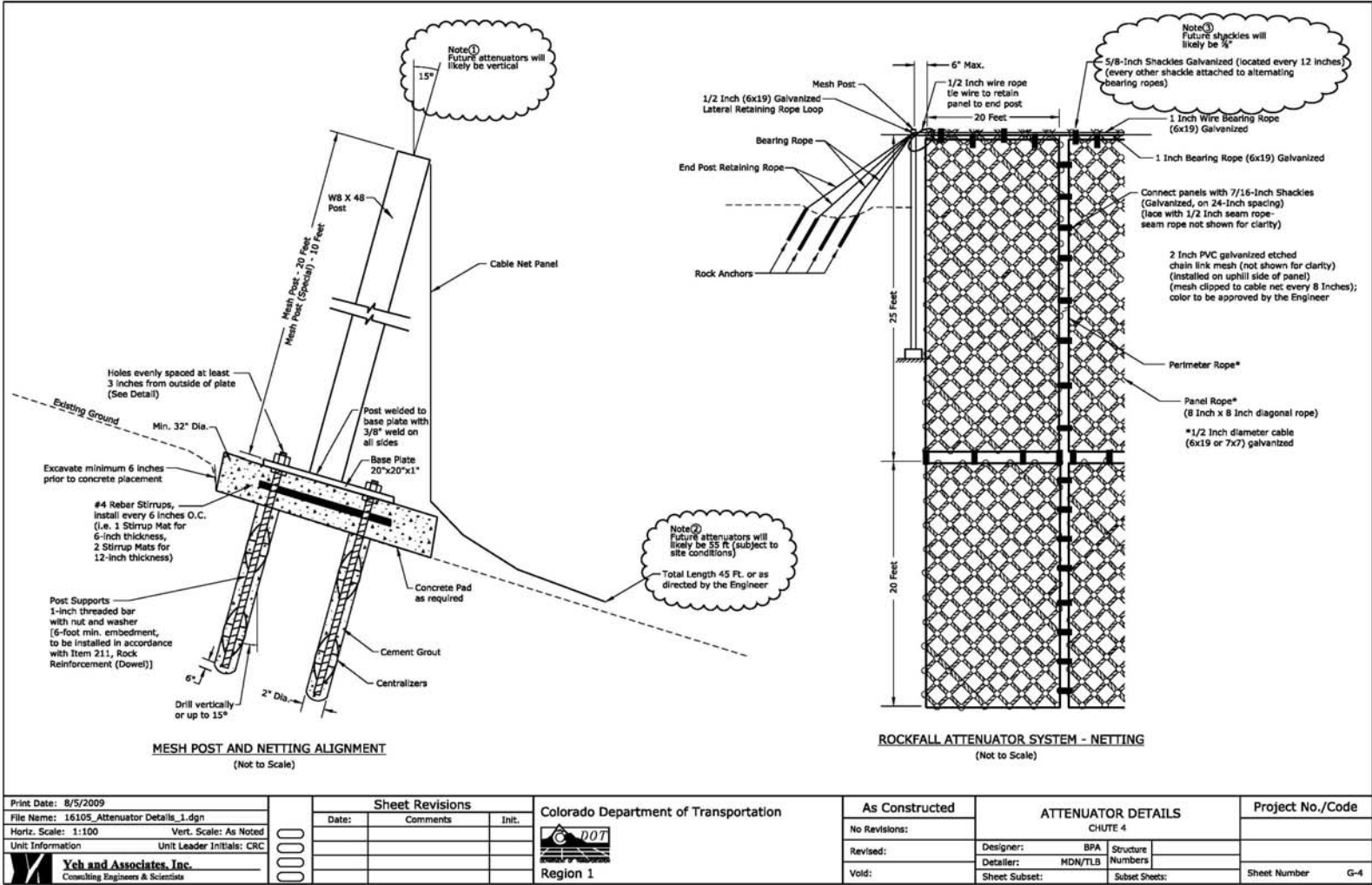
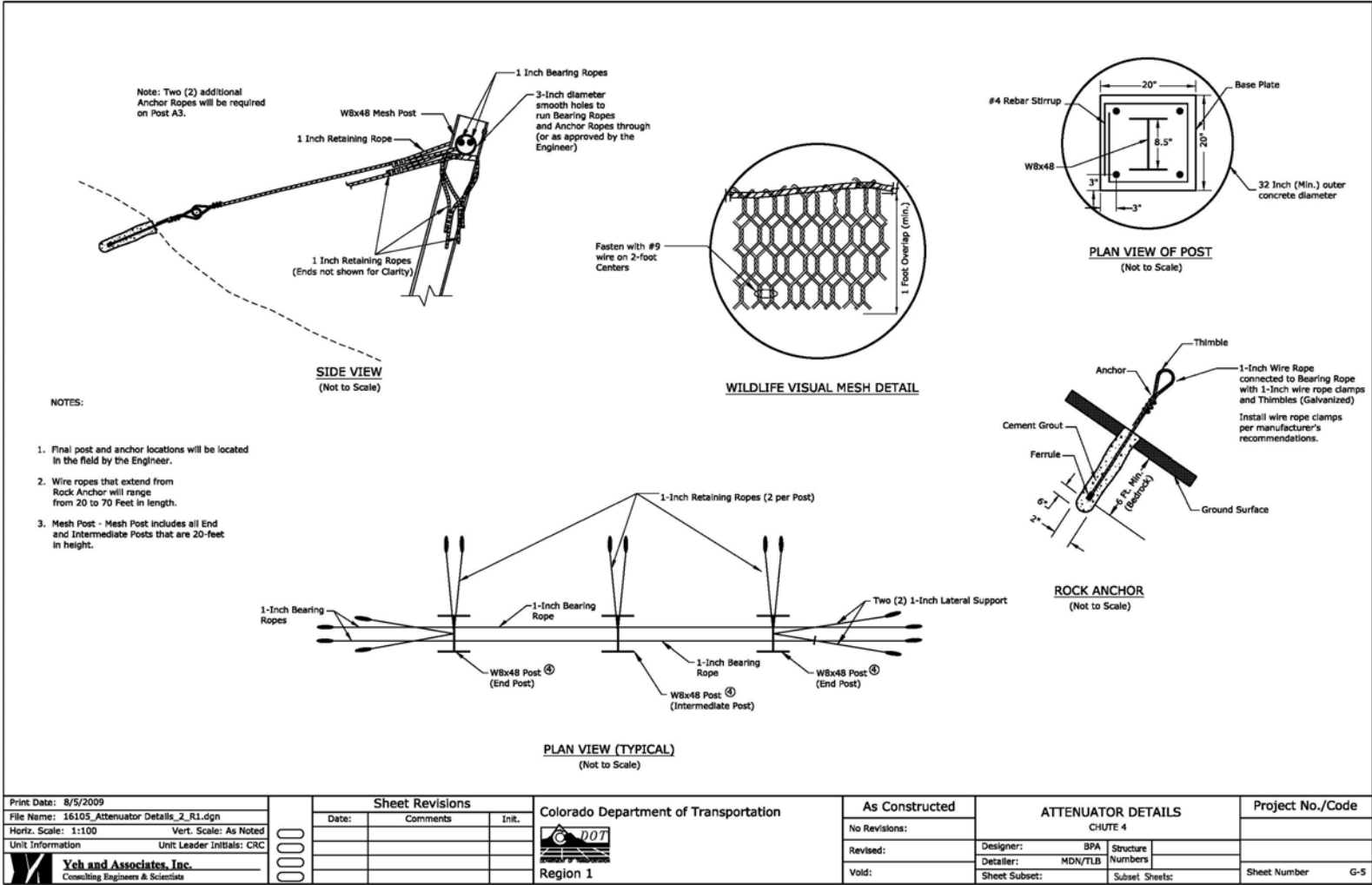**FIGURE G-4 Components used in attenuator installation.**

FIGURE G-5 Components used in attenuator installation.

THE NATIONAL ACADEMIES
Advisers to the Nation on Science, Engineering, and Medicine

The **National Academy of Sciences** is a private, nonprofit, self-perpetuating society of distinguished scholars engaged in scientific and engineering research, dedicated to the furtherance of science and technology and to their use for the general welfare. On the authority of the charter granted to it by the Congress in 1863, the Academy has a mandate that requires it to advise the federal government on scientific and technical matters. Dr. Ralph J. Cicerone is president of the National Academy of Sciences.

The **National Academy of Engineering** was established in 1964, under the charter of the National Academy of Sciences, as a parallel organization of outstanding engineers. It is autonomous in its administration and in the selection of its members, sharing with the National Academy of Sciences the responsibility for advising the federal government. The National Academy of Engineering also sponsors engineering programs aimed at meeting national needs, encourages education and research, and recognizes the superior achievements of engineers. Dr. Charles M. Vest is president of the National Academy of Engineering.

The **Institute of Medicine** was established in 1970 by the National Academy of Sciences to secure the services of eminent members of appropriate professions in the examination of policy matters pertaining to the health of the public. The Institute acts under the responsibility given to the National Academy of Sciences by its congressional charter to be an adviser to the federal government and, on its own initiative, to identify issues of medical care, research, and education. Dr. Harvey V. Fineberg is president of the Institute of Medicine.

The **National Research Council** was organized by the National Academy of Sciences in 1916 to associate the broad community of science and technology with the Academy's purposes of furthering knowledge and advising the federal government. Functioning in accordance with general policies determined by the Academy, the Council has become the principal operating agency of both the National Academy of Sciences and the National Academy of Engineering in providing services to the government, the public, and the scientific and engineering communities. The Council is administered jointly by both the Academies and the Institute of Medicine. Dr. Ralph J. Cicerone and Dr. Charles M. Vest are chair and vice chair, respectively, of the National Research Council.

The **Transportation Research Board** is one of six major divisions of the National Research Council. The mission of the Transportation Research Board is to provide leadership in transportation innovation and progress through research and information exchange, conducted within a setting that is objective, interdisciplinary, and multimodal. The Board's varied activities annually engage about 7,000 engineers, scientists, and other transportation researchers and practitioners from the public and private sectors and academia, all of whom contribute their expertise in the public interest. The program is supported by state transportation departments, federal agencies including the component administrations of the U.S. Department of Transportation, and other organizations and individuals interested in the development of transportation. **www.TRB.org**

www.national-academies.org

TRANSPORTATION RESEARCH BOARD
500 Fifth Street, NW
Washington, DC 20001

THE NATIONAL ACADEMIES™
Advisers to the Nation on Science, Engineering, and Medicine

The nation turns to the National Academies—National
Academy of Sciences, National Academy of Engineering,
Institute of Medicine, and National Research Council—
for independent, objective advice on issues that affect
people's lives worldwide.
www.national-academies.org